Electronic Thesis and Dissertation Repository

1-19-2024 2:00 PM

Exploring the Reactivity of Metal-Ligand Cooperative Complexes with Dioxazolones, Terminal Alkynes, and 2-Ethynylbenzyl Alcohol

megan A. Hoffer Miss, *Western University*

Supervisor: Blacquiere, Johanna M., *The University of Western Ontario*
A thesis submitted in partial fulfillment of the requirements for the Master of Science degree in Chemistry
© megan A. Hoffer Miss 2024

Follow this and additional works at: https://ir.lib.uwo.ca/etd

Part of the Inorganic Chemistry Commons, and the Organic Chemistry Commons

Abstract

N-Acyl ketenimines were attempted to be synthesized catalytically by [Ru(Cp)(P$^{Ph}_2$N$^{Ph}_2$)(NCMe)]PF$_6$ with phenylacetylene and 3-phenethynyl-1,2,4-dioxazol-5-one. Trapping agents were employed to identify the major product of the reaction, as many products were formed. [Ru(Cp)(P$^{Ph}_2$N$^{Ph}_2$)(NCMe)]PF$_6$ reacts with 3-phenethynyl-1,2,4-dioxazol-5-one generating an isocyanate *via* the Curtius rearrangement, confirmed by a forced Curtius rearrangement with 3-phenethynyl-1,2,4-dioxazol-5-one and 1,2,4-triazole. Rates of vinylidene formation using [Ru(Cp)(P$^{Ph}_2$N$^{Ph}_2$)(NCMe)]PF$_6$ and various terminal alkynes of different sterics and electronics were evaluated using a Hammett analysis for and simple rate comparisons. Negligible trends were observed at 70 ℃. The rate of vinylidene formation with [Ru(Cp)(P$^{Cy}_2$N$^{Ph}_2$)(NCMe)]PF$_6$ and phenylacetylene was faster than that of [Ru(Cp)(P$^{Ph}_2$N$^{Ph}_2$)(NCMe)]PF$_6$ due to the difference in steric and electronic properties of the metal. Hydrofunctionalization reactions of 2-ethynylbenzyl alcohol (2-EBA) using an [Ru(Cp)(P$^{Cy}_2$N$^{Ph}_2$)(NCMe)]PF$_6$ were spiked with different alkali salts which had a positive effect on 2-EBA consumption. Different weakly coordinating anions were coordinated *in-situ* to Ru(Cp)(P$^{Cy}_2$N$^{Ph}_2$)Cl for the hydrofunctionalization of 2-EBA. It was found that the PF$_6^-$ anion gave the highest consumption of 2-EBA.

Keywords

Metal-ligand cooperative complexes, P$^R_2$N$^{R'}_2$, dioxazolones, terminal alkynes, metal-vinylidenes, Curtius rearrangement, isocyanate, Hammett analysis, rates, GC-FID, 2-EBA, isochromene, weakly coordinating anions, NMR spectroscopy, trapping agent, ruthenium.

Summary for Lay Audience

In this study, complexes involving ruthenium and iron were unable to produce our target product. Rather, one of the ruthenium complexes was found to follow a known reaction to produce a highly reactive molecule. Five different substrates and two different ruthenium complexes were used to investigate factors influencing the time to generate a known compound. Alterations to the substrate had no impact on the formation. However, one ruthenium complex exhibited faster formation of the desired product than the other. Furthermore, we investigated factors affecting the known transformation of 2-ethynylbenzyl alcohol (2-EBA) to isochromene.

Co-Authorship Statement

All experiments were performed by M. Hoffer. Chapters 1-3 were written by M. Hoffer and edited by J. M. Blacquiere.

Acknowledgments

I have been at Western for six years now, and through all the ups and downs, my family has been the constant. Always by my side, in my corner, encouraging me to work hard, and motivating me when I can't find it within me. I would not be where I am without them. I love you all so much and am so grateful to have you.

I would also like to thank my boyfriend, Matt. Also being in academia, we can bond over the good times and the bad. We hold each other accountable and go to each other when we need a break. Matt, you always strive to be better, do better, and that motivates me to be the best version of myself, never give up, and stay consistent. I love you.

I next want to thank Johanna, my supervisor. You have taught me so much over these past three years. You taught me how important it is to be prepared, how to answer questions, how to make a presentation, how to give a talk, and how important spell check is. I appreciate your mentorship over the past few years, preparing me for the real world, and making me a better scientist. I appreciate all the hard work and time you dedicate to your students.

To the Blacquiere group, both past and present members. So many amazing laughs and stories, bonding moments in the lab, scares as well. But we did it all together. We lift each other, pass the knowledge we learn down to one another, and run a lab as a unit. You have all been amazing colleagues and friends.

I am so grateful and lucky to have such an incredible and motivating support system. Thank you all. I have learned so much during my master's and undergrad degrees. I will cherish these memories for the rest of my life.

Table of Contents

List of Schemes

Pinnick Oxidation of **9** to generate carboxylic acid **10**; iv) installation of hydroxamic acid on **10** to generate **11**; V) cyclization of hydroxamic acid **11** to generate final dioxazolone **12 .. 74**

List of Tables

List of Figures

List of Appendices

List of Equations

List Of Abbreviations

acetate = OAc^-

Acetonitrile = MeCN

CV = cyclic voltammetry

Cp = Cyclopentadienyl

Cp* = pentamethylcyclopentadienyl

CDI = 1,1′-carbonyldiimidazole

dppe = 1,2-bis(diphenylphosphino)ethane

Dioxazolones = 1,4,2-dioxazol-5-ones

hexafluoro phosphate = $PF_6{}^-$

hexafluoro antimonate = $SbF_6{}^-$

H = hour

Hex = hexanes

ISIP = Inner sphere ion pair

MeCN = acetonitrile

Min = minute

MLC = Metal-ligand cooperative

OSIP = Outer sphere ion pair

p-toluensolfonate = OTs^-

Ph = phenyl

$P^R{}_2N^{R'}{}_2$ = 1,5-diaza-3,7-diphosphacyclooctane

RDS = rate determining step

tetrakis(3,5-bis(trifluoro-methyl)-phenyl)-borate = BAr^{F-}

tetrafluoroborate = BF_4^{-}

trifluoromethanesulfonate = OTf^{-}

trifluoroacetate = TFA^{-}

TOF = Turn over frequency

VTNA = Variable time normalization analysis

WCA = Weakly coordinating anion

2-EBA = 2-ethynylbenzyl alcohol

Chapter 1

1   Introduction

1.1   Metal Ligand Cooperative Complexes

Breaking bonds involves the absorption of energy, and the specific method depends on the nature of the bonds and the substances involved. The attractive forces holding the atoms together must be overcome. In a traditional metal complexes, the ligands do not participate in the chemical reaction, but rather affect the stability, reactivity, electronic properties, steric effects, and solubility of the complex itself. Metal-ligand cooperative (MLC) complexes bear ligands that participate in bond breaking and/or formation during chemical reactions.[1] For example, the R' group on the amine portion of a 1,5-diaza-3,7-diphosphacyclooctane ($P^R_2N^{R'}_2$) ligand can act as a proton acceptor to facilitate rapid protonation and deprotonation steps (Figure 1.1b, green portion). There are many different types of MLC complexes, herein, MLC complexes bearing $P^R_2N^{R'}_2$ ligands will be the focus of this thesis. The R groups on the phosphorus of the $P^R_2N^{R'}_2$ ligand directly attached to the metal are in the primary coordination sphere part of the complex. The R groups on the phosphorus moiety directly affect the phosphorus *and* metal's electronic properties. If the R group is more electron-donating, the metal therefore becomes more electron-rich. On the contrary, if the R group is electron-withdrawing, the metal becomes more electron-poor. The R' groups on the nitrogen are in the secondary coordination sphere, where they do not directly affect the metal centre's electronic properties, but rather impact the ability of the ligand to perform proton transfers and stabilize the active metal species.
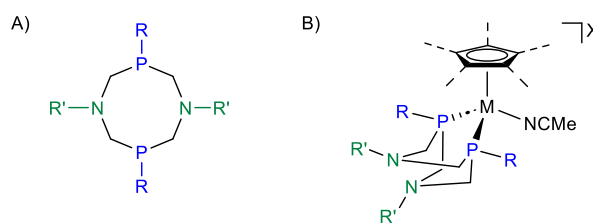
Figure 1.1. A) $P^R_2N^{R'}_2$ ligand; B) MLC complex bearing a $P^R_2N^{R'}_2$ ligand, dashed line = methyl groups can be present, blue = primary coordination sphere, green = secondary coordination sphere.

The amines of the $P^R_2N^{R'}_2$ ligands have been known to mediate proton transfer without the need for any added bases.[1] Examples of $[Ni(P^R_2N^{R'}_2)_2]^{2+}$ complexes have been used as electrocatalysts for oxidation and the production of H_2 studied by cyclic voltammetry (CV).[2] Addition of H_2 to $[Ni(P^R_2N^{R'}_2)_2]^{2+}$ complexes results in a two electron reduction of Ni(II) to Ni(0). The two hydrogens from H_2 bind to the pendant amines *via* a dihydrogen intermediate generating a mixture of the *endo-endo*, *endo-exo*, and *exo-exo* products (Scheme 1.1). More basic pendant amines were found to lower the free energy for the addition of H_2 to $[Ni(P^R_2N^{R'}_2)_2]^{2+}$.[2]
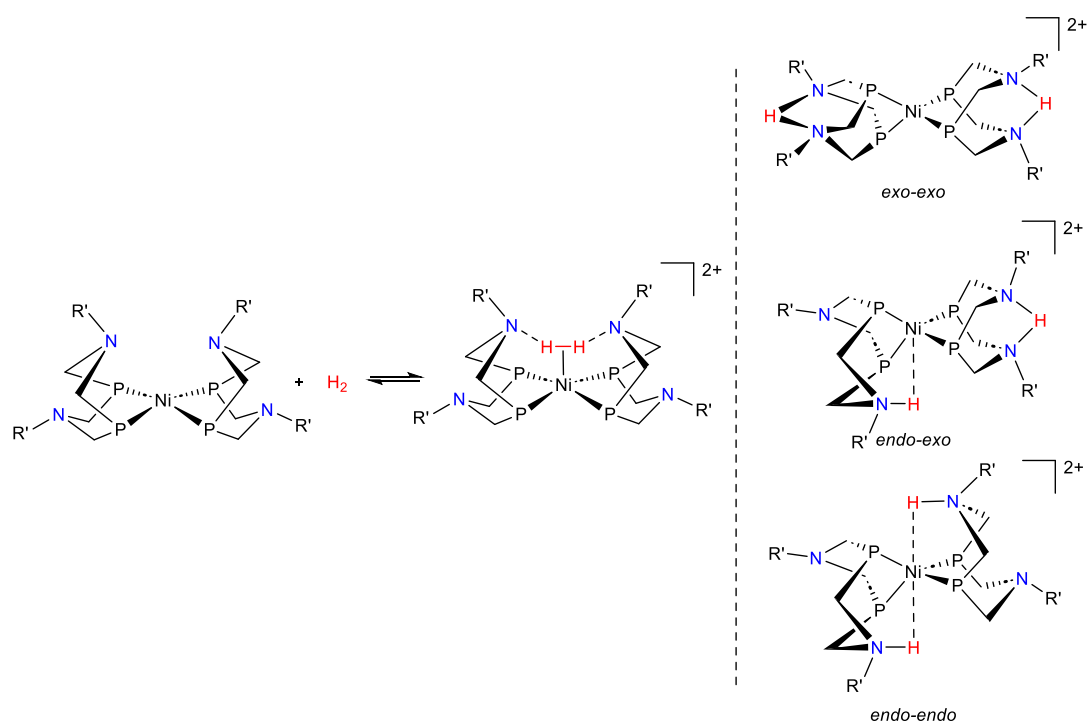
Scheme 1.1. Addition of H_2 to $[Ni(P^R_2N^{R'}_2)_2]^{2+}$ complex with both P_2N_2 ligands protonated, either *endo-endo, endo-exo,* or *exo* concerning the metal centre.[2] *P*-substituent removed for structure cleanliness.

In a study on catalysis with diphosphine ligands containing pendant amines, a Ni(I) complex bearing two $P^R_2N^{R'}_2$ ligands was evaluated for its use in H_2 production in protic ionic liquids.[2] This complex was most stable when both $P^R_2N^{R'}_2$ ligands were in their boat configurations. When this complex was added to protic ionic liquids, one of the pendant amines in the ligand was protonated. Following the *exo* Protonation step, the ligand could

adopt an *exo*-pinched isomer following a boat-to-chair isomerization of one of the amines. A kinetically and thermodynamically stabilized N-H-N linkage was furnished (Scheme 1.2). The pinched structure results in catalyst inhibition.
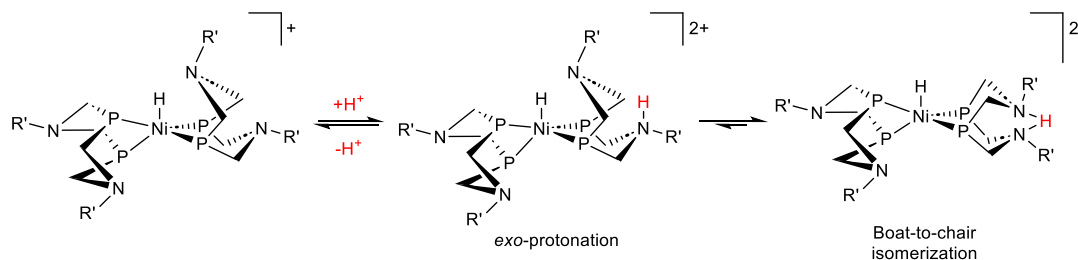
Scheme 1.2. *exo* protonation of $[Ni(P_2N^{R'}_2)H]^+$ followed by a boat-to-chair ring flip affording an *exo*-pinched isomer.[2] *P*-substituents removed for structure cleanliness.

1.1.1 Stabilities of MLC Complexes Bearing Cp/Cp* Ligands

The differences in stability between $[Ru(Cp)(P^{Cy}_2N^{Ph}_2)(MeCN)]PF_6$ and $[Ru(Cp^*)(P^{Cy}_2N^{Ph}_2)(MeCN)]PF_6$ have been studied. Higher lifetimes of the cyclopentadienyl (Cp) complex in comparison to the pentamethylcyclopentadienyl (Cp*) substituted ruthenium catalyst species for the hydroamination reaction of 2-ethynyl aniline to indole were observed.[3] Through computational modelling, the structures and energetics of the active catalysts with vacant coordination sites were calculated (Figure 1.2). The complexes with vacant coordination sites are the reference complexes, and deemed to have energies of 0 kJ/mol. The nitrogen adducts $[Ru(Cp/Cp^*)(P^{Cy}_2N^{Ph}_2)(N_2)]PF_6$ were calculated in order to observe the stabilization energies relative to their vacant coordination site complexes. The energies of the N_2 bound complexes were calculated to be -74.5 kJ/mol for the Cp* and -5.4 kJ/mol for the Cp analog. Instead of N_2 coordination, the Cp analog can achieve a κ^3-(*P,P,Ar*) configuration that greatly stabilizes the active catalyst *via* reversible π-coordination by -47.7 kJ/mol. The Cp* complex revealed that the κ^3-(*P,P,Ar*) isomer increases overall energy by 63.0 kJ/mol and is far less stable than its κ^2-(*P,P*) complex. The κ^3-(*P,P,Ar*) stabilization for Cp* complexes is prevented, likely by the steric clash between the phenyl group on the pendant amine and the Cp* methyl substituents.
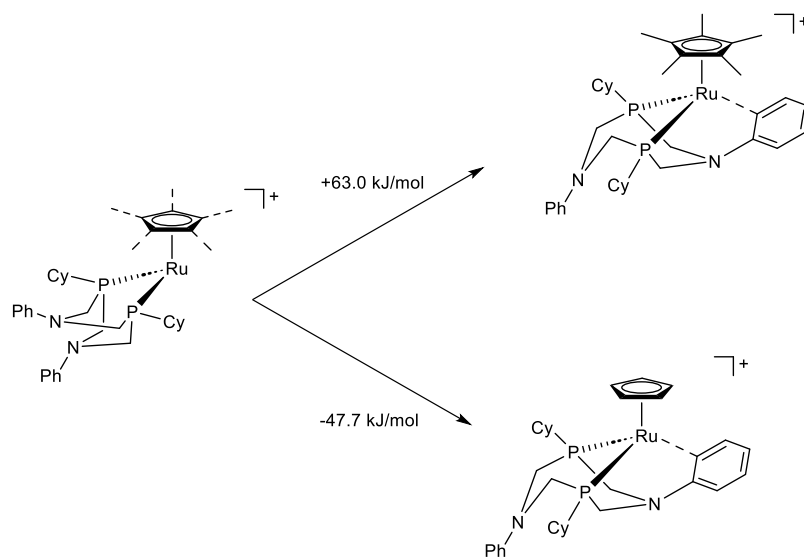
Figure 1.2. Differences in the energy of $[Ru(Cp)(P^{Cy}_2N^{Ph}_2)(N_2)]PF_6$ and $[Ru(Cp^*)(P^{Cy}_2N^{Ph}_2)(N_2)]PF_6$ for reversible π-coordination of the pendent amine phenyl substituent to the metal centre.[3]

1.2   Metal-vinylidenes

Metal-vinylidenes can be defined as a metal double-bonded to a carbon, which is subsequently double-bonded to a second carbon atom (Figure 1.3). The C_α atom which is bound directly to the metal is electrophilic, while C_β is nucleophilic, and their difference in reactivity have been extensively exploited in catalysis.[4,5]
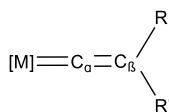
Figure 1.3. Depiction of a metal-vinylidene.

Transition-metal-vinylidenes are key intermediates in numerous synthetic transformations of alkynes.[4] Traditionally, nucleophiles have been added to metal-vinylidenes stoichiometrically to generate corresponding Fischer carbene complexes, reflecting the electrophilicity of the vinylidene α-carbon.[6] There have been many publications involving conversions of terminal alkynes to various products in which metal-vinylidenes serve as catalytic species.[3,7–9] The first instance of metal-vinylidenes was reported in 1985 by

Geoffroy for the polymerization of phenylacetylene (Scheme 1.3).[7] Irradiating $W(CO)_6$ at 366 nm in the presence of phenylacetylene generated the vinylidene complex $[W_o(CO)_5(=C=CHPh)]$, an active precursor for the polymerization of phenylacetylene. This was supported by the isolated $[W(CO)_5(=C=C(Me)(t\text{-}Bu))]$ vinylidene complex, which is the active species by photochemical displacement of a carbonyl ligand. Polymerization is triggered by the addition of additional phenylacetylene which reacts with the tungsten-vinylidene precursor following the loss of a CO ligand.[7]

Scheme 1.3. $W(CO)_6$ as an active precursor for the polymerization of phenylacetylene.[7]

There are many examples of ruthenium-based non-MLC complexes used towards the hydrofunctionalization of various substrates which proceed through metal-vinylidenes.[10–13] $Ru(Cp)(PPh_3)_2Cl$ can be used at 10 mol% catalytic loadings to cycloisomerize aromatic homo- and bis-homopropargylic amines and amides to generate indoles (Scheme 1.4).[13] The reaction requires pyridine as the solvent in order to aid in facilitating the proton transfer step to generate the intermediate metal-vinylidene. The high catalytic loadings and addition of bases or other additives to these reactions is quite inefficient as it adds additional workup steps along with low atom economy.

Scheme 1.4. Non-MLC ruthenium catalyzed cycloisomerization of aromatic homo-and bis-homopropargylic amines and amides to generate indoles.

In another example, [Ru(Cp)(Cl)(dppe)] in addition of NaBAr$^F_4$•3H$_2$O was used for the cycloisomerization of 2-aminodiphenylacetylene derivatives (Scheme 1.5).[12] No base additive was required for this reaction. However, product selectivity, high temperatures, and low yields became a concern. Using MLC complexes for these examples would allow for lower catalytic loadings, more optimal solvent use, and higher selectivity.
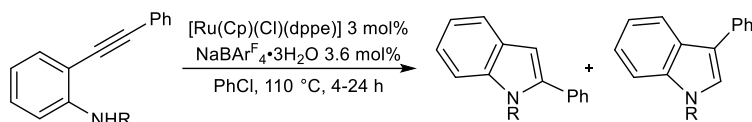
Scheme 1.5. Non-MLC ruthenium catalyzed cycloisomerization of 2-aminodiphenylacetylene derivatives with poor selectivity.

1.2.1   Vinylidene Formation

The preliminary step for vinylidene formation consists of the alkyne bonding in an η^2-binding mode to the metal, thus requiring the metal precursor to have a vacant coordination site generated by either the dissociation of a ligand or a switch in bonding mode by another ligand (Scheme 1.6).[4] The next step is dependent on the electronic nature of the ligands and metal complexes employed. For more electron-rich metal complexes, a formal oxidative addition of the C-H bond occurs giving an alkynyl hydride complex, followed by a 1,3-hydride migration resulting in the vinylidene.[14] Alternatively, the alkynyl hydrogen can undergo a 1,2-hydrogen atom migration giving the vinylidene intermediate, which is common for Ru(II) transition-metal complexes.[6]
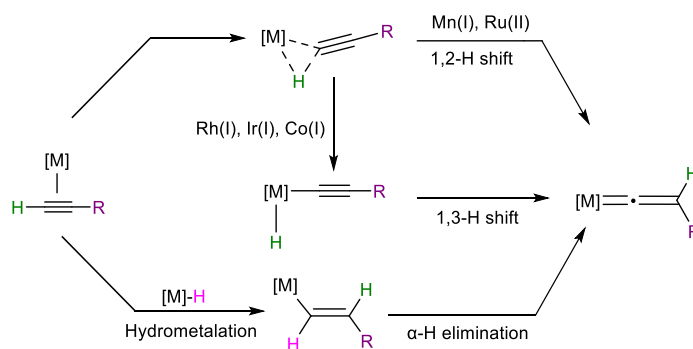
Scheme 1.6. Three well-established routes to form metal-vinylidenes.[6]

1.2.2   Stability of Metal-vinylidenes

The stability of metal-vinylidenes depends on the electronic properties of the metal and its ligands as well as the substituents on the alkyne. The electronics of the metal and alkyne must be tuned appropriately to ensure the species is not *too* stable so it can undergo subsequent reactivity. Metal-vinylidenes can be considered as tautomer pairs; the η^2-alkyne complex tautomerizes to a vinylidene like that of an enol to a ketone (Scheme 1.6).[14] Three main variables can be altered to affect metal-vinylidene formation; substituents on the alkyne, the metal used, and ligand effects.[14] In the computational study of energy differences between vinylidene and alkyne pairs, the electronic effects of investigated.[15] It was found that more electron-withdrawing terminal alkynes tend to favour the vinylidene tautomer over the η^2-alkyne complex.[14] Vinylidenes are electron-withdrawing ligands, therefor having electron-donating ligands on the metal has been shown to stabilize metal-vinylidenes.[6]

1.2.3   MLC Complexes and Vinylidene Formation

In an energetic study of vinylidene formation, the conversion of acetylene to vinylidene in the presence and absence of a cooperative ligand on the metal catalyst was investigated.[15] The paper presented a computational model of the mechanism of acetylene to a metal-vinylidene using two complexes; one bearing imidazole groups and one containing only methyl groups on the phosphorus substituents (Scheme 1.7). The single-step conversion of acetylene to vinylidene in the absence of imidazole on $CpRu(PMe_3)_2^+$ has a calculated barrier of 26.8 kcal/mol^{-1}. When replacing one methyl group on each phosphorus with an imidazole group, which are known to act as proton-shuttle, the calculated barrier was roughly 6 kcal/mol^{-1} lower.[2] The theoretical findings suggest that the use of MLC complexes greatly reduces the energy barrier for the conversion of terminal alkynes to vinylidenes.
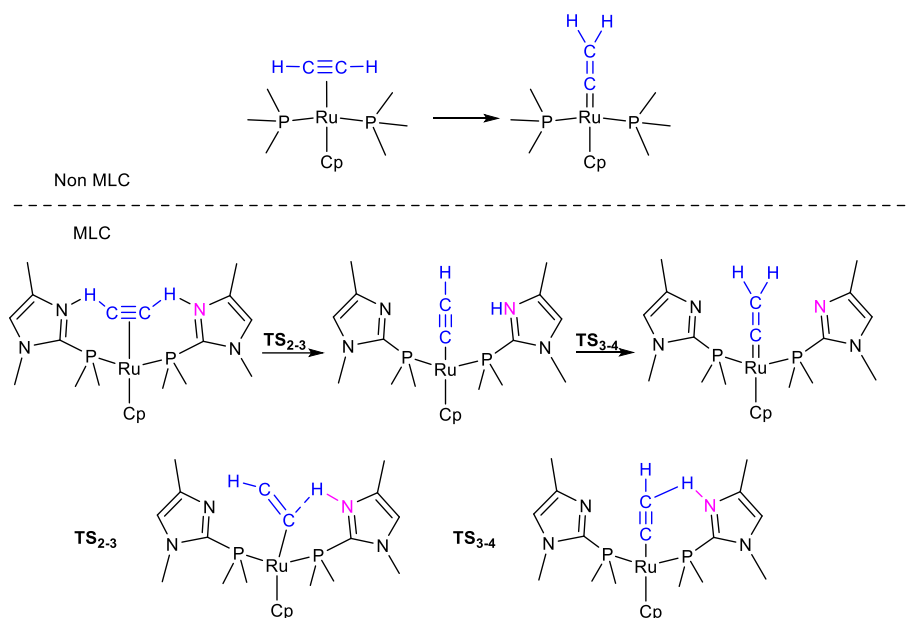
Scheme 1.7. The proposed mechanism *via* computational calculations of the imidazole-assisted proton-transfer for metal-vinylidene formation.

1.2.4   Hydrofunctionalization Reactions *via* Metal-vinylidenes

A hydrofunctionalization reaction is known as the addition of an EH group (E = O, NR, and others) across a double or triple bond (Scheme 1.8).[16] Many examples of the intramolecular hydrofunctionalization on metal-vinylidenes have been thoroughly explored, generating *endo*-heterocyclic products.[3,8,9,17] As summarized, metal-vinylidenes have been observed to require less energy to form using MLC complexes rather than non-MLC complexes. The Blacquiere group has previously reported on many different examples of ruthenium and iron MLC complexes bearing P_2N_2 ligands that generate metal-vinylidenes as the first step of their catalytic cycle in intramolecular alkyne hydroamination and hydroalkoxylation catalysis.[3,17,18]
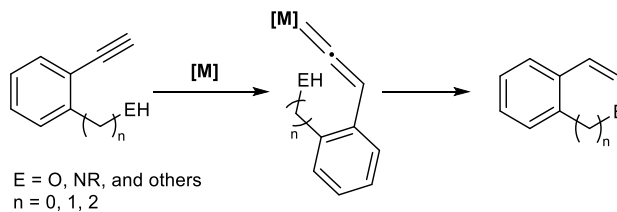
Scheme 1.8. General example of hydrofunctionalization reaction *via* metal-vinylidene.

In a recent mechanistic investigation by the Blacquiere group, the mechanism of hydrofunctionalization reactions of *N*- and *O*- containing compounds with the catalyst $[Ru(Cp)(P^{Cy}_2N^{Ph}_2)(MeCN)]PF_6$ was observed in detail (Scheme 1.9).[9] Through a series of kinetic and deuterium labelling studies, the rate-limiting step for the hydroalkoxylation of 2-ethynylbenzyl alcohol (2-EBA) to isochromene was proposed to be the formation of the vinylidene *via* a 1,2-proton migration. In addition, the effect of temperature on the yields of isochromene was observed. It was found that increasing temperatures from 40-70 °C increased conversions from 11 to 66%, indicating that catalytic activity increasing with increasing temperatures.[9]
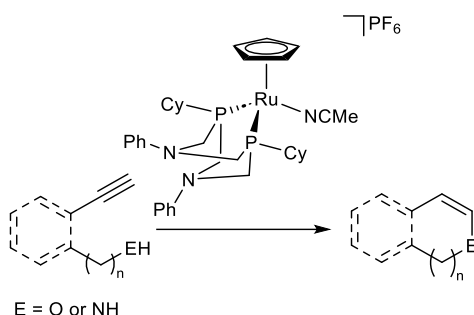
Scheme 1.9. Hydrofunctionalization reactions of *N*- and *O*- containing compounds using $[Ru(Cp)(P^{Cy}_2N^{Ph}_2)(MeCN)]PF_6$.[9]

1.2.5   Intramolecular Attack of Aprotic Internal Nucleophile on Metal-vinylidene

Successful cyclization of a nitrone-containing terminal alkyne species to afford an isoquinolone using the MLC complex $[Ru(Cp)(P^{Cy}_2N^{Ph}_2)(MeCN)]PF_6$ was observed (Scheme 1.10). The proposed mechanism begins with the formation of the vinylidene intermediate followed by the intramolecular addition of the nitrone oxygen to the alpha carbon.[9] This is of interest as it displays the capability to form organic products from vinylidenes using aprotic nucleophiles. The cyclic carbene then undergoes an electronic rearrangement to release a ketene intermediate. Ketenes are thermally unstable and decompose easily and are typically made *in situ*.[19] Therefore, the intermediate undergoes subsequent cyclization to afford the isoquinolone. The electronic rearrangement following

the intramolecular nucleophilic attack on the vinylidene is of specific interest, as the objective reactivity in Chapter 2 follows a similar pathway (Scheme 2.1).
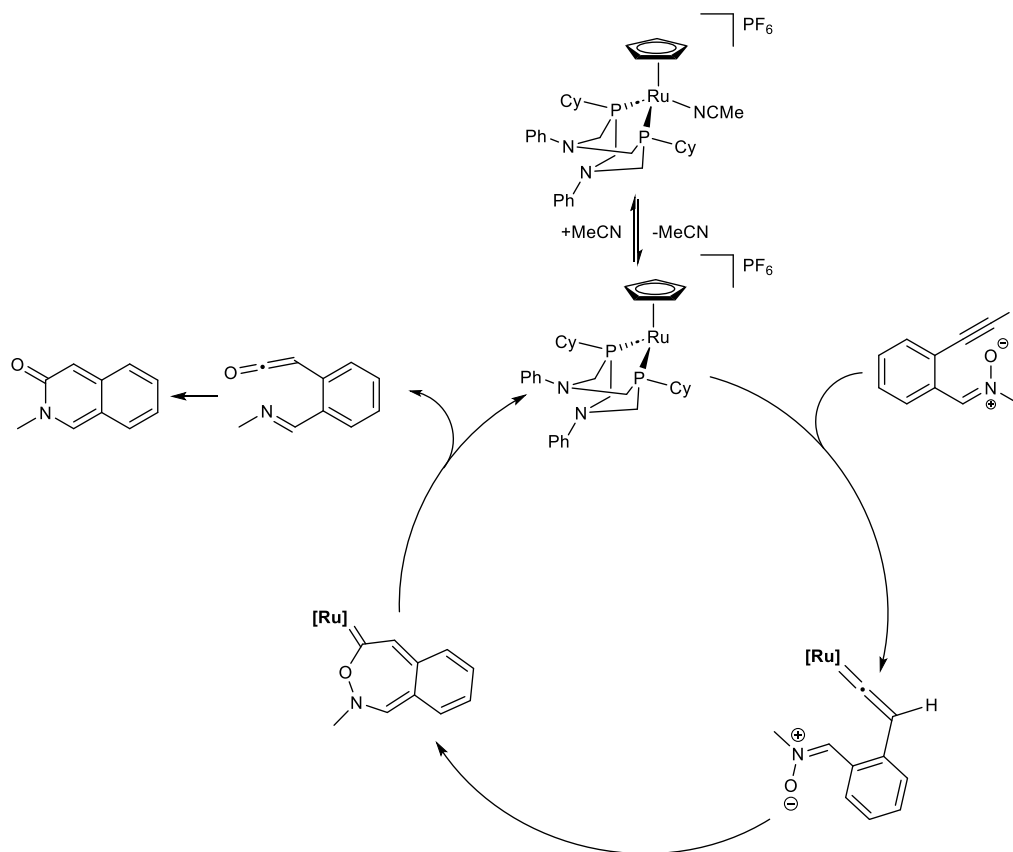
Scheme 1.10. Formation of 3(2*H*)-isoquinolone *via* metal-vinylidene followed by a cycloisomerization of ketene intermediate.[9]

1.3   Importance of Ketenimines and Their Reactivity

Ketenimines are a group of organic compounds that consist of a cumulated alkene and imine with varying substituents on each component (Figure 1.4). They are an important class of reactive species with several synthetic approaches and extensive investigation of their chemical characteristics being developed and investigated over the past two decades.[20,21]
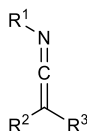
Figure 1.4. Ketenimine backbone.

1.3.1   General Reactivity of Ketenimines

Ketenimines are reactive intermediates that are susceptible to nucleophiles and electrophiles, given their resonance structures containing positive or negative charges on the N- or $C_{\alpha/\beta}$-positions (Scheme 1.11). Both the $C_\alpha=C_\beta$ and $N=C_\alpha$ bonds can participate in [n+m] cycloaddition reactions to afford cyclic and/or heterocyclic products. In addition, ketenimines with extended π-conjugation can undergo electrocyclic and sigmatropic rearrangements and their unusual reactivity has been applied to the synthesis of many complex and classically difficult-to-obtain organic compounds such as enamines, amines, and *N*-heterocycles.[20] Experimental and theoretical reports demonstrated that heteroatoms and conjugated functional groups affect the stability of ketenimines on their N- and C_β-terminus. [22] σ-Donating and π-accepting N- and C_β-substituents stabilize ketenimines which were found by plotting the stabilization energies against substituent group electronegativity.[22]
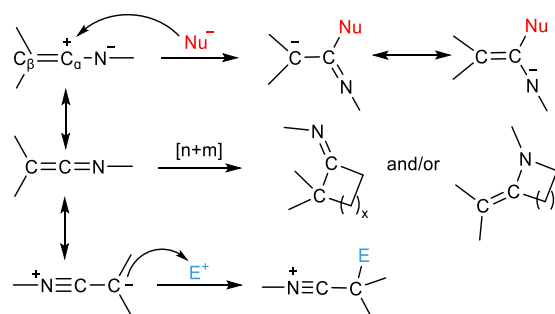
Scheme 1.11. Examples of nucleophilic, [n+m] cycloaddition, and electrophilic reactivity of ketenimines.

One of the most widely studied reactions of ketenimines involves the nucleophilic attack on the electron-deficient central carbon atom. Under such a mechanism, various

nucleophiles can react with the ketenimine to afford a series of functionalized organic compounds, such as amidines, imidates, and amides (Scheme 1.12).[20,23,24]
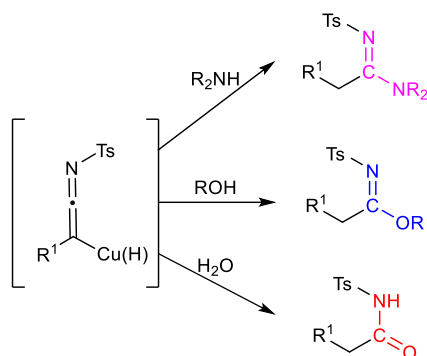
Scheme 1.12. Ketenimine reacts with amine to afford amidines, alcohol to afford imidates, and water to afford amides.[20]

1.3.2 Accessibility of *N*-Acyl Ketenimines

Absent from the discoveries and development of ketenimines is a well-formulated methodology to the corresponding *N*-acyl ketenimines. As stated above, σ-donating substituents on the *N*-terminus were found to stabilize the ketenimine. Therefore, the *N*-acyl substituent should offer resonance stability of the ketenimine allowing for isolation of a wide range of derivatives for downstream reactivity to access amides.[25,26] Methods to access isolable *N*-acyl ketenimines are reported, but they are scarce and suffer from the use of uncommon or difficult-to-obtain reagents, harsh conditions, and narrow substrate scope (Scheme 1.13).[27,28] Only two previous reports demonstrate the formation of *N*-acyl ketenimines, which were made *in situ* and reacted with nucleophiles to produce amide derivatives.[25,26] Generating isolable *N*-acyl ketenimines as well as proceeding *via* a ketenimine intermediate to access key functional groups could be a safe and efficient route to access a wide variety of amides.
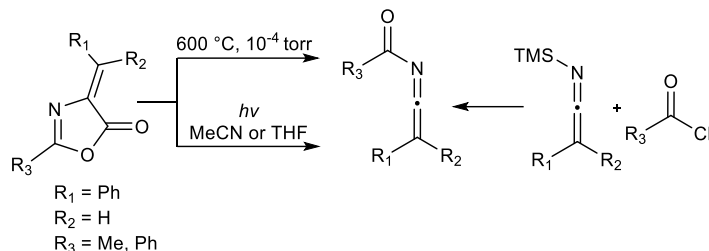
Scheme 1.13. Condensation reaction with amine after preparation of anhydride.[29]

1.3.3   Accessibility of Amides

Amide functionalities are common features in small or complex synthetic or natural molecules.[29–32] They play a crucial role in medicinal chemistry as they are present in a plethora of pharmaceuticals and make up the backbone of proteins which "facilitate virtually all biological processes".[29,30] Methods to access amides *via* ketenimine intermediates exist, however, they are restricted to a limited product scope as the ketenimines contain halogen substituents on the C_β position, and bulky alkyl groups and on the *N*-terminus that persist, limiting their scope (Scheme 1.14).[23,24,31,33–35]
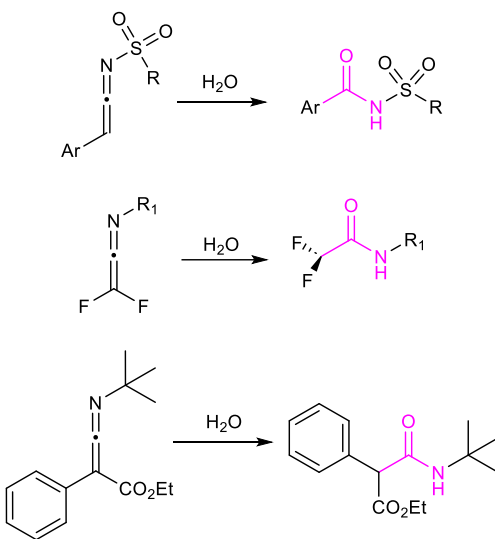
Scheme 1.14. Hydrolysis of ketenimines to access amides.[23,30,35]

Methods to access amides can involve the use of harsh chemicals and reaction conditions.[29] They can be accessed from carboxylic acid derivatives where upon heating at high temperatures, the corresponding symmetric anhydride is generated which then reacts with

an amine to afford the desired amide (Scheme 1.15). Acyl chlorides are used to react with the carboxylic acid to generate anhydrides at ambient temperatures, which then reacts with the amine, resulting in one equivalent of the desired amide, along with one equivalent of carboxylic acid (Scheme 1.15). To avoid the selectivity issue, acyl chlorides can react with ammonia, primary and/or secondary amines to generate amides.[36–38] Acyl chlorides are, however, highly flammable and toxic. Current synthetic routes to access *N*-acyl amidines usually rely on reactions of acylation of amidines with stoichiometric coupling reagents (Scheme 1.15).[39] Hexafluorophosphate azabenzotriazole tetramethyl uranium (HATU), is used, which can generate an active ester from a carboxylic acid. it is used along with *N,N*-diisopropylethylamine (DIPEA) to form amide bonds. This reaction also uses DMF, a very high boiling solvent, resulting in lengthy work-up steps, in addition to the stoichiometric amounts of waste generated from the coupling reagents.
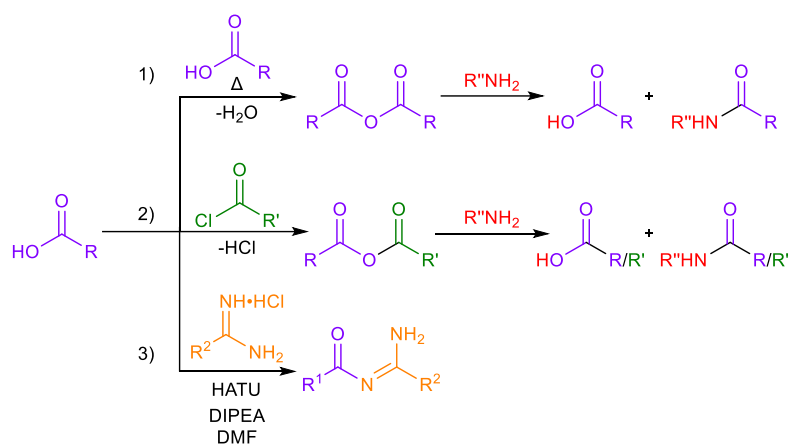
Scheme 1.15. Methods to access amides from carboxylic acids; 1) upon heating at high temperatures, the corresponding symmetric anhydride is generated which then reacts with an amine to afford the desired amide; 2) with acyl chlorides to generate anhydrides which then reacts with the amine to generate one equivalent of the desired amide e and one equivalent of carboxylic acid; and 3) with stoichiometric coupling reagents hexafluorophosphate azabenzotriazole tetramethyl uranium and *N,N*-diisopropylethylamine.

1.4   Accessibility of Dioxazolones

Dioxazolones (1,4,2-dioxazol-5-ones) are 5-membered rings containing a nitrogen at the 1-position, two oxygens at the 2- and 4- positions, a carbonyl group at the 3-position, and some substituent at the 5-position (Scheme 1.16). They can easily be prepared from a variety of their corresponding carboxylic acids which allows for alteration of the substituent at the 5-position. Upon stepwise addition of 1,1′-carbonyldiimidazole (CDI), followed by hydroxylamine hydrochloride, the carboxylic acid can be converted to the desired hydroxamic acid. This acid undergoes an addition reaction with CDI to generate the desired bench-stable dioxazolone without special precaution (Scheme 1.16).[40]
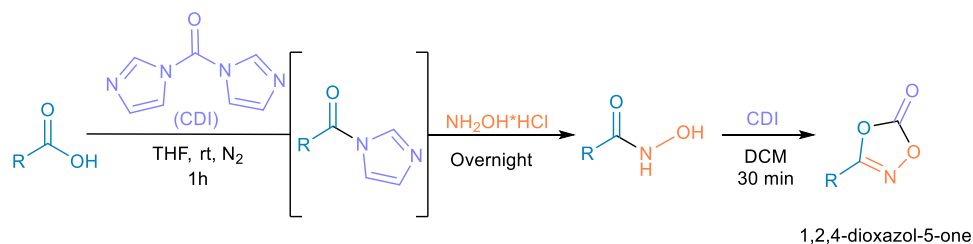
Scheme 1.16. General synthesis to access dioxazolones.

1.4.1   Dioxazolones and Nitrene Transfer Chemistry

A nitrene is classified as the nitrogen analogue of a carbene where the nitrogen is uncharged and univalent.[41] It is considered electrophilic due to its unsatisfied octet where it only has six valence electrons: two covalent and four non-bonding. Dioxazolones are a convenient class of acyl nitrene transfer reagents used for amidation reactions.[42] For example, in the metal-catalyzed directed C-H amidation of arenes, the generation of a metal nitrene occurs upon the elimination of carbon dioxide gas (Scheme 1.17).[42–44] Decarboxylative activation of the dioxazolone can result in the formation of a metal nitrene species at ambient temperature (Scheme 1.17).[42]
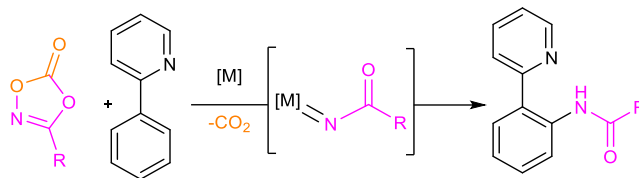
Scheme 1.17. Metal-catalyzed C-H amidation *via* nitrene intermediate. M = Co, Rh, Ir.[42]

1.4.2 Decarboxylative Decomposition of Dioxazolones

The Curtius rearrangement was discovered by Theodor Curtius, who described it as the thermal decomposition of an acyl azide to an isocyanate following the loss of N_2 (Scheme 1.18).[42] The transformation of a dioxazolone to an isocyanate occurs upon heating the dioxazolone to around 100 °C, depending on the dioxazolone used, where decarboxylative decomposition occurs. For the purpose of this thesis, this decarboxylative decomposition of the dioxazolone will be referred to as the Curtius rearrangement (Scheme 1.18). The loss of CO_2 gas drives the reaction forward entropically leaving the nitrene which decomposes to the isocyanate which can react with various nucleophiles. This Curtius rearrangement can also be favoured using a transition metal, where the intermediate metal nitrene species is released as an isocyanate (Scheme 1.18).[45]
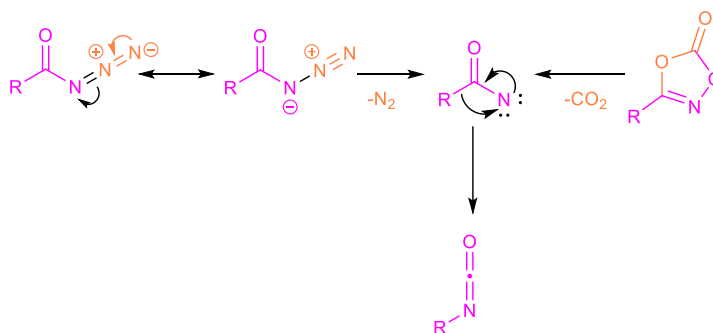
Scheme 1.18. Curtius rearrangement drawn on the left, decarboxylative decomposition of dioxazolones drawn on the right.

Fe(II) complexes have been reported to cleave N-O bonds or N-N bonds in functionalized hydroxamates and acyl azides to generate iron-nitrenoid complexes. In this example, the authors found that these Fe^{2+} complexes can undergo a Curtius-like rearrangement to generate the corresponding isocyanates to generate bisindolylmethanes (Scheme 1.19).[45]
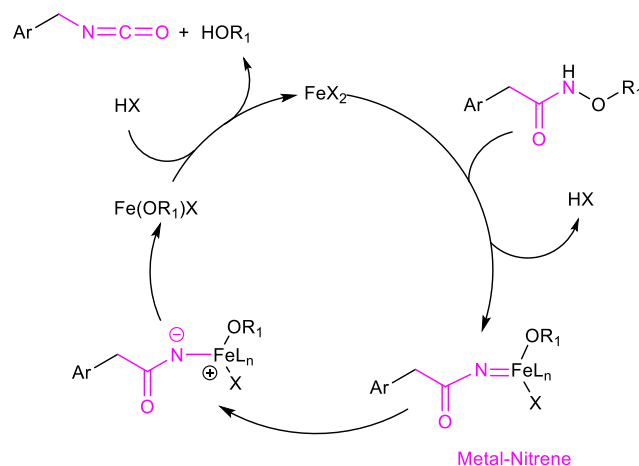
Scheme 1.19. Transition metal assisted isocyanate formation from metal-nitrene *via* Curitus-like rearrangment.[45]

1.4.3   Reactivity of Isocyanates

Isocyanates are an organic functional group made up of a carbonyl group double bonded to an amide. They are highly reactive and electrophilic, making them difficult to isolate and are typically synthesized *in-situ*. Common ways to synthesize them include the phosgenation of amines, which is hazardous to perform and requires special precautions (Figure 1.5), Curtius rearrangements (Scheme 1.18), and Lossen rearrangements (Scheme Figure 1.5). They can undergo cyclization reactions with themselves to form substituted isocyanuric acids, participate in Diels-Alder reactions where they function as dienophiles, and are susceptible to various nucleophiles (Figure 1.5).[46–49]
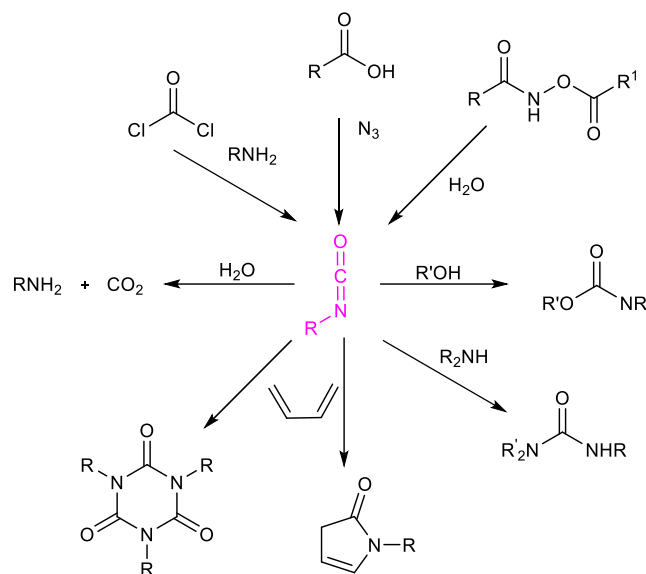
Figure 1.5. Synthesis and reactivity of isocyanates.

1.4.4   Dioxazolones and Vinylidene Reactivity

The reactivity of dioxazolones regarding nitrene transfer chemistry is thoroughly established,[42,43,50–52] however, there are no examples exploring the reactivity of dioxazolones with metal-vinylidenes. There are, however, examples where dioxazolones react with activated keteniminium ions to generate oxazole motifs (Figure 1.6).[51] Keteniminium ions are similar to vinylidenes given that they are heterocumulenes that can act as electrophiles in several organic transformations.[53] In the metal-free acid-catalyzed cycloaddition of ynamides and dioxazolones, forming polysubstituted 4-aminooxazoles, the dioxazolone acts as a nucleophile, attacking the alpha carbon on the activated keteniminium ion.[51] This intermediate then undergoes electronic rearrangement to release carbon dioxide followed by an intramolecular attack on the internal positive charge to form a 5-membered ring. This cyclic intermediate is then deprotonated to generate the desired oxazole.[51]
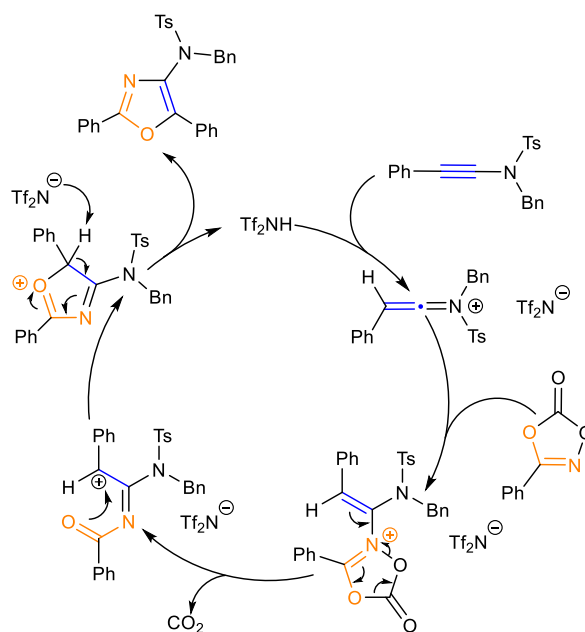
Figure 1.6. Proposed catalytic cycle for the acid-catalyzed cycloaddition of ynamides and dioxazolones *via* keteniminium ion intermediate.[51]

1.4.5   *N*-Acyl Ketenimines from Dioxazolones

In the example of the copper-catalyzed multicomponent synthesis of *N*-acyl amidines *via* acyl nitrenes, an *N*-acyl ketenimine is proposed to be generated *in-situ*. The dioxazolone forms a metal-nitrene with a copper-acetylide species. A new C-N bond is furnished, and this species is released as an *N*-acyl ketenimine. The ketenimine has an electrophilic carbon centre which reacts with diisopropylamine, a base in the reaction mixture that is required to generate the copper-acetylide species, to give a variety of *N*-acyl amidines (Scheme 1.20). [26] The reagents using in this paper are nearly identical to those used for the proposed chemistry of this thesis, differing in the catalyst and base used (Scheme 2.1). In the proposed chemistry of this thesis, all transition metal catalysts contain P_2N_2 ligands bearing basic pendant amines (Figure 1.7). If the proposed *N*-acyl ketenimine is formed, the basic amines are not likely to be a part of the final product given that they are lower in concentration in the mixture. In the chemistry using the copper catalyst, the added base, diisopropylamine, is required to generate a key intermediate, therefore must be present in stoichiometric amounts.
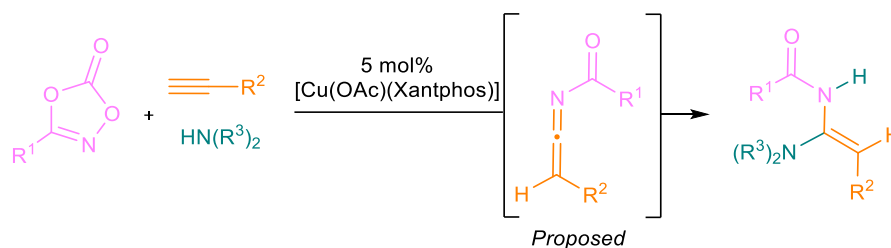
Scheme 1.20. Formation of *N*-acyl amidine *via* proposed ketenimine intermediate.[26]

1.5   Non-Coordinating Anions

A non-coordinating anion is a negatively charged species that weakly interacts with positively charged species. They are commonly found as counterions for cationic metal complexes with an unsaturated coordination sphere.[54] The coordinating ability of an anion is limited by its most basic site. The anion will always weakly coordinate by its most nucleophilic, sterically accessible moiety. Therefore, the term weakly coordinating anions (WCAs) will be used from here on out. The level of coordination of the anion relies on its structure. Using WCAs with sterically encumbered inaccessible basic sites results in lower degrees of coordination.[55] The ideal WCA should have a charge of -1 and be delocalized over the entire anion. When coordinated to a complex, WCAs should serve a minimal role, primarily acting as spectators for reactive cations while remaining intact during the course of reactivity.[56] Some WCA examples include; tetrakis(3,5-bis(trifluoro-methyl)-phenyl)-borate (BAr^{F-}), tetrafluoroborate (BF_4^-), trifluoromethan-esulfonate (OTf^-), hexafluoro phosphate (PF_6^-), and hexafluoro antimonate (SbF_6^-) (Scheme 1.21). WCAs are commonly used to study the reactivity of cationic species. They have little function other than to be spectators for reactive cations.[56] When using WCAs for charge balance on cationic catalytic species, it is proposed that the more weakly coordinated the anion, the higher the catalytic activity.
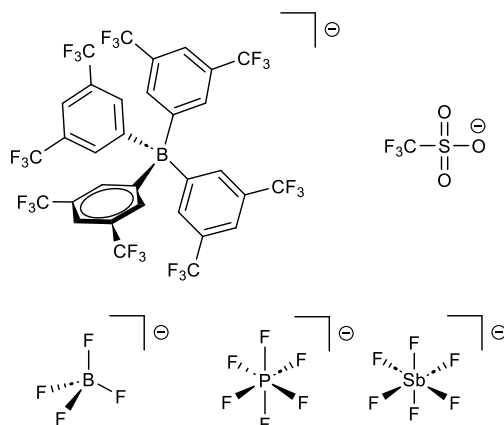
Scheme 1.21. WCA examples; BF_4^-, $BAr^F{}^-$, SbF_6^-, OTf^-, and PF_6^-.

1.5.1   Methods to Prepare Metal Complexes with WCAs

Common methods to access cationic complexes supported by WCAs are well-established. Silver salts of WCAs are commonly used as halide abstracting reagents and are commercially available with a wide variety of counter anions.[57] However, there is competitive oxidation reaction where the silver salts' oxidizing potential is highly dependent on the solvent used for the reaction in addition to them being expensive. They are also hygroscopic and photosensitive, limiting their applicability. Many other salts can be used for halide abstractions, specifically, potassium salts, which have a lower lattice energy, therefore, react less harshly.[58]
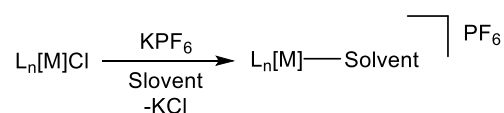
Scheme 1.22. General halide abstraction reaction.

1.5.2   Effects on Catalysis Using Different WCAs

Many studies have been performed evaluating the effects the WCAs have on cationic metal complexes for catalytic transformations. The intermolecular alkoxylation of 3-hexyne with MeOH using cationic gold(I) catalysts with different WCAs has been explored.[59] This transformation was studied using an *N*-heterocyclic carbene-based gold catalyst stabilized by various anions; $BAr^F{}^-$, BF_4^-, OTf^-, *p*-toluensolfonate (OTs^-), trifluoroacetate (TFA^-

) and acetate (OAc⁻). The trends in turnover frequencies (TOF) values did not reflect the coordinating power of the anions. The key step in the reaction is the catalyst's ability to abstract a proton from methanol during a nucleophilic attack which is linked directly to the anion's basicity. The catalytic performance is compromised when the anion exhibits higher coordination power or basicity, as it hinders alkyne coordination and leads to the excessive generation of free methoxide, thereby poisoning the catalyst. OTs⁻ was found to be the best anion for this catalytic transformation. The pre-equilibrium with this anion is shifted toward the outer sphere ion pair (OSIP). Prevention of catalyst deactivation to a gold–methoxide is achieved, with its distinctive basicity facilitating the nucleophilic attack. The intermediate coordinating power and basicity of the OTs⁻ anion provides the best compromise to achieve efficient catalysis.
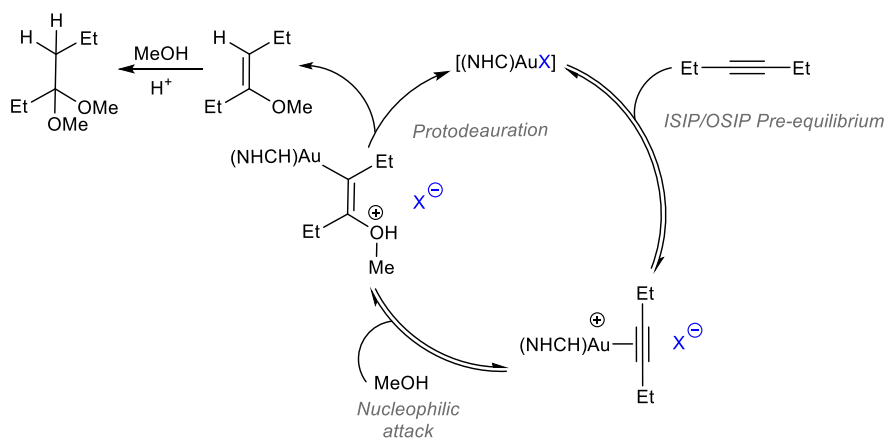
Scheme 1.23. Intermolecular alkoxylation of alkynes using cationic gold(I) catalysts with different WCAs (X).[59]

Over the last two decades, observations have indicated that in complexes where the counterion assumes a spectator role, the presence of larger, less coordinating counterions has positively influenced catalytic efficiency.[60,61] Iridium(I) *N*-heterocyclic carbene-phosphine complexes have been used to perform hydrogen isotope exchange (HIE) processes.[62] In this paper, the authors looked at using PF_6^-, BF_4^-, OTf⁻, and BArF⁻ as counterions for their iridium complexes. Application of these complexes as catalysts in hydrogen isotope exchange has demonstrated improved catalytic activity at lower catalyst loadings in the order X = BArF⁻ ≈ OTf⁻ > PF_6^- > BF_4^-. This does not follow the expected

trend of larger, therefore, less coordinating, indicating that this trend does not apply to all systems. Despite ongoing investigations, a comprehensive understanding of the roles WCA plays in reactions is required.
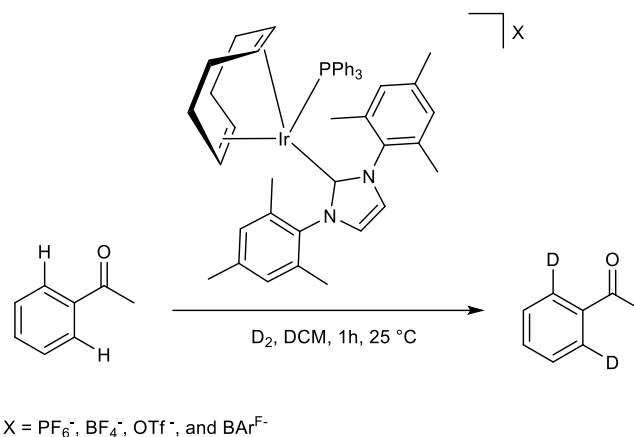
Scheme 1.24. HIE of acetophenone using iridium(I) *N*-heterocyclic carbene-phosphine complexes and different WCAs.

1.6   Project Scope

In this project, various MLC complexes will be used to investigate their capabilities to form metal-vinylidenes and explore their catalytic potentials. First, the reactivity of dioxazolones will be exploited towards the goal of forming a variety of *N*-acyl ketenimines using five different MLC complexes (Figure 1.7). The Blacquiere group has previously reported catalysts that undergo the first step of the catalytic cycle, in intramolecular alkyne hydroamination and hydroalkoxylation catalysis. Five previously reported Fe or Ru catalysts will be used (**Fe-1**, **Fe-2**, **Ru-1**, **Ru-2**, **Ru-3**), that differ in the tunable $P^R_2N^{R'}_2$ ligands, and the Cp/Cp*. Two iron-based catalysts were chosen for this reactivity due to the presence of a cheap, earth-abundant metal centre, combined with tunable $P^R_2N^{R'}_2$ ligands, specifically designed for proton-shuttling. The two basic pendant amines can reversibly shuttle protons to and from the metal centre during vinylidene formation which is a key step of the proposed catalytic cycle. The ruthenium-based catalysts were selected due to their increased stability and greater performance regarding functionalization reactions.[3,17,18] Further efforts have been focused on measuring the rate of formation of metal-vinylidenes with **Ru-3**, **Ru-4**, and different terminal alkynes. The

hydrofunctionalization of 2-ethynylbenzylalcohol and 2-ethynylaniline derivatives using MLC complexes has been extensively explored by the Blacquiere group.[3,8,9,17,18] The use of additives for these reactions is avoided to ensure high atom economy and simple purification of products. It has not yet been investigated if the addition of alkali salts has any effect on these reactions. Other anions have not been used for these complexes. It is unknown whether the $PF_6{}^-$ anion is the most weakly coordinating anion to use for the highest catalytic conversions. In this section, an *in-situ* halide abstraction will be performed on complex **Ru-5** to generate various MLC complexes with different anions to see if changing the counterion affects the hydroalkoxylation of 2-EBA to isochromene.
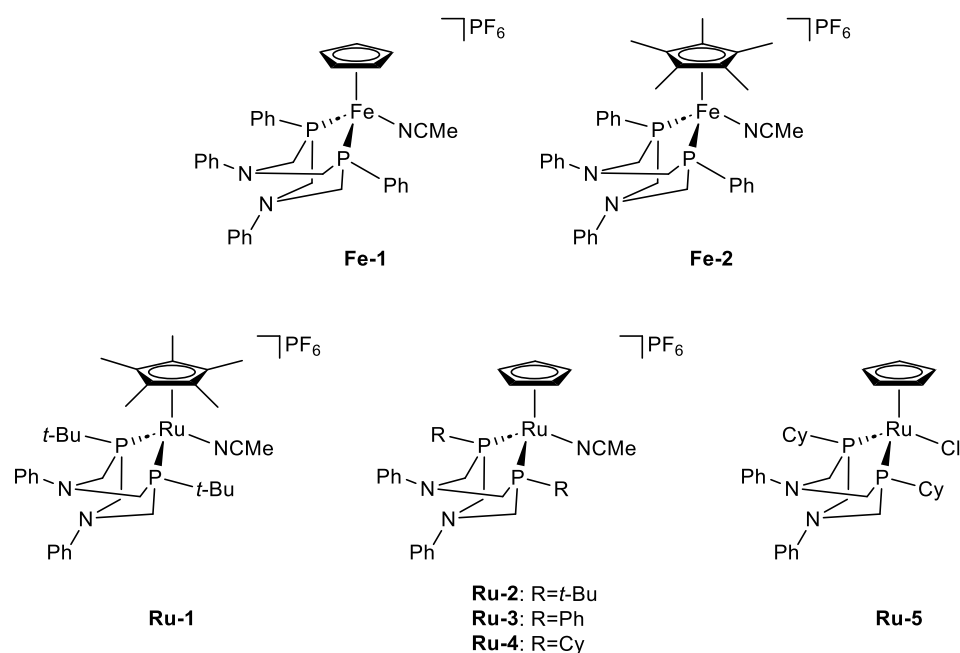
Figure 1.7. MLC complexes used throughout this study.

Chapter 2

2   Overview

The proposed catalytic approach for accessing *N*-acyl ketenimines from dioxazolones relies on the hypothetical catalytic cycle below (Figure 2.1). The first step, which involves the formation of a metal-vinylidene with terminal alkynes, is well established.[14] Upon the formation of the vinylidene, the dioxazolone then acts as a nucleophile, resulting in addition to the electron-poor C_α of the vinylidene, a reactivity not yet observed for dioxazolones. This intermediate will then undergo electronic rearrangement to release carbon dioxide and the desired *N*-acyl ketenimine product.
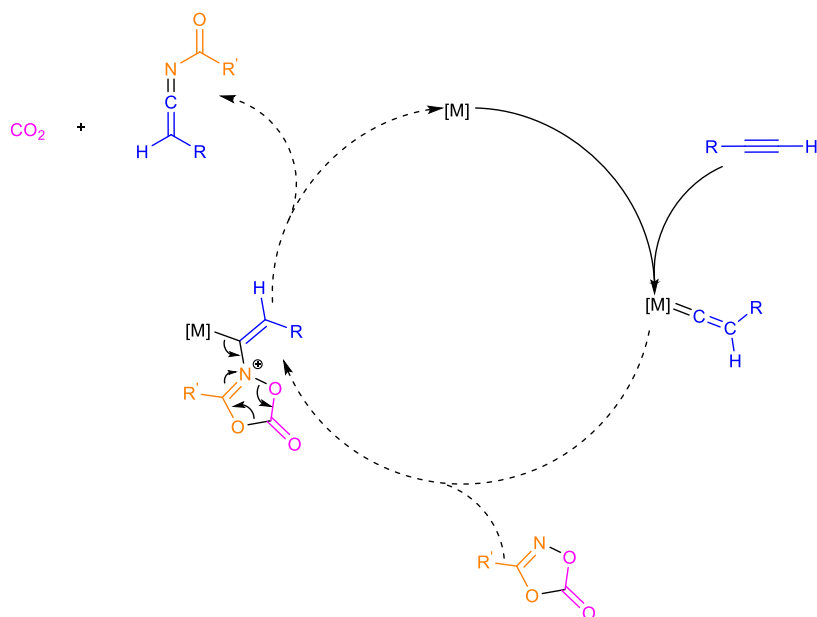
Scheme 2.1. Proposed catalytic cycle for targeted reactivity.

2.1 Dioxazolone Synthesis

Dioxazolone **1a** was synthesized according to reported procedures.[40] The two-step synthesis began with converting benzenepropanoic acid to the corresponding hydroxamic acid using carbonyldiimadazole (CDI) followed by reaction with hydroxylamine hydrocholoride to afford *N*-hydroxy-benzenepropanamide, *via* a hydroxylamine intermediate.[63] The crude hydroxylamine product was treated with additional CDI, and

reactant consumption was monitored by TLC. Purification by recrystallization in hexanes afforded the desired product, consistent with evidence from the reported ^{1}H NMR spectroscopic data. [63]
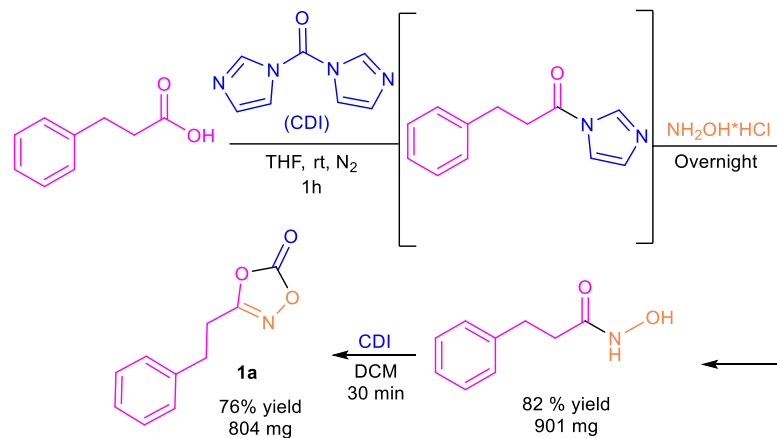
Scheme 2.2. Synthesis of dioxazolone **1a**.

Phenyl-substituted dioxazolone **1b** was synthesized using the same procedure as above, using benzoic acid. The desired product was formed in 71% overall yield, and the ^{1}H NMR spectroscopic signals were consistent with literature reports.[63]
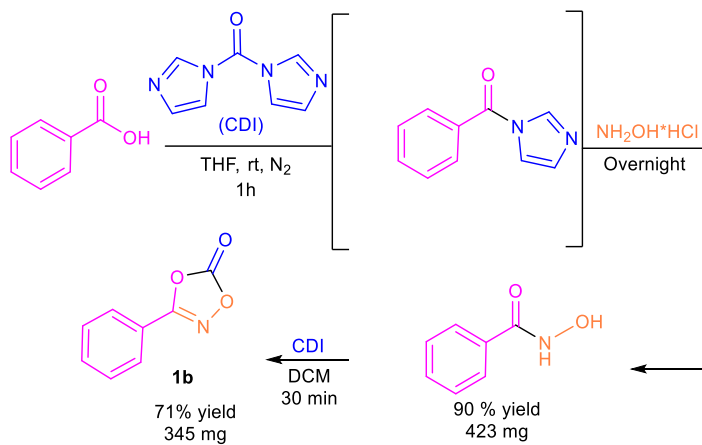
Scheme 2.3. Synthesis of dioxazolone **1b**.

2.2 Attempts to form *N*-Acyl Ketenimines Using MLC Vinylidene Complexes and **1a**.

The proposed reactivity in Figure 2.1 is novel to the Blacquiere group herein that the intermolecular reactivity of metal-vinylidenes and nucleophiles has not yet been explored. In this section, attempts at forming these *N*-acyl ketenimines are the main focus where the nucleophilic reactivity between dioxazolones and metal-vinylidenes will be explored both catalytically and stoichiometrically.

2.2.1 Stoichiometric Reactions Between MLC Vinylidenes and **1a**

Scheme 2.3 shows the proposed stoichiometric reaction between all five MLC complexes and **1a**. Dioxazolone **1a** was selected for experimentation because of its ethylene hydrogens that appear as two diagnostic triplets at approximately 3 ppm in the ^{1}H NMR spectrum. If two new triplets of different chemical shifts are observed this would clearly indicate formation of a new product. The proposed catalytic cycle involved the intermolecular attack of the dioxazolone on the electron-poor C_α of the metal-vinylidene. To determine if the desired *N*-acyl ketenimine is formed from this step, stoichiometric reactions between the dioxazolone and vinylidene complexes were tested. The same procedure for all five complexes was performed; a 1:1 mixture of the metal complex and alkyne **2a** were dissolved in anisole and stirred 2 h at 110 °C. Full conversion of the acetonitrile complex to the vinylidene was observed by ^{31}P{^{1}H} NMR spectroscopy for all complexes. Once one equivalent of **1a** was added, only the reaction with vinylidene complex $[Ru(Cp)(P^{Ph}_2N^{Ph}_2)(=C=CPhH)]PF_6$ (**V-5**) synthesized by **Ru-3** and **2a** resulted in full conversion back to the acetonitrile complex. Therefore, it was determined that a less electron-rich metal centre was required. The product from this reaction was not able to be isolated, therefore, these conditions proved unsuccessful.
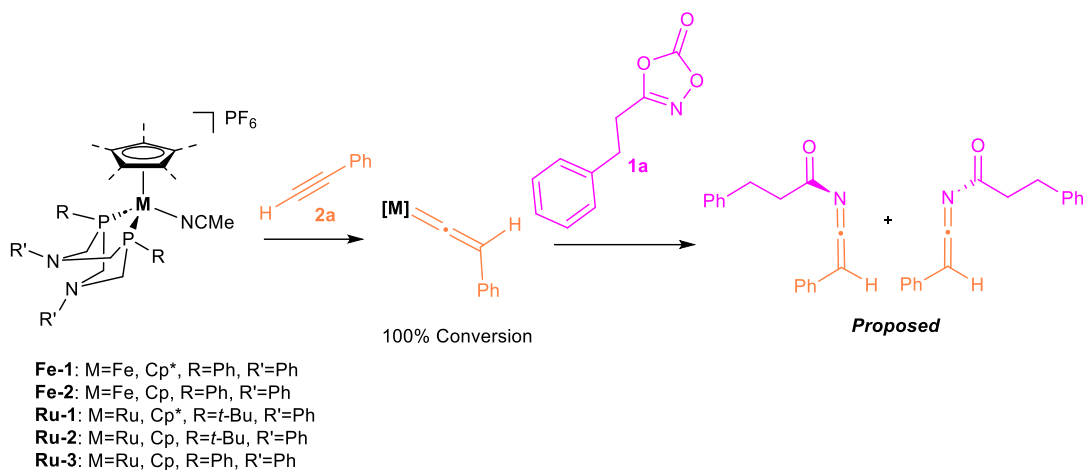
Scheme 2.4. Formation of vinylidene with **2a** and all five MLC complexes followed by proposed reactivity between **1a** and metal-vinylidene to form the desired *N*-acyl ketenimine.

A 1:1.5 mixture of **Ru-3** and alkyne **2a** was dissolved in anisole and stirred 2 h at 110 °C (Scheme 2.4). 1.5 equivalents of **2a** was selected to ensure **Ru-3** was completely consumed, as to avoid side reactivity with **1a**. Full conversion of the acetonitrile complex **Ru-3** to the vinylidene **V-5** was observed by ^{31}P{^{1}H} NMR spectroscopy where the **Ru-3** chemical shift was observed at 38.7 ppm and **V-5** complex was observed at 37.4 ppm (Figure 2.2). In addition, a distinct colour change from yellow to reddish-orange was observed. Subsequently, 1 equivalent of dioxazolone **1a** was added to the mixture and the reaction was heated at 70 °C for an additional 16 h. It was proposed that once **1a** reacts with **V-5**, **Ru-3** was expected to regenerate. It is important to note that the alkyne reagent was in excess, therefore, the remaining 0.5 equivalents of unreacted **2a** can re-form complex **V-5** *via* reaction with **Ru-3**, which was observed by ^{31}P{^{1}H} NMR spectroscopy. A 1:2 ratio of the acetonitrile complex and its vinylidene were expected to be formed after this reaction. Rather, a 1:1 ratio of vinylidene complex relative to the starting metal complex was observed, along with some unknown byproduct at 38.9 ppm (Figure 2.2).
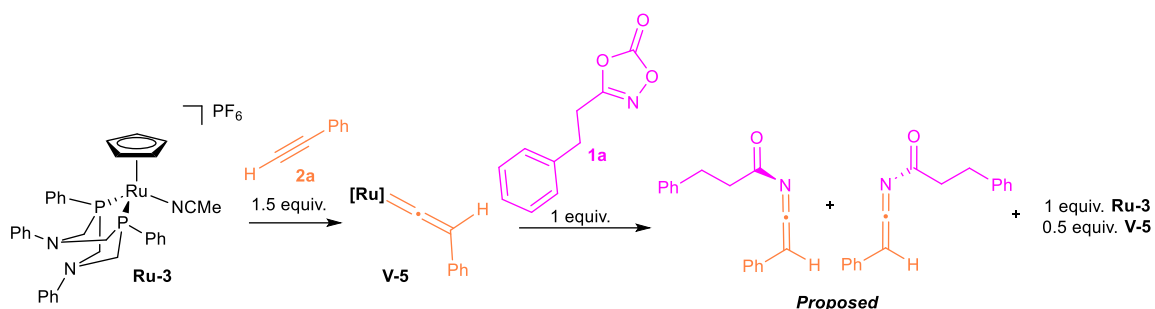
Scheme 2.5. Formation of vinylidene **V-5** *via* 1:1.5 mixture of **Ru-3** and **2a** followed by proposed reactivity between **1a** and **V-5** to form the desired *N*-acyl ketenimine.
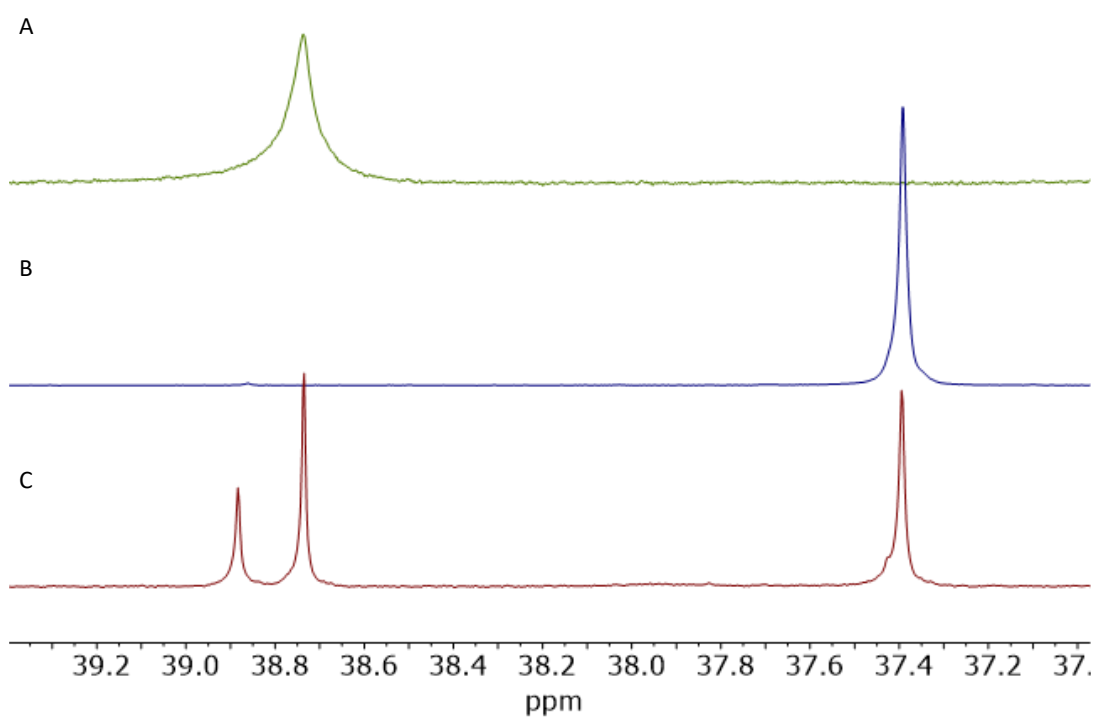
Figure 2.1. ^{31}P{^{1}H} NMR spectra (600 MHz, anisole) of A) **Ru-3**; B) 1:1.5 mixture of **Ru-3** and **2a** heated at 110 °C for 2 h to give *in situ* formation of **V-5**; and C) 1 equivalent of **1a** added to B and left to stir for 16 h at 70 °C.

The solvent was removed under an inert atmosphere, and the organic products were collected by washing the dried crude material with diethyl ether. Two new sets of triplets, in different locations from the dioxazolone starting material, were observed in the product

obtained from the organic wash. X as the major product with triplets at 2.94 and 2.48 ppm, and minor product Z with triplets at 3.55 and 2.90 ppm, in a 2:1 ratio (Figure 2.3). Based on the integrations and multiplicities, these sets of peaks are likely two different products representing the hydrogens of the CH_2CH_2Ph linker connecting the dioxazolone backbone to the aromatic ring.
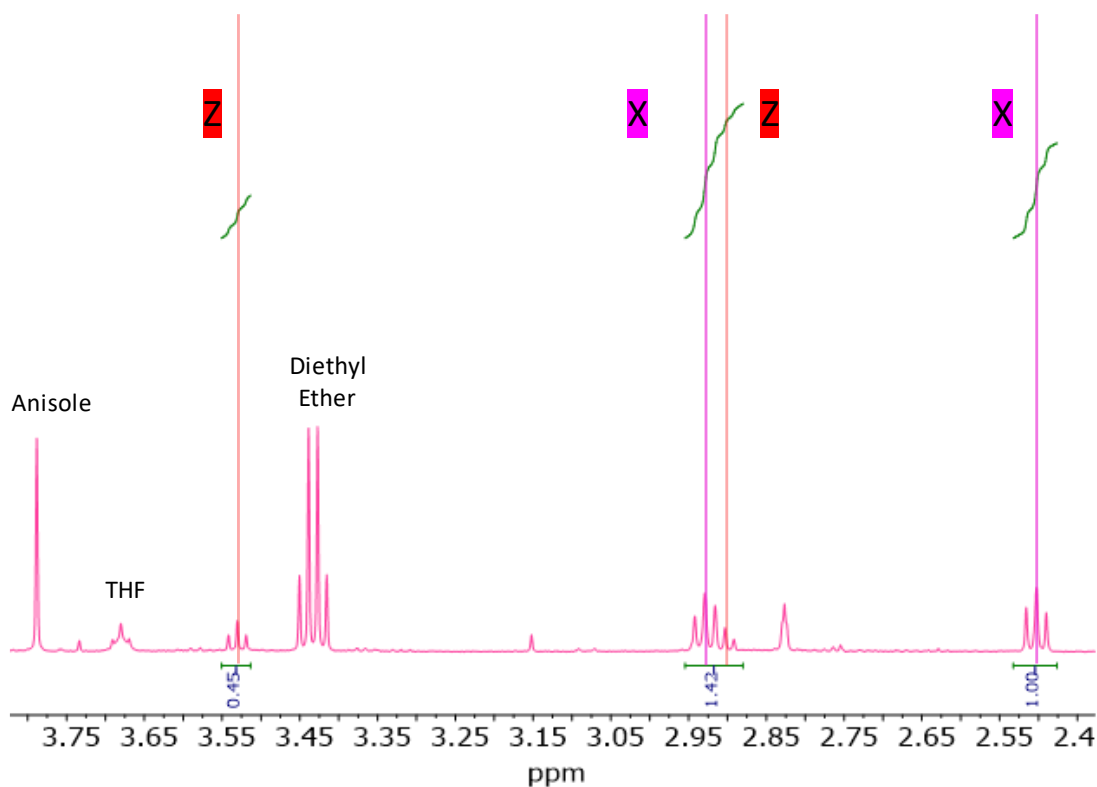
Figure 2.2. ^{1}H NMR spectrum (600 MHz, CD_2Cl_2) of organic ether wash from the 1:1.5:1 mixture of **1a**, **2a** and **Ru-3** dissolved in anisole and heated at 70 °C for 24 h.

A control reaction was performed with a 1:1 ratio of dioxazolone **1a** and **Ru-3**. The metal complex and dioxazolone were dissolved in anisole and heated at 70 °C for 24 h. The reaction mixture was concentrated *in vacuo* and the product was extracted from the residue with diethyl ether. The filtrate was then dried *in vacuo* to afford the final product. ^{1}H NMR spectroscopic analysis in CD_2Cl_2, revealed the formation of two sets of triplets in a 2:1 ratio: X, as was previously observed as the minor product; and Y, as the major product of this reaction. All three reagents of the stoichiometric reaction were required to form product Z. Products X and Y were both formed when **2a** was absent from the reaction

mixture. Product X was formed in both reactions, which was most likely a side product from the reaction of **1a** and **Ru-3**. Importantly, no signals were observed in the $^{31}P\{^{1}H\}$ NMR spectra of these samples.
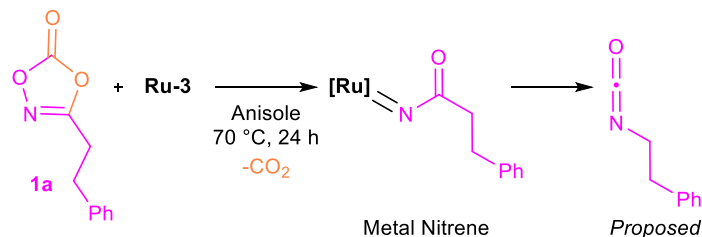
Scheme 2.6. Proposed product from the stoichiometric reaction of **1a** and **Ru-3** at 70 °C for 24 h.
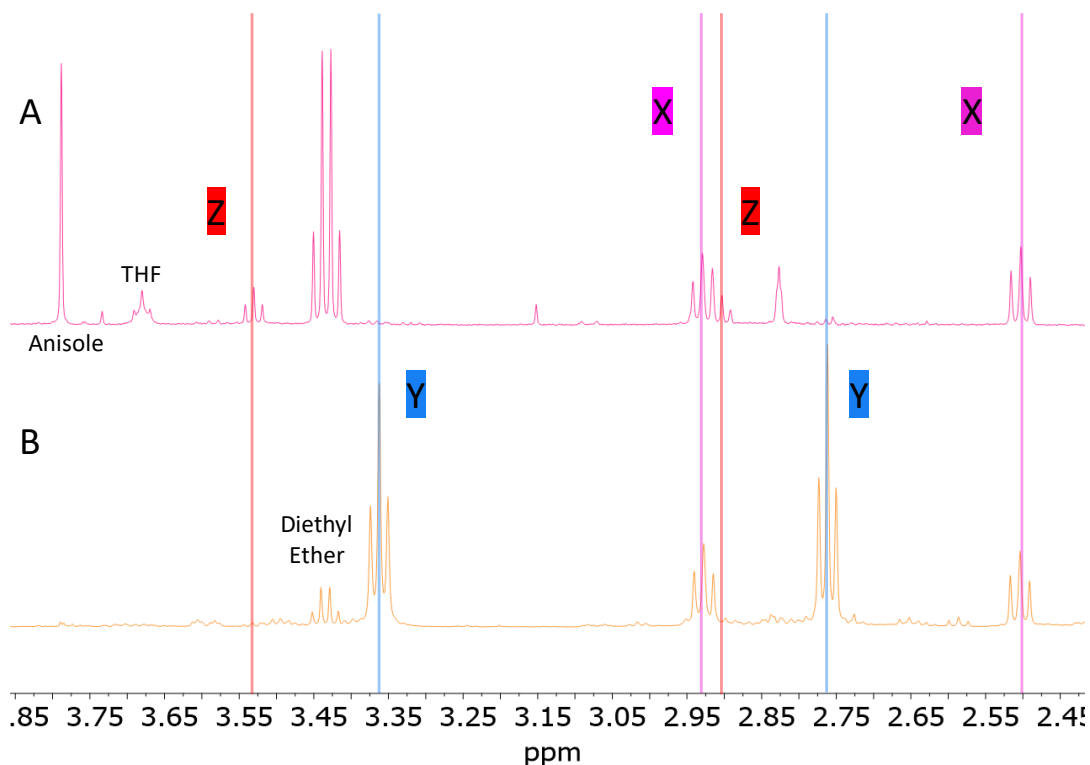
Figure 2.3. ^{1}H NMR spectra (600 MHz, CD_2Cl_2) of organic ether wash from the reactions dissolved in anisole and heated at 70 °C for 24 h: A) 1:1.5:1 mixture of **1a**, **2a** and **Ru-3**; and B) 1:1 **1a** and **Ru-3**.

Initial test reactions were done on a milligram scale to conserve the metal complex. However, to fully identify and characterize the products being formed, reaction scale-up was necessary. Subsequent efforts were focused on the catalytic reactivity between **Ru-3**, **1a**, and **2a** to scale up the reaction.

2.2.2   Catalytic Reactions with **Ru-3**, **1a** and **2a**

Catalytic reactions were performed by combining 1:1 mixture of **1a** and **2a** with 5 mol% of **Ru-3**. The reaction was heated at 70 °C for 24 h and a workup was required to remove the catalyst. The anisole was removed *in vacuo*, and the residue was washed with diethyl ether to collect the organic products. The diethyl ether was then removed *in vacuo* and a ^{1}H NMR spectrum was collected of the reaction mixture in CD_2Cl_2. The spectrum, and corresponding TLC analysis, both indicated the presence of several species, requiring separation by chromatography. A mixture of two of the products, X and Y, was isolated, and the sample was analyzed by ^{1}H NMR spectroscopy. The other products were not able to be isolated by column chromatography due to incompatibility, and subsequent decomposition on silica, as indicated by the ^{1}H NMR spectra acquired from the later fractions collected. The ^{1}H NMR spectrum of the isolated product showed two triplets that were consistent with compound X, in addition to their integrations matching to each other. Two additional peaks were observed: one triplet that has the same chemical shift as a previously observed triplet at 2.76 for product Y, and a complex multiplet that overlapped with a previously observed triplet at 3.36 ppm for product Y. These new peaks showed a similar pattern of integration when compared to previous experiments, suggesting they belong to the same molecule. Furthermore, the crude mixture was deemed to not contain the *N*-acyl ketenimine due to lack of diagnostic signals in both the IR, where a peak at 2000 cm^{-1} is expected, and ^{1}H NMR spectra, where the proton on C_β is expected to have a chemical shift of *ca.* 5 ppm.[64,65] X is proposed to be the product of a reaction between only **1a** and **Ru-3** but was not isolated for full characterization.
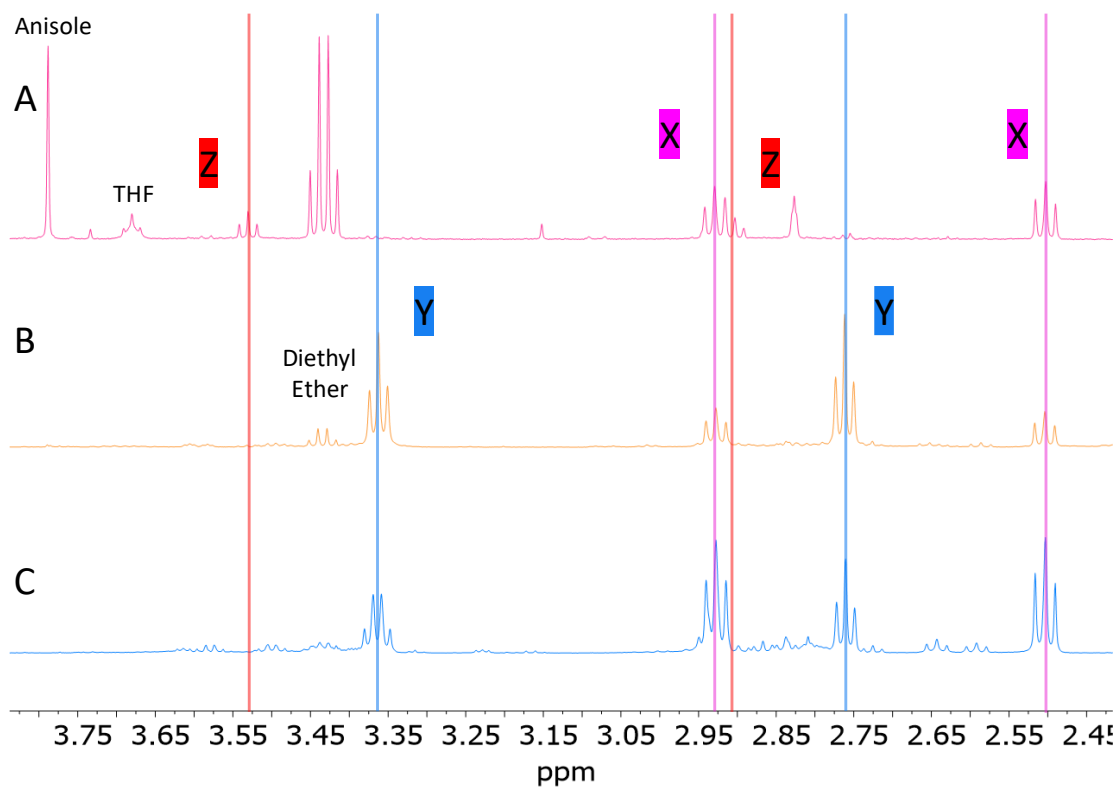
Figure 2.4. ^{1}H NMR spectra (600 MHz, CD$_2$Cl$_2$) of organic ether wash from the reactions dissolved in anisole and heated at 70 °C for 24 h: A) 1:1.5:1 mixture of **1a**, **2a** and **Ru-3**; B) 1:1 **1a** and **Ru-3**; and C) Isolated crude mixture post column from catalytic reaction of a 1:1 mixture of **1a** and **2a** with 5 mol% of **Ru-3**.
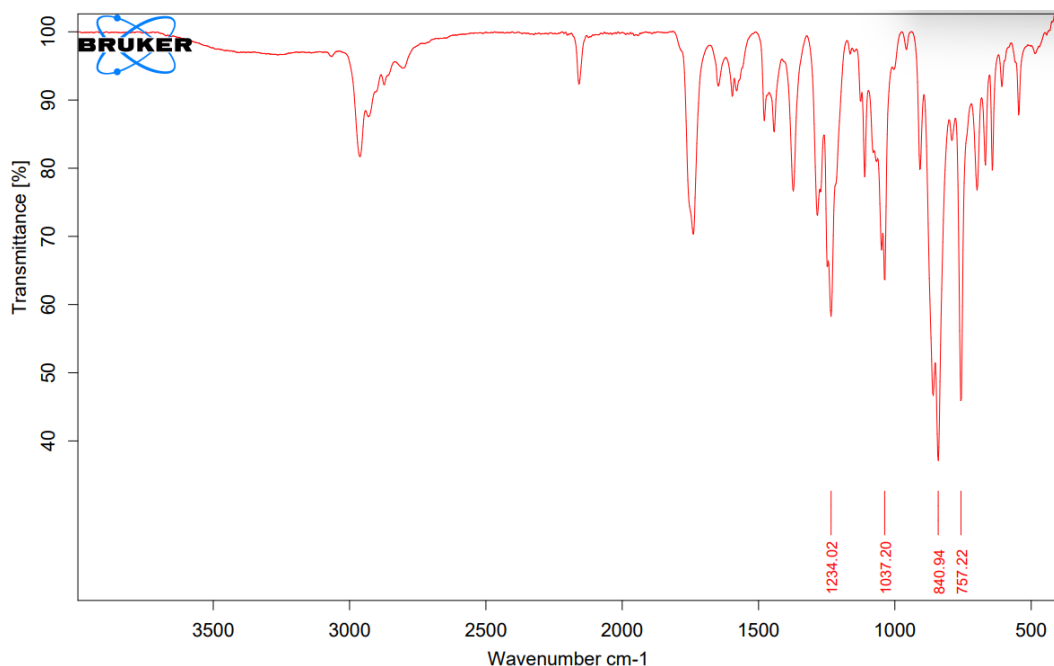
Figure 2.5. IR spectra of isolated crude mixture post column from the catalytic reaction of a 1:1 mixture of **1a** and **2a** with 5 mol% of **Ru-3**.

2.3 Trapping Reactive Intermediates with Various Species

As evident from Figure 2.5C with the plethora of minor products in the baseline of the ^{1}H NMR spectrum, many different products are being formed in the catalytic reaction between **Ru-3**, **1a**, and **2a**. Several distinct products were seen to be formed but proved difficult to isolate due to low yields and rapid decomposition. There are many different possible reaction pathways between the dioxazolone and MLC complex. In this section, various trapping agents were used to isolate the major product of reaction between **1a** and **Ru-3** to determine the reaction pathway.

2.3.1 Product Trapping with Diisopropylamine and Water

It was proposed that if an *N*-acyl ketenimine was made, it may subsequently react with another equivalent of dioxazolone or terminal alkyne in the mixture. Bruin *et. al.* reported the proposed insertion of an acyl nitrene from a dioxazolone into a Cu-C acetylide bond. Subsequent C-N bond formation occurred to liberate an *N*-acyl ketenimine. This proposed

mechanism was supported by DFT calculations.[26] Diisopropylamine was a required additive in this reported reaction to form the active copper-acetylide species in the catalytic cycle. Diisopropylamine subsequently reacted with the ketenimine intermediate to afford *N*-acyl amidine products (Scheme 2.5).[26]
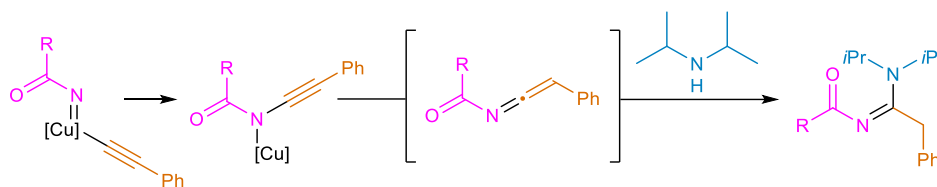
Scheme 2.7. Formation of *N*-acyl amidine *via* proposed *N*-acyl ketenimine intermediate.[26]

Control experiments without copper resulted in the formation of *N,N*-diisopropyl-*N'*-phenethylurea after 10 h, through the reaction of dioxazolone and diisopropylamine at room temperature (Scheme 2.6). The dioxazolone was shown to undergo decarboxylative decomposition, through a Curtius rearrangement, affording a highly reactive isocyanate intermediate accompanied by the loss of CO_2. This reactive isocyanate is unstable and reacted with the diisopropylamine to afford the *N,N*-diisopropyl-*N'*-phenethylurea as the product.[26]
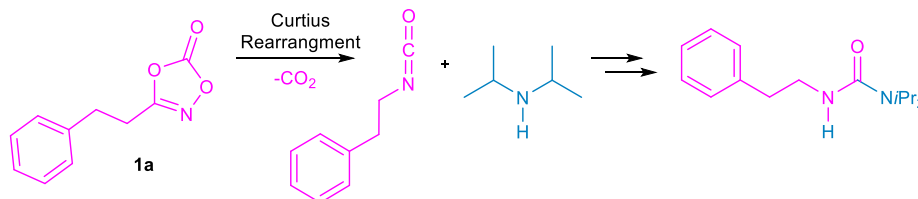
Scheme 2.8. Control reaction between dioxazolone and diisopropylamine to form of *N,N*-diisopropyl-*N'*-phenethylurea after 10 h at room temperature.

To determine if the product made through catalysis with substrates **1a**, **2a**, and 5 mol% of **Ru-3** was an *N*-acyl ketenimine, diisopropylamine was employed as a trapping agent. If the proposed *N*-acyl ketenimine was formed during catalysis, the amine would trap the product and form the corresponding *N*-acyl amidine (Scheme 2.7).[26] 1 equivalent of **1a** and **2a** along with 10 equivalents of diisopropylamine were combined in anisole. 5 mol% of **Ru-3** was added to the mixture and left to stir for 24 h at 70 °C. Elevated temperatures

were required to form the vinylidene in the proposed catalytic cycle. Upon working up the reaction mixture, it was determined that the product of the reaction was *N,N*-diisopropyl-*N'*-phenethylurea, confirmed by [^1]H NMR spectroscopic data consistent with literature reports.[26] Dioxazolones are known to decompose to isocyanates at room temperature with diisopropylamine present.[42,52] At elevated temperatures, dioxazolone decomposition would occur more readily, causing the unwanted formation of urea byproducts. The instability of dioxazolone under the conditions needed to form the vinylidene required the use of a different trapping agent than diisopropylamine.
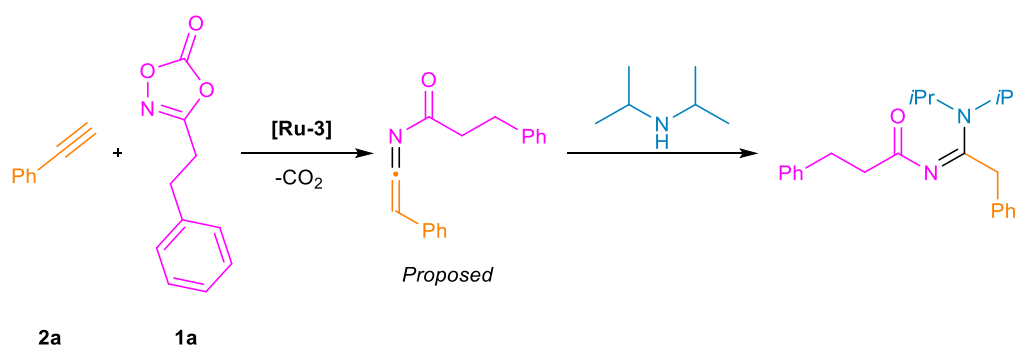
Scheme 2.9. Expected reactivity between amine and proposed *N*-acyl ketenimine.

The same type of reactivity was observed when using water instead amine trapping reagents, where *N*-(2-phenylethyl)carbamic acid was observed as the product, confirmed by [^1]H NMR spectroscopy matching that of literature reports.[66] It was later discovered that substrate **1a** was reacting catalytically with **Ru-3** in the same fashion with or without the presence of **2a** in the mixture. It is hypothesized that the dioxazolone and catalyst form a metal nitrene, which can then react in two different fashions. The formed metal nitrene intermediate can either undergo electron rearrangement to afford an isocyanate or have a nucleophilic species present in the mixture attack the nitrene affording unwanted side products (Scheme 2.8).[67,68] Attack on the metal-nitrene is the desired pathway since the isocyanate product can be generated without the need for a transition metal catalyst.
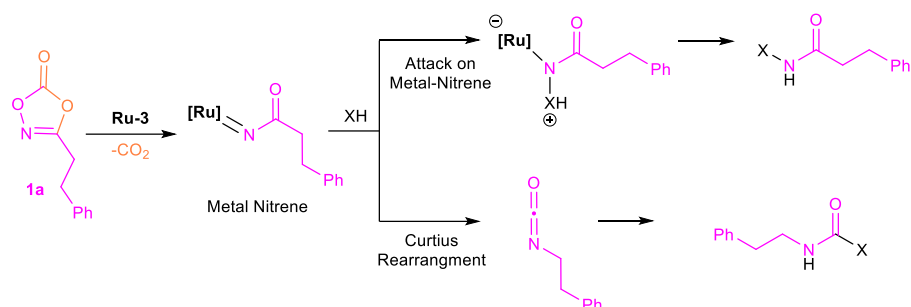
Scheme 2.10. Possible reactivity pathways for **1a** and **Ru-3** with trapping agent XH.

2.3.2 Control Reactions of **1a** and Trapping Agents

Diisopropylamine and water were ineffective reactants to bias the chemistry of a proposed Ru-nitrene intermediate to nitrene transfer chemistry, rather than isocyanate release. It was unclear from the previous reactions if the dioxazolone was simply decomposing and reacting with the additive or if the catalyst was promoting isocyanate formation. In this section, various molecules that do not react with the dioxazolone under standard catalytic conditions were employed as intermediate trapping reagents between the dioxazolone and **Ru-3**. Multiple screening tests were performed with a variety of reagents to probe the reactivity of **1a** with each trapping reagent with absence of the catalyst (Scheme 2.9). 1-butyric acid, 4-acetamidobenzene sulfonylazide, and 2,3-dimethyl-1,3-butadiene all demonstrated consumption of **1a** greater than 20% and thus would not allow for a clean reaction for identification of the 'trapped' product (Figure 2.7). It was found that 3-methyl-1-butanol, 1,2,4-triazole, 4-phenyl-1,2-triazoline-3,5-dione, and TMS-azide demonstrated less than 20% conversion of the dioxazolone to a new unknown species. This negligible amount of conversion would allow for use of these reagents to trap the products formed under catalytic conditions without any other competitive side reactivity.
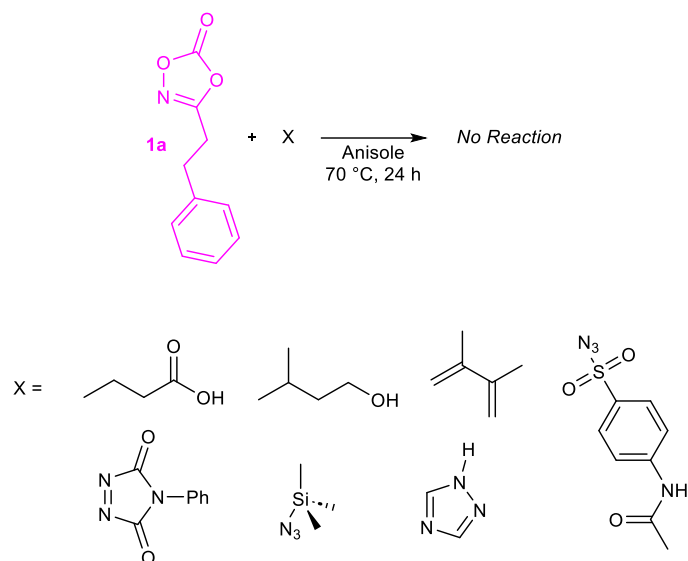
Scheme 2.11. Control reaction with dioxazolone **1a** and various trapping agent candidates. Dioxazolone is proposed to remain intact.
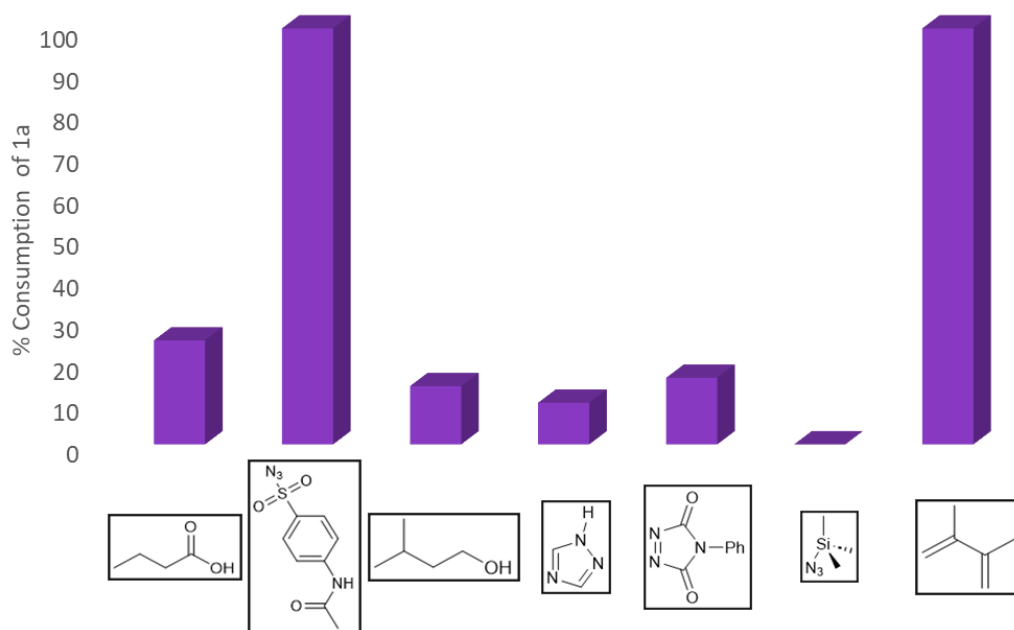
Figure 2.6. Percent consumption of **1a** after reaction with various trapping agents heated in anisole at 70 °C for 24 h.

2.3.3   Trapping Product of Catalytic Reaction of **1a** and **Ru-3**

Catalytic reactions were performed with **1a**, an excess of 3-methyl-1-butanol, 1,2,4-triazole, 4-phenyl-1,2-triazoline-3,5-dione, or TMS-azide, and 5 mol% of **Ru-3**. Reaction mixtures upon testing 3-methyl-1-butanol, 4-phenyl-1,2-triazoline-3,5-dione, or TMS-azide all resulted in a complex mixture of products in ^{1}H NMR spectra. Reaction of **1a** with excess 1,2,4-triazole and 5 mol% of **Ru-3** resulted in complete consumption of **1a** with the generation of what appeared to be one product. Purification *via* column chromatography was performed in order to obtain clean sample. The organic products of the reaction were separated from the catalyst and attempts at isolation of the major species from minor side products were performed. The proposed product was expected to result from either the reaction between a metal nitrene and the trapping agent or the reaction between the isocyanate byproduct and trapping agent both having the chemical formula $C_{11}H_{12}N_4O$ and expected molecular weight of 216 g/mol.
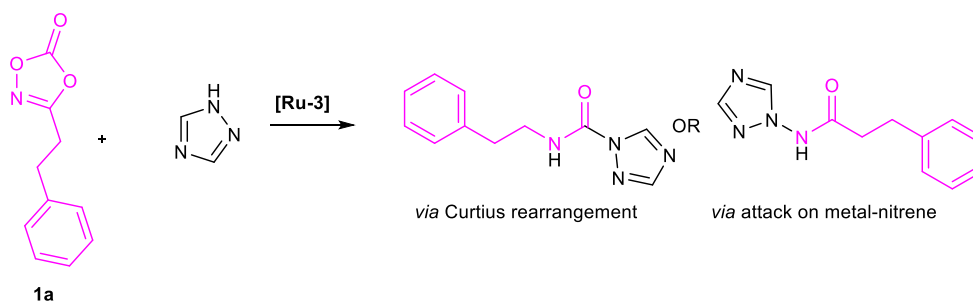
Figure 2.7. Proposed reaction products for reaction of **1a** and trapping agent 1,2,4-triazole using 5 mol% of **Ru-3**.

EI-MS data was collected of the material, which did not indicate formation of the proposed product. There are no major peaks at 217 *m/z*, representative of the proposed $[M+H]^+$ product. In addition, if catalyst remained in the sample, it would be expected to give a major signal at 662 *m/z* for the ruthenium cation, which was not present. Thus, further investigation into what product is formed was required.
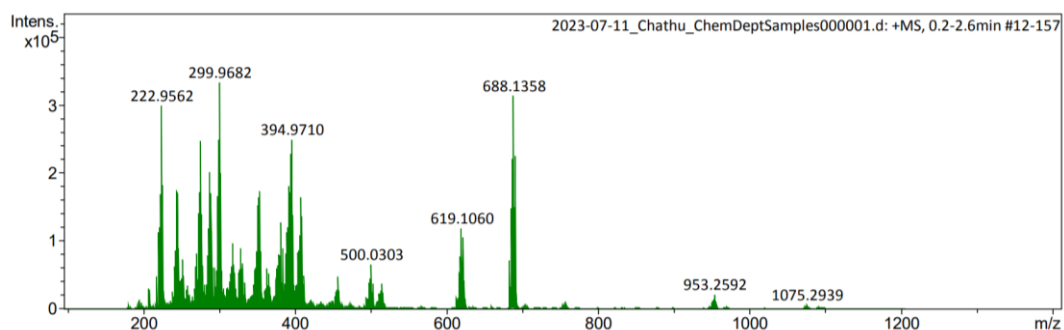
Figure 2.8. EI-MS spectra of organic product of reaction of **1a** and 1,2,4-triazole in anisole using 5 mol% of **Ru-3**.

^{1}H NMR analysis showed a pair of triplets that are not consistent with the dioxazolone starting material at 2.95 and 3.70 ppm, both integrating to two hydrogens. The aromatic peaks integrated to 8, higher than expected likely to do with the presence of $CHCl_3$ - residual from the NMR solvent, consistent with incorporation of a single phenyl group in the major product. In addition, an amide proton was expected between 5.5-8.5 ppm. A singlet was observed at 7.94 ppm which was proposed to be the amide hydrogen on the proposed structures (Scheme 2.10), as it also integrated to one relative to the peaks that were assigned to the ethylene linker.
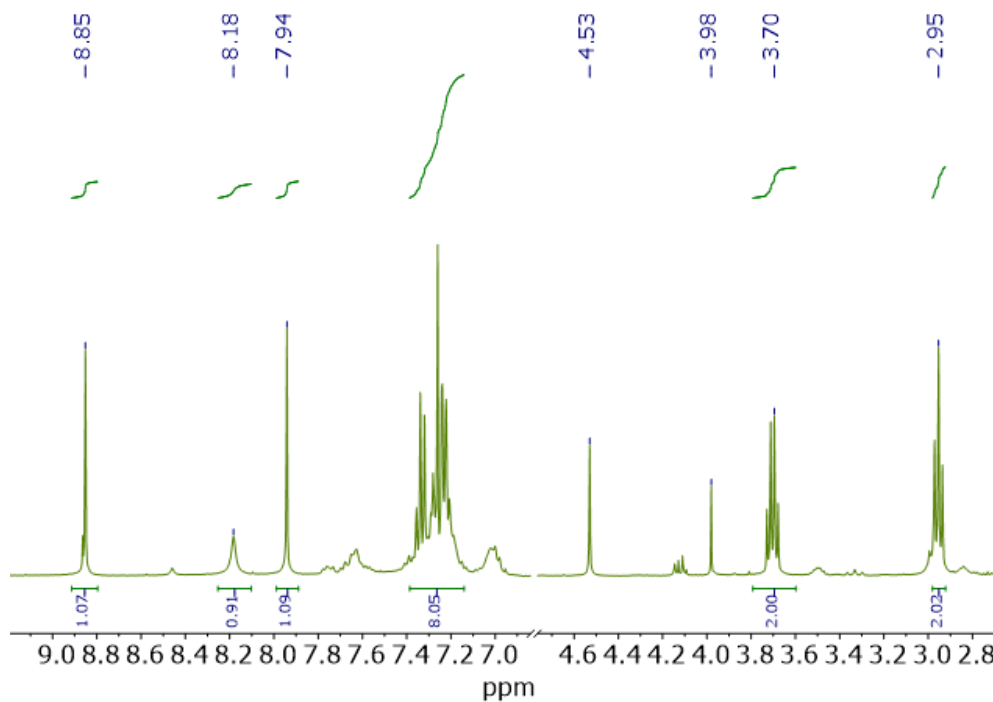
Figure 2.9. ^{1}H NMR spectrum (600 MHz, CDCl$_3$) of isolated product from reaction between **1a,** excess of 1,2,4-triazole, and 5 mol% of **Ru-3**.

The triazole fragment is expected to have two protons appear at approximately 8 ppm.[69] The two products can be distinguished by a ^{1}H–^{1}H COSY NMR experiment where the aromatic protons on the triazole functionality of the molecule correlated to the amide proton for the nitrene product. This correlation would not be present for the Curtius rearrangement product. ^{1}H–^{1}H COSY NMR data did not show correlation to any other protons within 3 bonds (Figure 2.9).
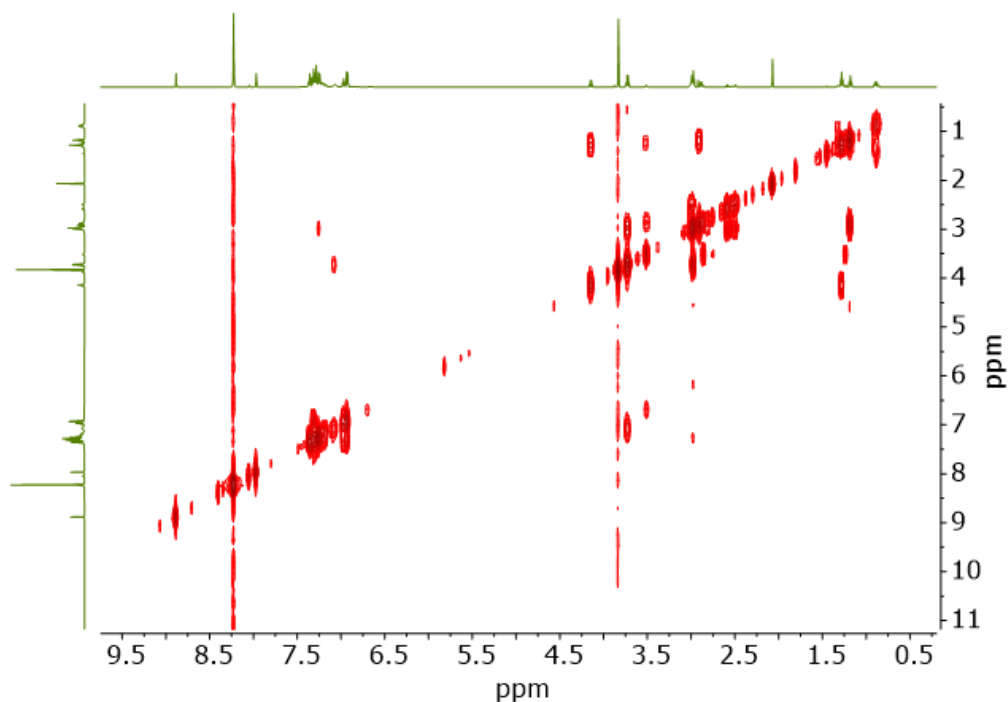
Figure 2.10. ^{1}H ^{1}H COSY NMR spectrum (600 MHz, CDCl$_3$) of isolated product from reaction between **1a,** excess of 1,2,4-triazole, and 5 mol% of **Ru-3**.

2.3.4   Forcing the Curtius Rearrangement of **1a** with 1,2,4-Triazole

To further probe the reaction pathway between **1a** and **Ru-3**, an experiment was conducted to bias the formation of the Curtius rearrangement product with **1a** and 1,2,4-triazole. If the product of this reaction was the same as previously observed, it will be evident that the Curtius rearrangement pathway is favoured under these reaction conditions. Dioxazolones similar to **1a** are known to undergo decarboxylative decomposition at temperatures above 110 °C.[42] Therefore, **1a** and an excess of 1,2,4-triazole were combined in anisole and heated to 110 °C for 24 h. The crude ^{1}H NMR spectrum indicated the presence of more than one species; therefore, column chromatography was employed in attempts to separate the products from each other. The major product was not isolated cleanly; therefore, evaluation of products was performed on the crude material. The mixture from this reaction contained a triplet at 2.95 ppm and a quartet at 3.70 ppm with integrations in its ^{1}H NMR spectrum. These were previously observed in the product mixture from the catalytic reaction with **Ru-3**, **1a**, and 1,2,4-triazole. The amide proton that was previously assigned

at 8.39 ppm was not observed. This was proposed to be attributed to hydrogen exchange with other products present in the mixture. In addition, the peaks at 8.85 and 7.94 ppm which were previously observed and assigned to the triazole aromatic protons were observed. ^{1}H-^{1}H COSY NMR analysis was acquired where there were correlations observed to the triplet at 2.95 ppm and a quartet at 3.70 ppm, consistent with product expected for the formation of the Curtius rearrangement product.
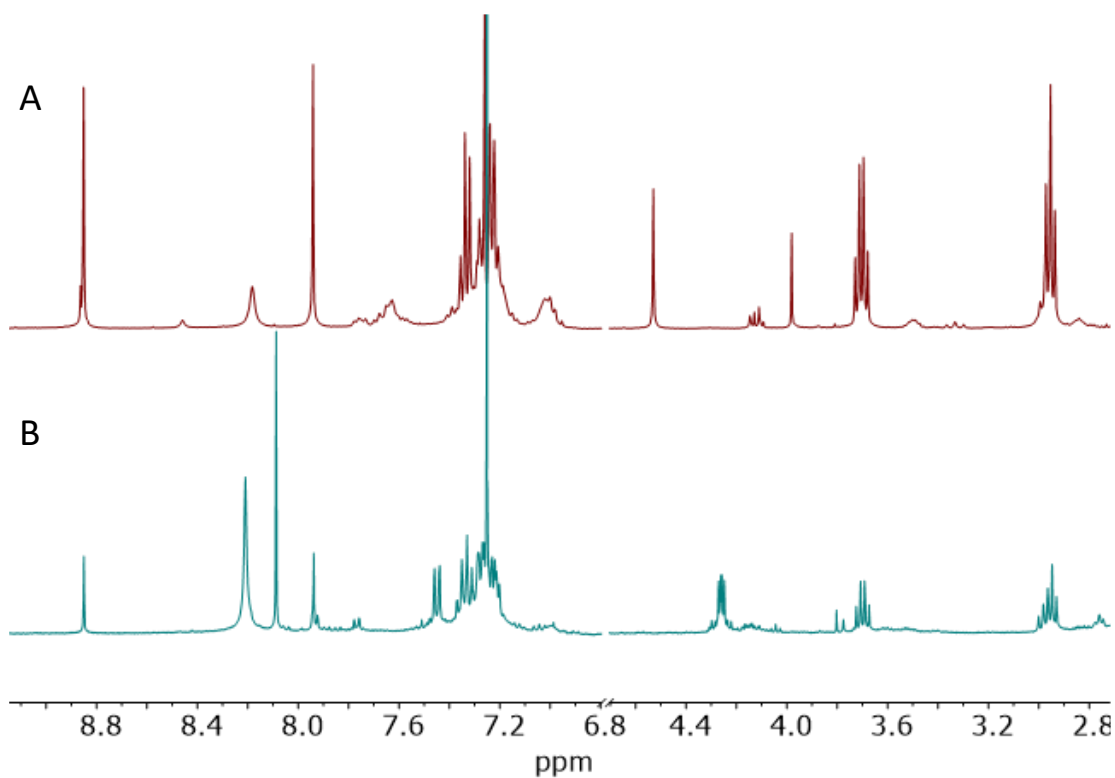
Figure 2.11. ^{1}H NMR spectrum (600 MHz, CDCl$_3$) of isolated product from; A) reaction between **1a**, excess of 1,2,4-triazole, and 5 mol% of **Ru-3**; and B) product of reaction between **1a** and excess of 1,2,4-triazole.
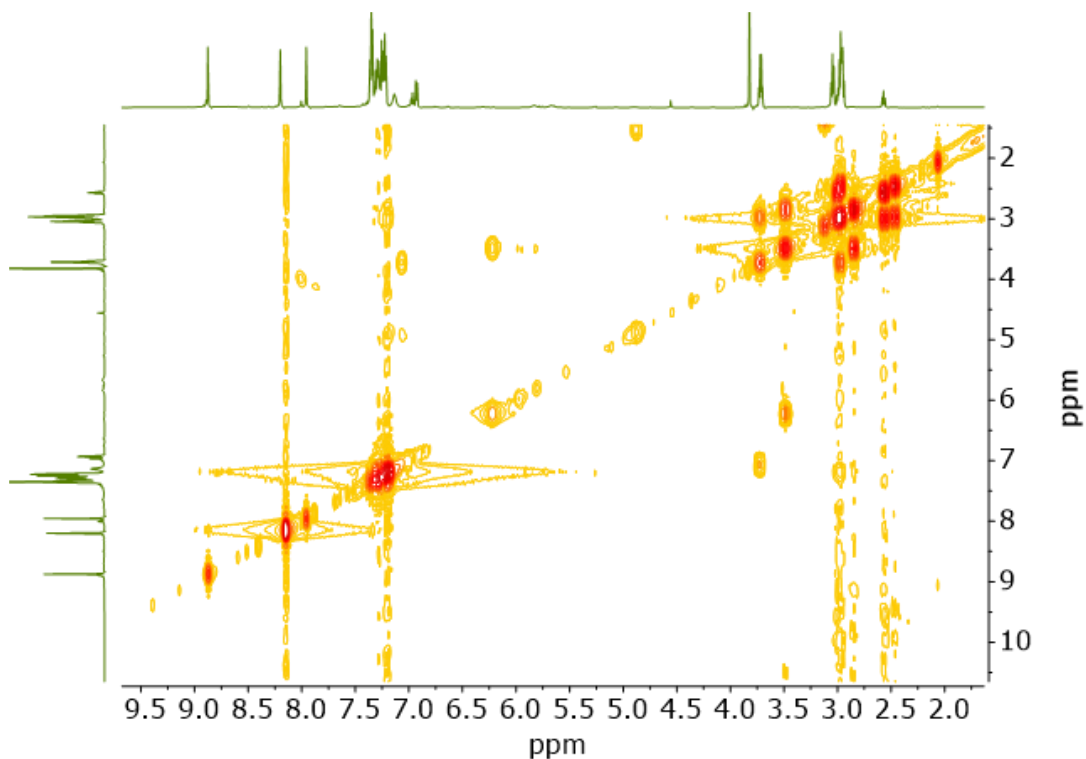
Figure 2.12. ^{1}H ^{1}H COSY NMR spectrum (600 MHz, CDCl$_3$) of crude mixture from reaction between **1a** and excess of 1,2,4-triazole.

2.4 Exploration of the Intramolecular Catalytic Reactivity Between Dioxazolones and MLC Vinylidenes

Due to the lack of success with the intermolecular reactivity of the dioxazolone and metal-vinylidene, attempts were put towards probing the intramolecular reactivity between dioxazolones and terminal alkynes. It was hypothesized that the desired reactivity would be more favorable due to lower entropy, given the two reactive functionalities are part of one molecule as opposed to forcing two molecules to come together. Therefore, compounds **1c,** 3-{2-(ethynyl)phenyl}-1,4,2-dioxazol-5-one, and **1d,** ethynyl-1,4,2-dioxazol-5-one, were attempted to be synthesized using a combination of reported and novel procedures. To synthesize **1c**, the first step involved a Sonagashira coupling reaction with 2-bromo-benzoic acid, **3**, to install a TMS-protected alkyne, which could easily be deprotected to generate the terminal alkyne.[70] Attempts to replicate reported procedures gave products with agreement to reported spectroscopic data.[70]
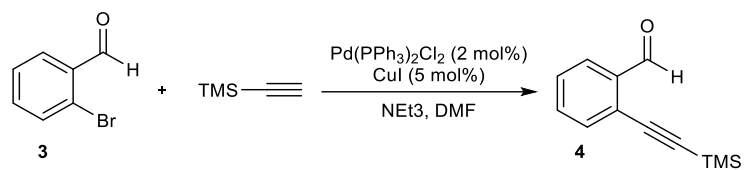
Scheme 2.12. Sonagashira coupling reaction of **3** to generate **4**.
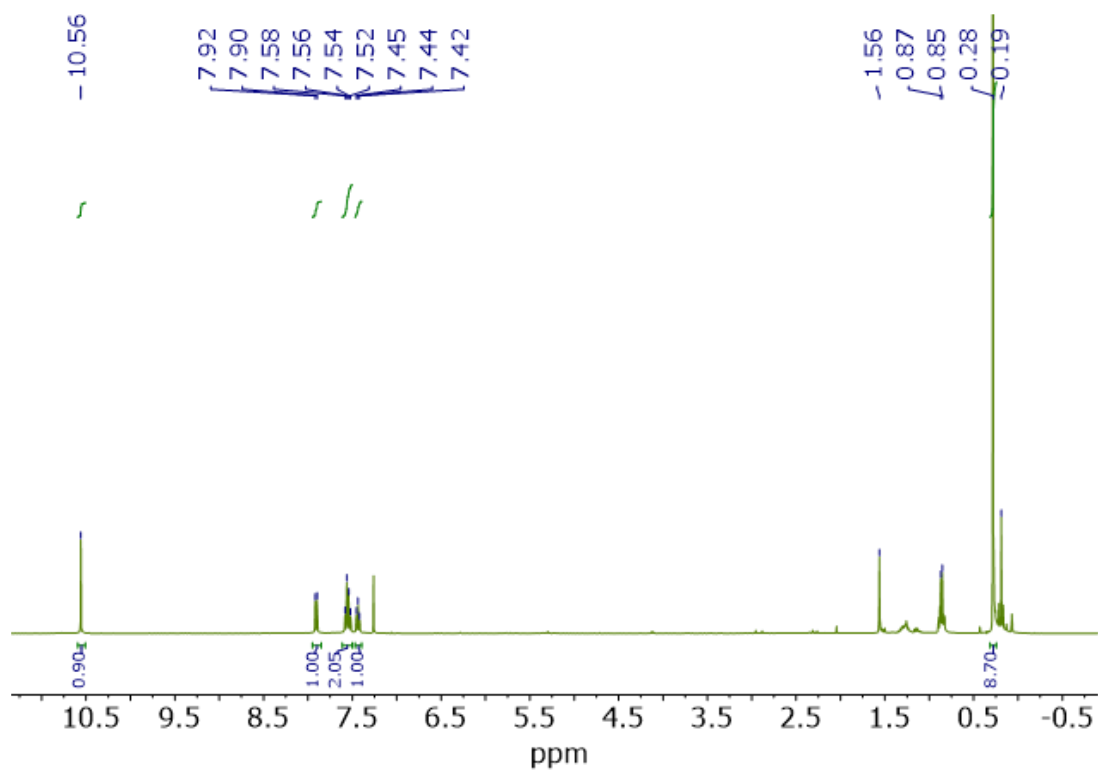
Figure 2.13. ^{1}H NMR spectrum (400 MHz, CDCl$_3$) of **4**.

Subsequently, this intermediate species, **4**, underwent a Pinnick oxidation reaction to generate a carboxylic acid, **5**, which was the precursor for the dioxazolone portion of the aryl linked product. The formation of **5** was confirmed by ^{1}H NMR spectrum matching previously reported data. [71]
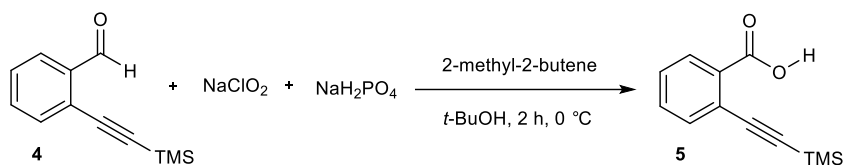
Scheme 2.13. Pinnick Oxidation reaction of **4** to generate a carboxylic acid **5**.
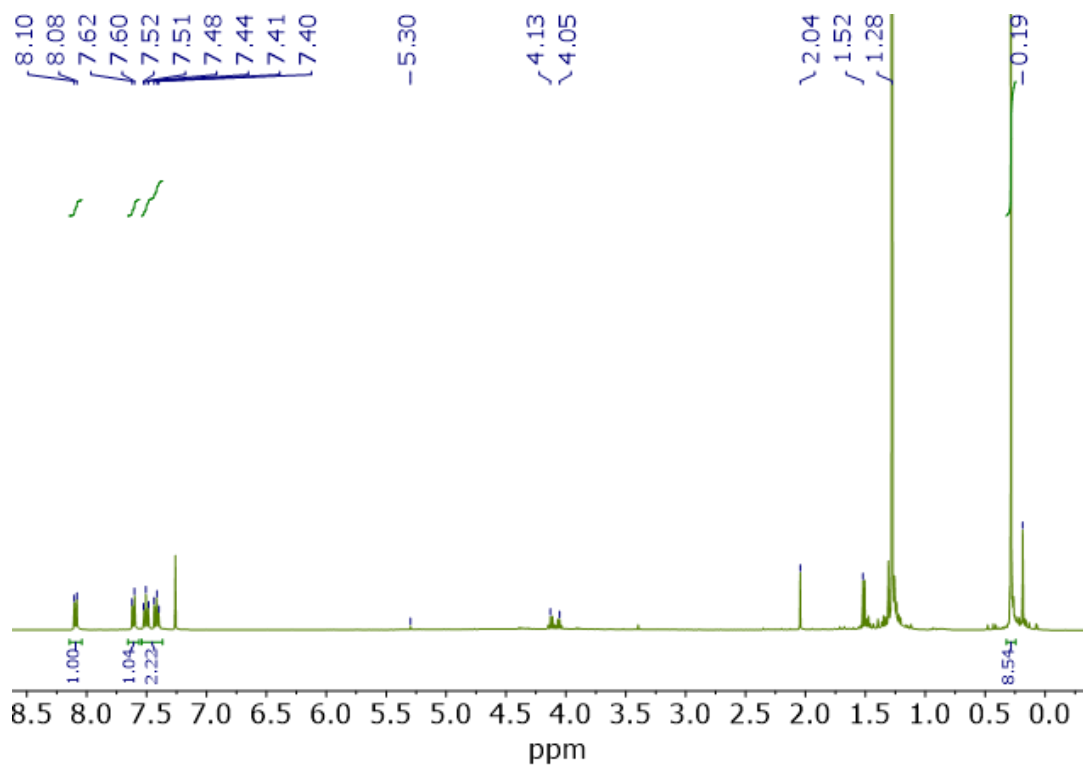
Figure 2.14. ¹H NMR (400 MHz, CDCl₃) spectrum of **5**.

The next two steps involved the formation of the dioxazolone by using CDI and hydroxylamine hydrochloride to generate the intermediate *N*-acyl hydroxylamine, **6**, confirmed using IR and ¹H NMR (Figures 2.17 & 2.18).[40]
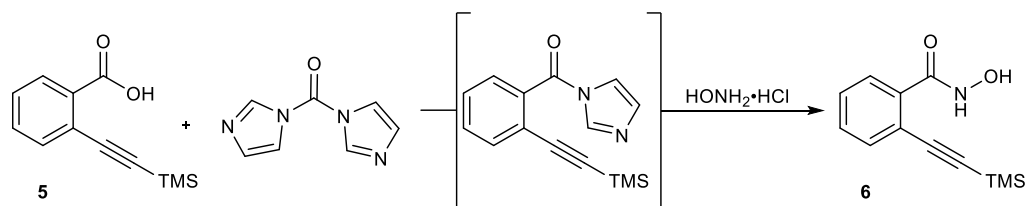
Scheme 2.14. Formation of intermediate *N*-acyl hydroxylamine **6** from **5**.
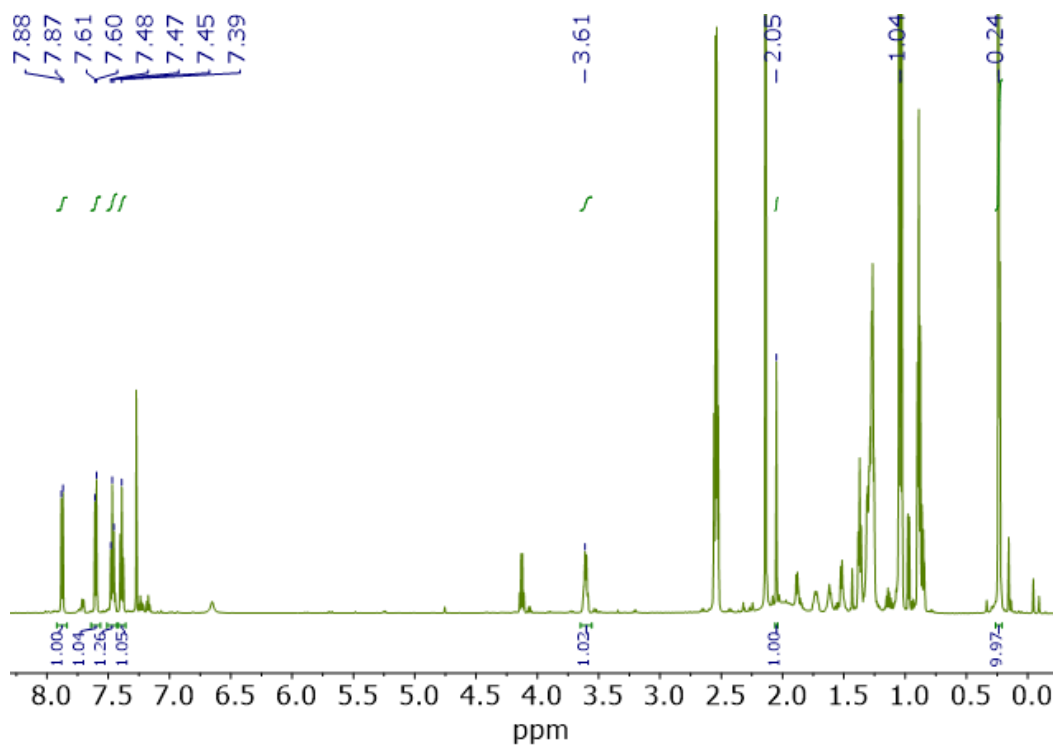
Figure 2.15. ^{1}H NMR (400 MHz, Acetone-d$_6$) spectrum of **6**.
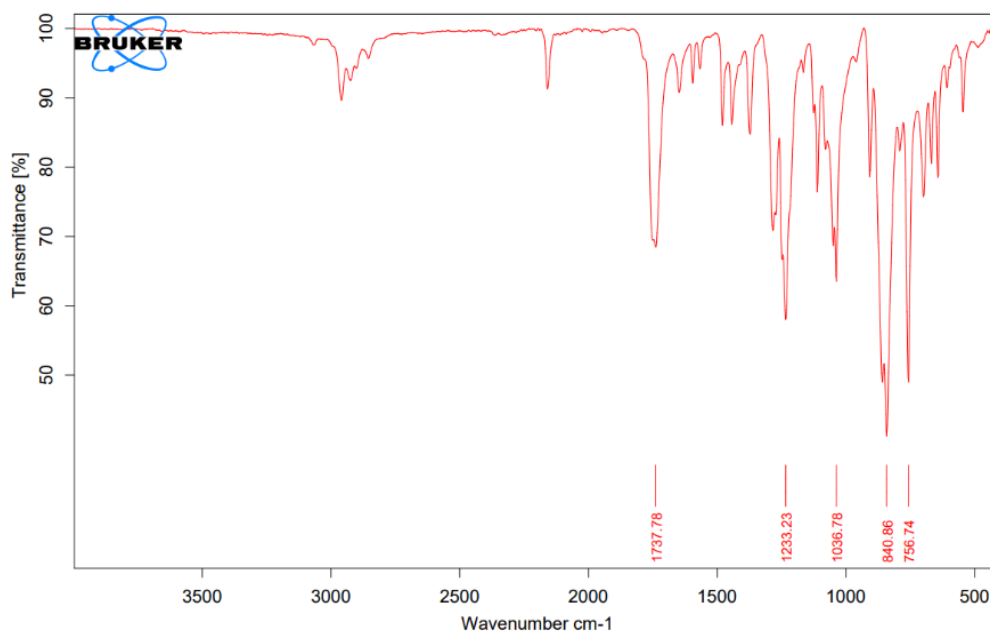
Figure 2.16. IR spectrum of **6**.

Product IV was then combined with CDI to form the desired dioxazolone V via a cyclization step. ^{1}H NMR proved ineffective due to the loss of an exchangeable amide proton upon the formation of V, therefore, FTIR was used to confirm the formation of the desired product, through a newly formed C-O bond stretch. However, the desired dioxazolone C-O vibration was not observed in FTIR following product isolation. Thus, the hydroxylamine moitey was determined to remain intact and was used for further synthesis. Deprotection of the terminal alkyne was required for the catalytic reactivity of the hydroxamic acid or dioxazolone functionality to be investigated. A control reaction was performed on **1b**, the phenyl-substituted dioxazolone, to confirm the stability of dioxazolones during TMS deprotection (Scheme 2.14). Upon dissolving 1 equivalent of **1b** and 1 equivalent of K_3CO_2 in methanol, ^{1}H NMR indicated complete decomposition of the dioxazolone after one h, suggesting the deprotection step cannot be performed as proposed in Scheme 2.14. Ongoing work is being conducted to first deprotect the alkyne prior to dioxazolone formation. Further, synthetic attempts are required to obtain the final product and determine if the proposed catalytic reactivity is attainable.
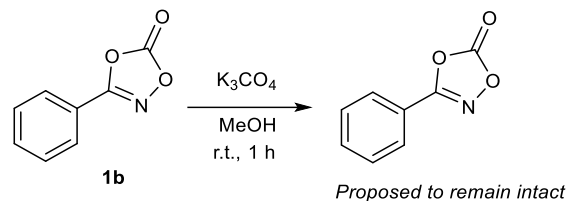
Scheme 2.15. Control reaction of **1b** to test the stability to deprotection conditions.
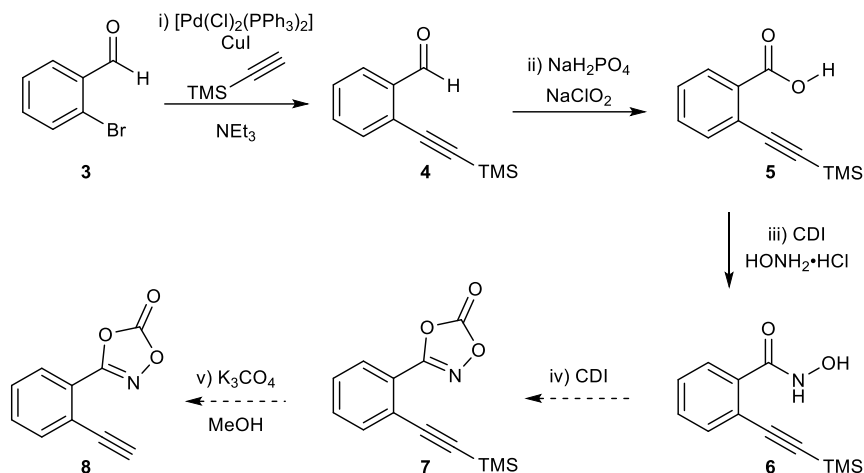
Scheme 2.16. i) Transformation of **3** to **4** *via* a sonogashira reaction; ii) Pinnick Oxidation of **4** to generate carboxylic acid **5**; iii) installation of hydroxamic acid on **5** to generate **6**; iv) cyclization of hydroxamic acid **6** to generate dioxazolone **7**; v) removal of TMS-protecting group on **7** to generate final complex **8**.

2.5   Summary and Conclusion

Chapter 2 demonstrated that the catalytic transformation of *N*-acyl ketenimines using dioxazolones and terminal alkynes with **Ru-3** was not possible. The reactivity between **1a** and **Ru-3** was explored, where it was found that they undergo a competitive the Curtius rearrangement instead of the target chemistry outlines in Scheme 2.1. A subsrtate containing both a terminal alkyne and dioxazolone functionality was attempted to be synthesized, but this was unsuccessful. In order to understand how to favour vinylidene formation, Chapter 3 focuses on exploring variables influencing the kinetics of vinylidene formation. Additionally, ruthenium MLC complexes similar to those explored in Chapter

2 will be used to examine the impact various alkali salts has on the hydroalkoxylation process of 2-EBA to isochromene

Chapter 3

3 Overview

It is important to better understand the rates of vinylidene formation using [Ru(Cp)(P$^R_2$N$^{R'}_2$)(NCMe)]PF$_6$ complexes to maximize catalytic activity for the hydrofunctionalization of complexes containing terminal alkynes, for both inter- and intramolecular reactions. Using different terminal alkynes with different electronic and steric properties will allow for a greater understanding of rates of formation of this often rate-determining step concerning other chemistry. Vinylidene formation can easily be monitored by ^{31}P{^{1}H} NMR spectroscopy, as the ancillary phosphorus ligands exhibit a distinct upfield shift of 0-3 ppm in the vinylidene complex relative to the starting acetonitrile complex of **Ru-3**. In addition, a direct comparison of vinylidene formation with phenylacetylene using **Ru-3** and [Ru(Cp)(P$^{Cy}_2$N$^{Ph}_2$)(NCMe)]PF$_6$ (**Ru-4**) will be conducted to probe how the electronic and steric properties of the metal centre affect the rate of vinylidene formation. The hydrofunctionalization of 2-EBA to isochromene has been well explored to obtain high conversion with optimal conditions using **Ru-4**. It is important to test the effect that salt additives may have on catalytic conversions to acquire reproducible and accurate data. In this chapter, multiple tests were performed for the hydroalkoxylation of 2-EBA using **Ru-4** and various alkali salt additives. Complex **Ru-4** has a PF$_6^-$ anion, which is known to be weakly coordinating due to its low overall charge of -1 and large size for high levels of charge delocalization. Ru(Cp)(P$^{Cy}_2$N$^{Ph}_2$)Cl (**Ru-5**) will be used to install different weakly coordinating anions (WCAs) to probe how these anions interfere/assist with the hydroalkoxylation of 2-EBA.

3.1 Vinylidene Rate Study

The targeted reactivity in Chapter 2 required the first step of the catalytic cycle to be vinylidene formation. Vinylidene formation is favourable with alkyne **2a**; however, it cannot compete with the Curtius rearrangement of dioxazolone **1a**. It is crucial to gain a greater understanding of how the rates of formation of the vinylidene complexes are affected to exploit the possible reactivity, specifically, intermolecular reactivity, of **Ru-3** and **Ru-4**. This prompted a rate study of vinylidene formation with different terminal

alkynes with **Ru-3** and **Ru-4**. By altering the electronic properties of the terminal alkyne and tracking vinylidene formation over time with **Ru-3**, a Hammett analysis can be performed. It is also necessary to see if steric hindrance on the terminal alkyne affects vinylidene formation. Additionally, by using the same terminal alkyne but altering the structure of the MLC complex used, trends relating to the steric and electronic properties of the metal can be observed.

3.1.1 Hammett Analysis of Vinylidene Formation with **Ru-3** and Different Terminal Alkynes

Four different terminal alkynes; phenylacetylene (**2a**), 4-ethynyl toluene (**2b**), 4-ethynyl anisole (**2c**), and 4-(trifluoromethyl)phenylacetylene (**2d**) were tested for the formation of metal-vinylidenes with **Ru-3** in a five-to-one ratio (Scheme 3.1). The formation of the vinylidene species was tracked using $^{31}P\{^1H\}$ NMR spectroscopy. The reactions were prepared in NMR tubes and loaded into a spectrometer to acquire an initial time point where no vinylidene species was present. Subsequently, each terminal alkyne was added into the tube, loaded back into the spectrometer. A spectrum was acquired every 10 mins for 80 mins. The spectrometer was heated from 25 ℃ to 70 ℃ over 10 mins, resulting in the first timepoint as unreliable. Therefore, the rate was determined from data in the time range of 20 to 80 mins. Triphenylphosphine oxide was used as the internal standard for calculation of vinylidene formations.
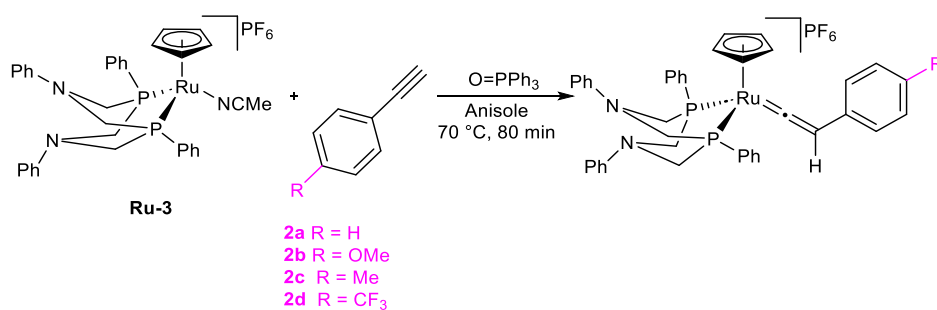
Scheme 3.1. *In-situ* vinylidene formation with phenylacetylene, 4-ethynyl toluene, 4-enthynyl anisole, and 4-(trifluoromethyl)phenylacetylene using **Ru-3**, monitored by $^{31}P\{^1H\}$ NMR spectroscopy using O=PPh$_3$ as an internal standard.

All complexes were observed to convert to only one product, which was consistently observed over all three runs for each terminal alkyne. MeCN complexes with respect to their vinylidene complexes have very little change in $^{31}P\{^1H\}$ NMR chemical shifts, approximately 1-5 ppm. Upfield shifts are typically observed for vinylidene complexes with respect to their MeCN complexes.[8,17,18,58] This is what was observed in this study, where complex **Ru-3** had a $^{31}P\{^1H\}$ NMR chemical shift of 44.4 ppm. Vinylidene complexes with **2a**, **2b**, **2c**, and **2d** displayed chemical shifts of; 42.6, 43.0, 42.6, and 41.7 ppm respectively. In addition to this, all samples were observed to have a distinct colour change from yellow to reddish orange after reaction completion.

The rates of vinylidene formation were plotted relative to the alkyne sigma para value where σ_p values are; -0.27 for *p*-OMe, -0.17 for *p*-Me, 0 for *p*-H, and 0.54 for *p*-CF$_3$ (Figure 3.1). The line of best fit of the Hammett analysis does not give a good linear correlation. The negative linear slope ($\rho = -0.5533$) of the Hammett analysis is between -1 and 0, which tells is insignificant. This small and negative ρ value indicated that this reaction does not depend on electronic parameters. This indicates that there were no distinct trends when altering the electronic properties of the terminal alkyne for vinylidene formation with **Ru-3** under these conditions (Figure 3.1). Vinylidene formations after 80 mins all fall within 10% of each other when using **2a**, **2b**, and **2c**, ranging from 23 to 33%. Vinylidene formation for **2d** was observed to have the lowest rate of vinylidene formation in comparison to the others. This was proposed to be the case due to competitive reactivity with the empty coordination site on **Ru-3** and the fluorines of the -CF$_3$ substituent, as halogenated solvents have been observed to be incompatible with these complexes at elevated temperatures. In addition, the R^2 value for the trendline is 0.811, indicating that 81% of the regression accounts for the specific measurement. This presents the possibility that electronic effects were not directly impacting rate of vinylidene formation at the specified temperature.
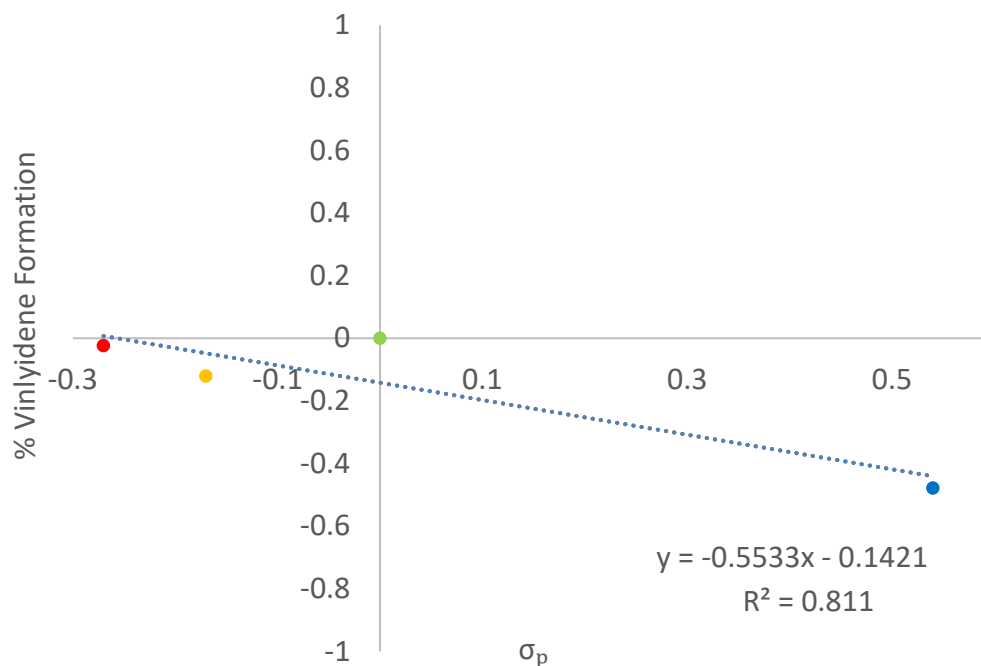
Figure 3.1. Hammett analysis of vinylidene formation of phenylacetylene (green) 4-ethynyl toluene (orange), 4-enthynyl anisole (red), and 4-(trifluoromethyl)phenylacetylene (blue) with **Ru-3**.

It is important to note that three steps in vinylidene formation can affect the rate; 1) dissociation of acetonitrile, 2) side-on bonding of the alkyne to the vacant coordination site, and 3) hydrogen migration (Scheme 3.2). It is proposed that acetonitrile dissociation was the rate-determining step at this temperature, as electronic effects of the alkyne were expected to affect step 2 or 3 of vinylidene formation. The intermediate metal species bearing a vacant coordination site is electrophilic, therefore, a more electron-rich alkyne would favour the second step of vinylidene formation, the side-on bonding of the alkyne to the vacant coordination site. In contrast, as previously stated, more electron-withdrawing terminal alkynes tend to favour the vinylidene tautomer over the η^2-alkyne complex, favouring the final step of vinylidene formation.[14]
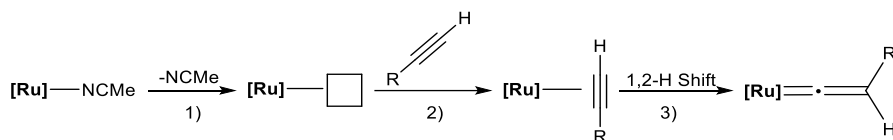
Scheme 3.2. Steps of vinylidene formation; 1) dissociation of acetonitrile, 2) side-on bonding of the alkyne to the vacant coordination site, and 3) hydrogen migration.

3.1.2 Vinylidene Formation with **Ru-3**, Phenylacetylene, and 1-Octyne

Under these conditions, 1-octyne (**2e**) was used as a direct comparator to phenylacetylene with **Ru-3** (Scheme 3.3). Interestingly, the chemical shift observed for vinylidene increased from 44.4 ppm for **Ru-3** to 45.3 ppm when **2e** was added. It is possible that the vinylidene was not formed, but rather the π-bound alkyne was formed (Scheme 3.2, step 3). The alkyl chain of **2e** is more electron donating than the phenyl ring on **2a**. More electron donating terminal alkynes tend to favor the η^2-alkyne complex over the vinylidene complex. In the η^2-alkyne complex, the C-C triple bond is donating electron density to the metal centre and the metal is backbonding to the alkyne. The absence of aromaticity in **2e** results in negligible hyperconjugation from the π-backbonding from the metal to the C-C triple bond. Thus, resulting in a greater electronic density on the metal centre and therefore the phosphorus substituents causing the downfield chemical shift.
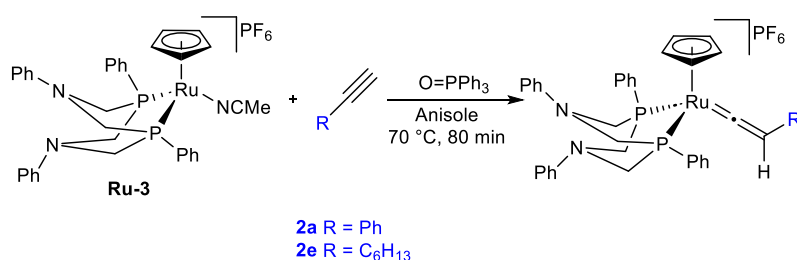
Scheme 3.3. *In-situ* vinylidene formation with phenylacetylene and 1-octyne using **Ru-3**, monitored by ^{31}P{^{1}H} NMR spectroscopy using O=PPh$_3$ as an internal standard.

The rate of vinylidene formation is greater for phenylacetylene than that of 1-octyne based on the line of best fits. The rate of vinylidene formation with phenylacetylene is 0.223 min$^-$^{1} greater than that of vinylidene formation with 1-octyne. As stated previously, more

electron-withdrawing terminal alkynes tend to favour the vinylidene tautomer over the η^2-alkyne complex. **2a** is less electron rich than **2e**, therefore resulting in a greater rate.
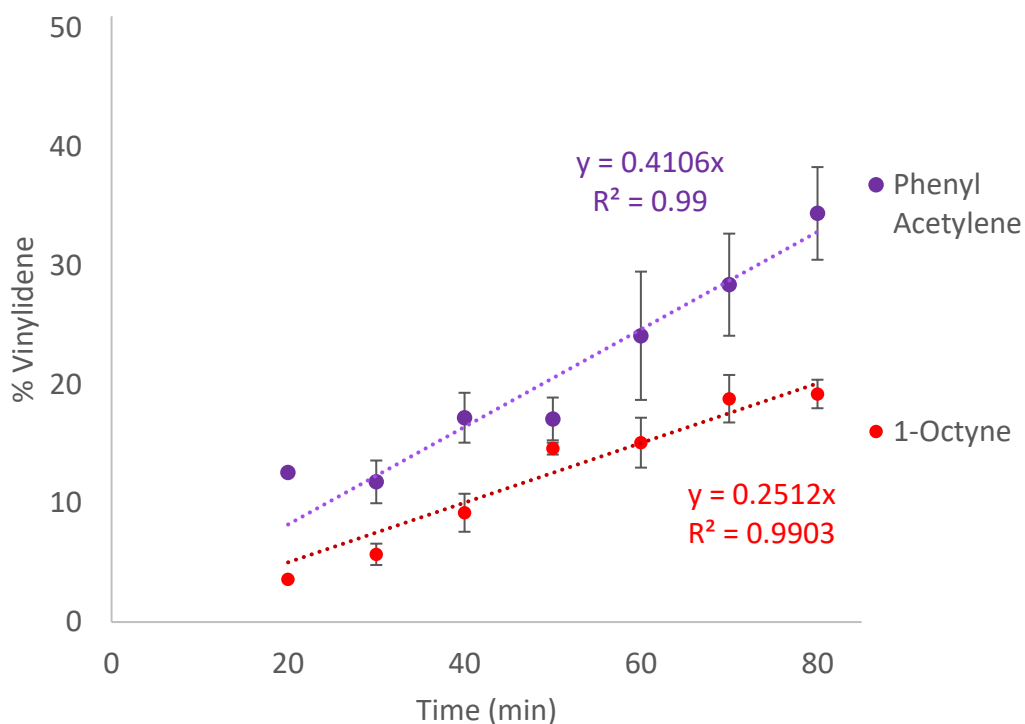
Figure 3.2. Conversion vs. time plot of vinylidene formation of 1-octyne (red) and phenylacetylene (purple) with **Ru-3**. Error bars were calculated using the standard deviation of the three runs for vinylidene formation with MLC complex.

3.1.3   Altering the Electronic and Steric Properties of Ruthenium for Vinylidene Formation with Phenyl Acetylene

To validate the hypothesis that the rate-determining step of vinylidene formation at this temperature is dissociation of MeCN, two ruthenium MLC complexes were used with different phosphine substituents, **Ru-3** (R = Ph) and **Ru-4** (R = Cy). **Ru-3** is less electron-rich and less sterically hindered about the metal centre than **Ru-4**, given that the phenyl substituent on the phosphorus in **Ru-3** is less electron donating and smaller than the cyclohexyl group in **Ru-4**. As previously mentioned, vinylidenes are electron-withdrawing ligands, therefor having electron-donating ligands on the metal has been shown to stabilize metal-vinylidenes.[6]
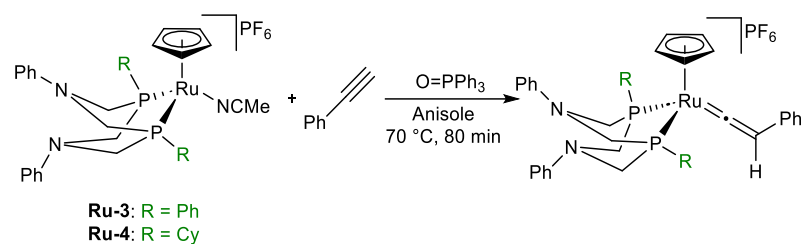
Scheme 3.4. *In-situ* vinylidene formation with phenylacetylene using **Ru-3** and **Ru-4**, monitored by ^{31}P{^{1}H} NMR spectroscopy using O=PPh$_3$ as an internal standard.

Ru-3 was 0.64 times slower in rate than **Ru-4**. It is proposed that the more electron-rich and sterically encumbered metal centre should promote ligand dissociation at a higher rate due to the lower required energy to promote ligand dissociation. The metal complex was proposed to be more stable with a vacant coordination site with a more electron-rich metal centre. **Ru-4** was observed to form its vinylidene complex at a higher rate than **Ru-3**. Thus, supporting the hypothesis that the rate-determining step at this temperature is most likely due to acetonitrile dissociation. In addition, sterics may have also played a role in enhancing MeCN dissociation. In a previous study, the crystal structure of [Ru(Cp)(P$^{t\text{-}Bu}_2$N$^{Ph}_2$)(MeCN)]PF$_6$ revealed that the two metallocycles comprised of the ruthenium metal centre and the P$^{t\text{-}Bu}_2$N$^{Ph}_2$ ligand are both in a boat conformation. One of the pendent amines is close in proximity to the labile acetonitrile ligand. Typically, the proximal metallocycle will crystalize in a chair conformation for structures of [Ru(Cp/Cp*)(P$^R_2$N$^{R'}_2$)(L/X)]$^+$ complexes (L = MeCN with PF$_6^-$; X = Cl), with the tertiary amine positioned away from the active site.[18] The labile ligand of **Ru-4** is much more sterically encumbered than that of **Ru-3**, therefore, dissociation of MeCN would result in less steric clash about the metal centre and therefore be more favorable for **Ru-4**.
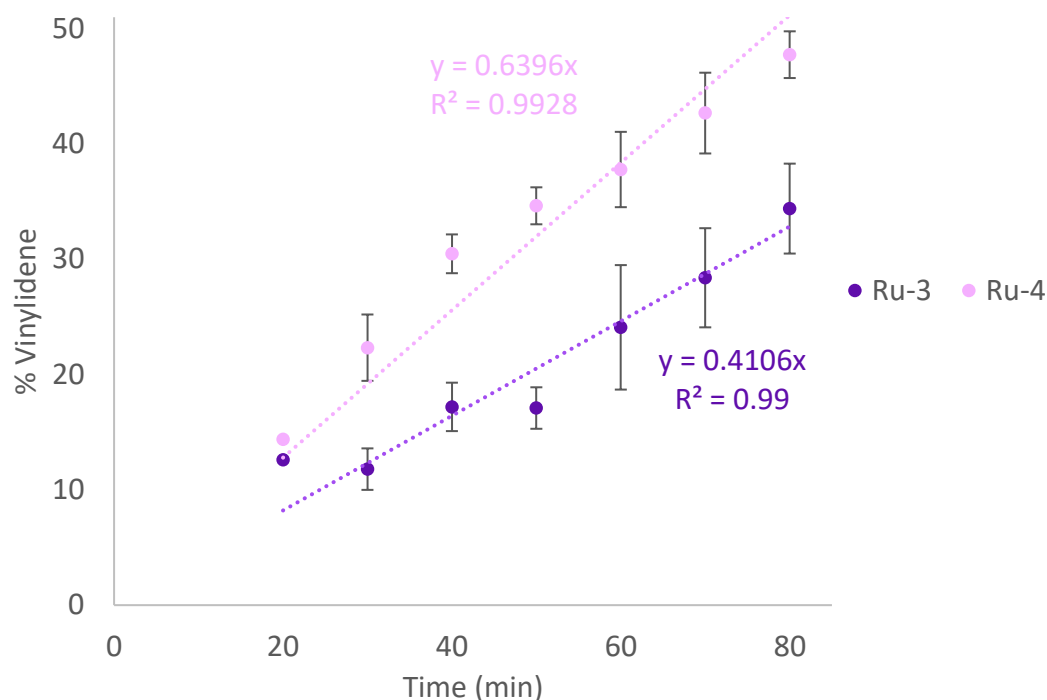
Figure 3.3. Conversion vs. time plot of vinylidene formation of phenylacetylene with **Ru-3** and **Ru-4**. Error bars were calculated using the standard deviation of the three runs for vinylidene formation with MLC complex.

3.2   Hydroalkoxylation of 2-EBA with **Ru-4**

Due to the higher observed formation of vinylidene with **Ru-4** observed from the previous study, subsequent reactions were performed with this complex. The hydrofunctionalization of 2-EBA using complex **Ru-4** has been previously explored in the Blacquiere group.[9] **Ru-4** was able to achieve a 66% *in-situ* yield of isochromene from 2-EBA at 70 ℃ over 24 h.[3] In this section, the effects of alkali salt additives on the catalytic performance will be explored.

3.2.1   Alkali Salt Additives Effect on the Hydroalkoxylation of 2-EBA

It was of interest to see if using various hexafluorophosphate alkali salts as an additive into the previously established hydroalkoxylation facilitated by **Ru-4** has any effect on overall catalytic conversion. The consumption of 2-EBA was calculated using GC-FID. A calibration curve was constructed by preparing vials of 2-EBA differing in concentrations

ranging from 0.5 mM to 15 mM in GC vials using a dilution scheme (Table 5.7.). Due to the high price point of isochromene and the level of difficulty in cleanly isolating the product from catalysis, a calibration curve for this species was not created. Thus, for the remainder of this Chapter, 2-EBA consumption will be used for the measurement of catalytic activity, based on previous studies using **Ru-4** for the hydroalkoxylation of 2-EBA.[3] Solubility tests were performed on $NaPF_6$, $LiPF_6$, and KPF_6 to identify solubilizing solvents that are compatible with catalytic reaction conditions (Table 3.1). The salts were insoluble in many organic solvents and were only found to be soluble in dimethyl sulfoxide and dimethylformamide.

Table 3.1. Solubility test results of alkali salts with various organic solvents.

Solent	$NaPF_6$	$LiPF_6$	KPF_6
Acetonitrile	X	X	X
Acetone	X	X	X
Anisole	X	X	X
Methyl-THF	X	X	X
Dioxane	X	X	X
DMSO	✓	✓	✓
DMF	✓	✓	✓

The salts must be added as a solution rather than a solid to the catalytic mixtures to ensure they were in the homogeneous solution during course of reaction. It was proposed that the addition of DMSO and DMF could result in catalyst inhibition, as these solvents could coordinate to the active catalyst species. Therefore, a control reaction was performed with **Ru-4** and 2-EBA with the addition of 40 µL of dimethyl sulfoxide or dimethylformamide to ensure baseline reactivity is not affected by the presence of these solvents. The reaction with only Me-THF had an overall consumption of 66% 2-EBA, which is consistent with

previously acquired data (Figure 3.4).[3] The reaction with DMF as the additive had an overall conversion of 72% 2-EBA which is only 6% different from the baseline reaction. The reaction with DMSO as the solvent additive showed little consumption of 2-EBA, with only 17% consumption. While dimethyl sulfoxide was shown to be incompatible with catalysis, dimethylformamide had no effects on overall conversion, therefore it was selected as the solvent for the alkali salt stock solutions.
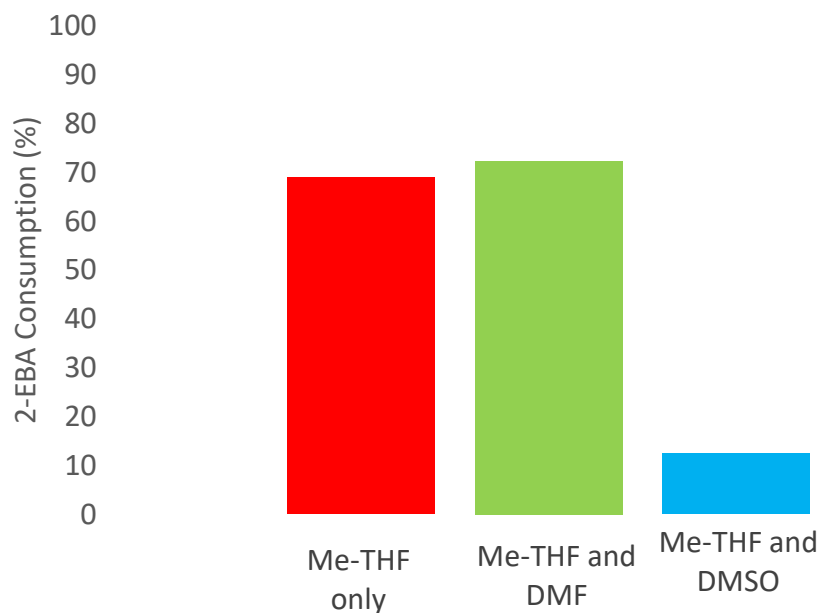
Figure 3.4. Catalytic consumption of 2-EBA with 5 mol% of **Ru-4** at 70 ℃ for 24 h in solvents: Me-THF only (red), Me-THF with 6.7%$_{vol}$ DMF (green), and Me-THF with 6.7%$_{vol}$ DMSO (blue).

Eight reactions were conducted to test the effect of various alkali salt additives on the catalytic hydrofunctionalization of 2-EBA using **Ru-4** (Scheme 3.6). The vials differed in their contents of alkali salt additive, 2-EBA, and **Ru-4**. All vials were subjected to catalytic conditions where they were heated at 70 ℃ for 24 h which were then analyzed by GC-FID.
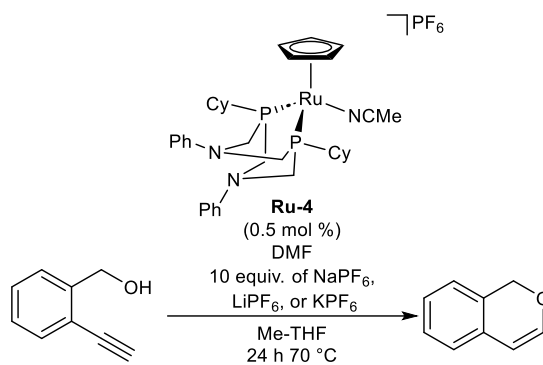
Scheme 3.5. Hydroalkoxylation of 2-EBA to isochromene using **Ru-4** and alkali salt additives with 6.7% DMF by volume.

When comparing the results of reaction between the vial containing **Ru-4** and 2-EBA to those with **Ru-4**, 2-EBA, and the alkali salt additives, there is a clear effect of these salts on the overall reactivity. The reactions with $NaPF_6$ as the alkali salt additive gave the highest consumption at 92%, significantly higher than the reaction without any additive at 67% conversion. The reaction with $LiPF_6$ and KPF_6 also affected consumptions of 2-EBA at 81% and 78%, slightly higher than the reaction without any additive. It is important to note that no additional peaks of significant value were observed on the chromatogram besides 2-EBA and isochromene. The error bars for the baseline catalytic reaction between 2-EBA and **Ru-4** compared to the reactions between 2-EBA and **Ru-4** with the salt additives do not overlap (Figure 3.5). Thus, there must be some enhanced reactivity occurring between the catalyst and these salt additives. It is possible that the alkali salt was coordinating to the pendant amine resulting in a change in orientation of the $P^{Cy}_2N^{Ph}_2$ ligand on complex **Ru-4**, as alluded to in Section 1.1. The $P^R_2N^{R'}_2$ ligand is very bulky in its energetically favored boat conformation. It is possible that one of the 6-memberd rings of the ligand could flip to a chair conformation to coordinate to the salt. This could aid in coordination of the terminal alkyne to the vacant coordination site on the catalyst as it could be less sterically hindered in the proposed Na^+ coordinated form (Scheme 3.5). Assuming this coordination is quick and reversible and occurs after the proton shuttling steps, this orientation could aid in quicker formation of isochromene.
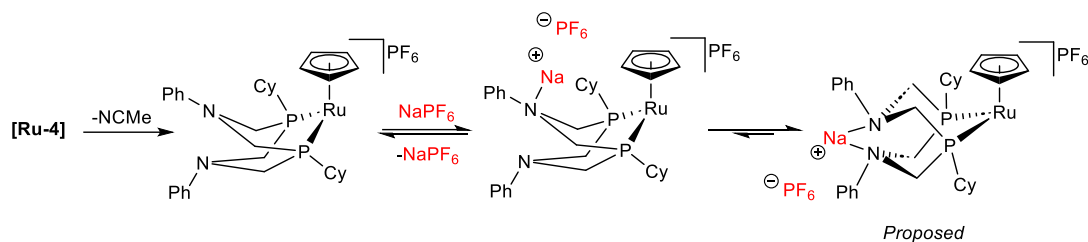
Proposed

Scheme 3.6. Loss of MeCN on **Ru-4** followed by proposed *exo* addition of Na$^+$ and boat-to-chair ring flip of one of the 6-member metalocycles affording an *exo*-pinched isomer.[2]

When the salts and 2-EBA are subjected to catalytic conditions without **Ru-4**, 7-13% consumption of 2-EBA is observed. A control reaction was performed where 2-EBA was subjected to catalytic conditions without **Ru-4** or any additives, and 2-10% consumption of 2-EBA was observed. It is also possible that the additives could promote Markovnikov addition of the alcohol to the terminal alkyne, generating the 5 *endo-dig* product.The addition of water to alkynes results in the formation of enols that spontaneously tautomerize to ketones.[72] In examples of the hydration reactions when employing H_2SO_4, H_2O, and $HgSO_4$ on 1-(1-hydroxycyclohexyl)ethanol, the Markovnikov product, 1-ethinylcyclohexan-1-ol, is obtained (Scheme 3.7). The alkali salts could be promoting the formation of the Markovnikov addition product of alcohol across the alkyne bond where the product is overlapping with the known isochromene product in the chromatograph using the selected method for GC-FID analysis. The hydration requires very strong acids, therefore, it is proposed that the alkali salts could be using in place of these reagents.
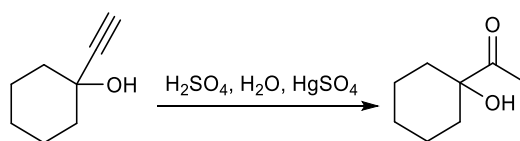
Scheme 3.7. Markovnikov product, from the hydration of ethinylcyclohexan-1-ol when employing H_2SO_4, H_2O, and $HgSO_4$ on 1-(1-hydroxycyclohexyl)ethanol.[72]

The error bars for all reactions of 2-EBA and alkali salts as well as that of the control without **Ru-4** or the salt additives all overlap. Thus, it is unclear whether the salts themselves react with 2-EBA. This indicates that the salts themselves may be reacting with 2-EBA in some fashion, however, further mechanistic investigation is required.
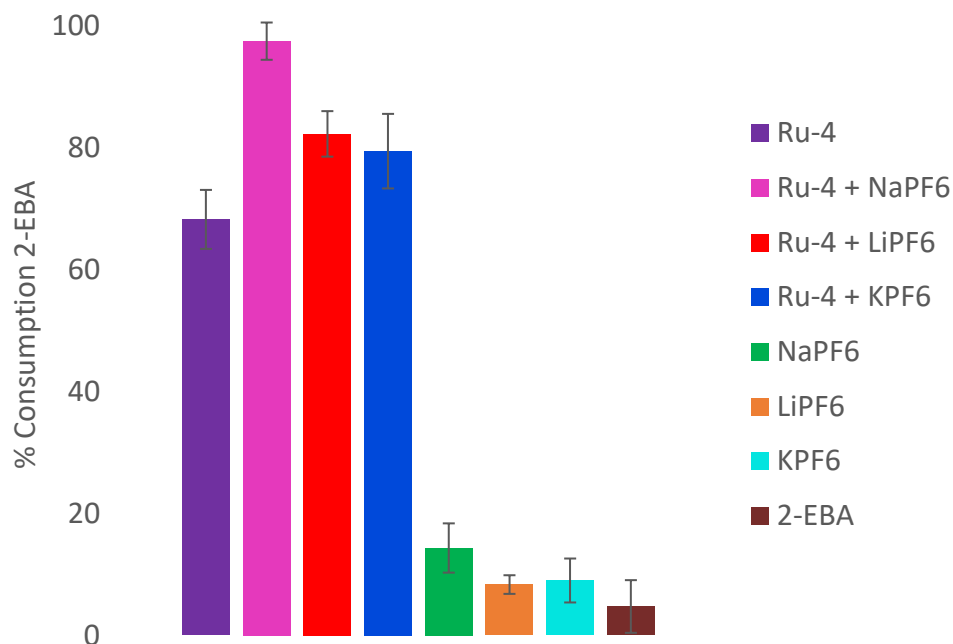
Figure 3.5. Consumption of 2-EBA in Me-THF with 6.6%$_{vol}$ DMF with different additives using; **Ru-4**, (purple); **Ru-4** with NaPF$_6$ additive (pink); **Ru-4** with LiPF$_6$ additive (red), **Ru-4** with KPF$_6$ additive (dark blue); NaPF$_6$ additive (green); LiPF$_6$ additive (orange); KPF$_6$ additive (light blue); no additives (brown). Error bars were calculated using the standard deviation of the three runs for 2-EBA consumption.

3.3   Hydroalkoxylation of 2-EBA with **Ru-5**

All MLC complexes used to this point in the Blacquiere group are stabilized by a PF$_6^-$ counterion. The hydroalkoxylation of 2-EBA has been optimized with the use of catalyst **Ru-4**. This transformation, however, has never been explored using [Ru(Cp)(P$^R_2$N$^{R'}_2$)(NCMe)]$^+$ with different WCAs. Therefore, three different potassium salts with anions that are known to be weakly coordinating were used to generate different ruthenium MLC complexes *via* a halide abstraction with RuCl(Cp)(P$^{Cy}_2$N$^{Ph}_2$) (**Ru-5**). The complexes were then subjected to catalytic conditions with 2-EBA to probe the effects each WCA had on the hydroalkoxylation of 2-EBA.

3.3.1   Synthesis of [Ru(Cp)(P$^{Cy}_2$N$^{Ph}_2$)Cl (**Ru-5**)

Complex **Ru-5** was synthesized following literature procedures.[3,73] The only alteration made on the procedure was the work up to remove excess free ligand. This was simply removed by dissolving the crude mixture in toluene and passing it through a plug of Celite. Yields were lower than expected for both steps of the reaction than that of literature. The first step was proposed to have a low yield due to oxidation of the PPh$_3$ reagent, as there was a large amount of O=PPh$_3$ that persisted in the crude reaction mixture which subsequently resulted in additional workup steps. The low yield for the ligand coordination step was attributed to the extensive workup required to remove excess ligand to ensure clean complex for catalytic use.
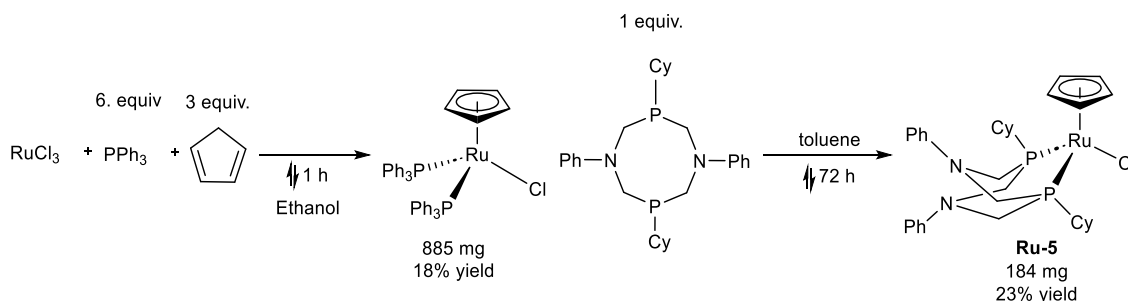
Scheme 3.8. Synthesis of **Ru-5**.

3.3.2   Attempts at Halide Abstraction from **Ru-5** with KOTf

The preliminary step for these reactions was to generate new ruthenium complexes with different anions. The goal for these reactions was to make stock solutions of [Ru(Cp)(P$^{Cy}_2$N$^{Ph}_2$)(NCMe)]X (where X = PF$_6$⁻, OTf⁻, and BF$_4$⁻) complexes by performing *in-situ* halide abstractions with KPF$_6$, KOTf and KBF$_4$ (Scheme 3.9). Using known amounts of MeCN, Me-THF and **Ru-5**, a desired concentration could be obtained. It was proposed that the KCl salt would crash out of solution and the remaining homogenous solution would contain only the desired complex, which would subsequently be used for catalysis.
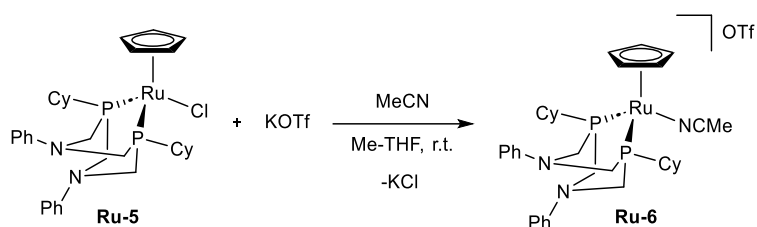
Scheme 3.9. Proposed method for generating ruthenium complexes bearing different anions *via in-situ* halide abstraction. X = PF_6^-, OTf^-, and BF_4^-.

The time to perform these in-situ halide abstractions must occur quantitatively and in short reaction times. KOTf was first used for this test reaction in attempts to synthesize [Ru(Cp)(P$^{Cy}_2$N$^{Ph}_2$)(NCMe)]OTf (**Ru-6**) (Scheme 3.10). After a few hours the sample was checked by ^{31}P{^{1}H} NMR spectroscopy. The emergence of a new peak was observed at 45.9 ppm, which is downfield from **Ru-5** at 46.6 ppm. This is consistent with ^{31}P{^{1}H} NMR spectroscopic data of isolated **Ru-4**, which appears at 45.9 ppm. The chemical shifts of **Ru-4** and **Ru-6** should be extremely close as the electronics of the metal centre would not be greatly affected by the WCA present for charge balance.[54,55,74] After allowing this solution to sit at room temperature under an inert atmosphere for 30 h, 59% of **Ru-6** was generated. This test showed that the halide abstraction was feasible under these conditions, however, the signal-to-noise ratio decreased dramatically (Figure 3.6). Because these samples were intended to be used as the stock solution for the hydrofunctionalization reaction, the purity of the sample needed to be as close to 100% as possible. The decrease in signal-to-noise is an indicator of catalyst decomposition, therefore, altering the overall concentration of the stock solutions, thus providing incorrect catalytic loadings for hydroalkoxylation reactions, in addition to the 30-h reaction time being unfeasible.
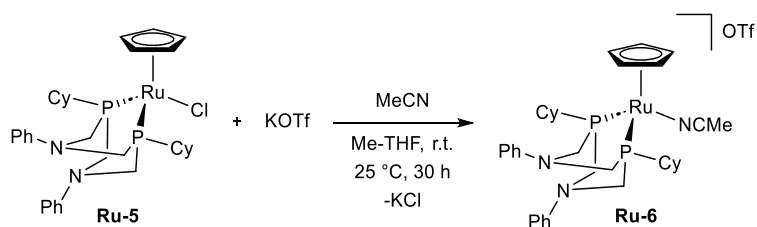
Scheme 3.10. Attempt at *in-situ* halide abstraction of **Ru-5** and KOTf.
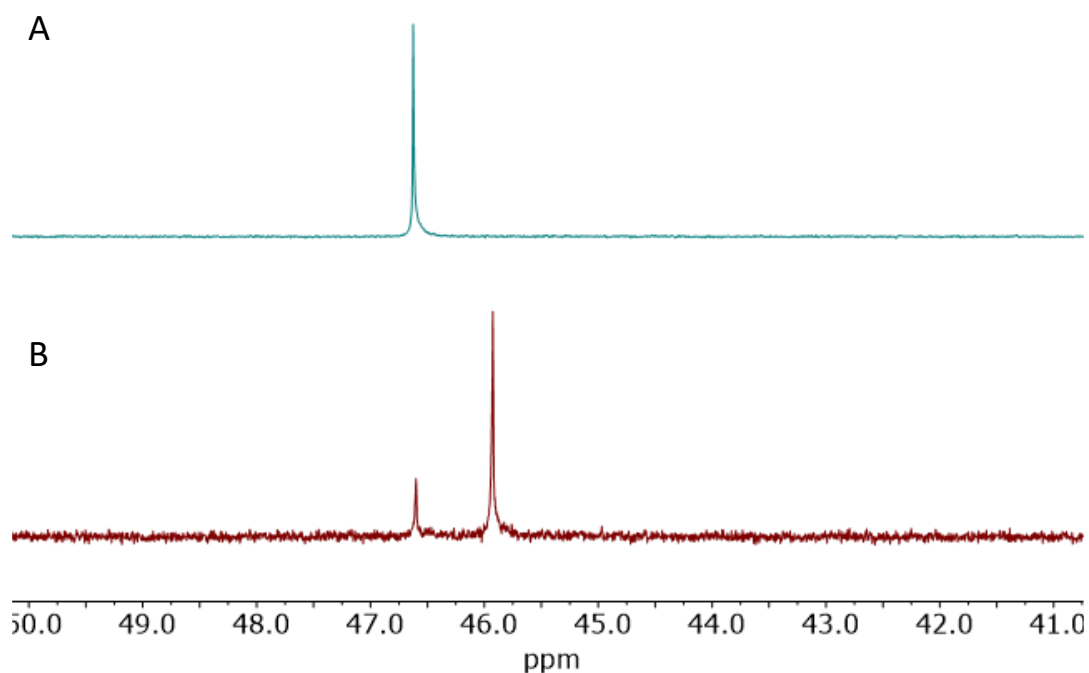
Figure 3.6. $^{31}P\{^1H\}$ NMR spectra (600 MHz, Me-THF) of A) **Ru-5;** and B) **Ru-5** combined with 10 equivalents of KOTf after 30 .

It was proposed that the formation of $[Ru(Cp)(P^{Cy}_2N^{Ph}_2)(NCMe)]OTf$ at elevated temperatures would occur quicker and could result in less decomposition. Therefore, **Ru-5** and KOTf were heated to 70 ºC for one h. A conversion of 32% to $[Ru(Cp)(P^{Cy}_2N^{Ph}_2)(NCMe)]OTf$ was observed by $^{31}P\{^1H\}$ NMR spectroscopy. The signal-to-noise ratio also decreased greatly likely resulting from decomposition, thus affecting the purity of this sample and making it not eligible for use as a stock solution for catalysis (Figure 3.7). The duration of reaction is too long, therefore, this methodology does not align with the desired criteria for these *in-situ* halide abstractions.
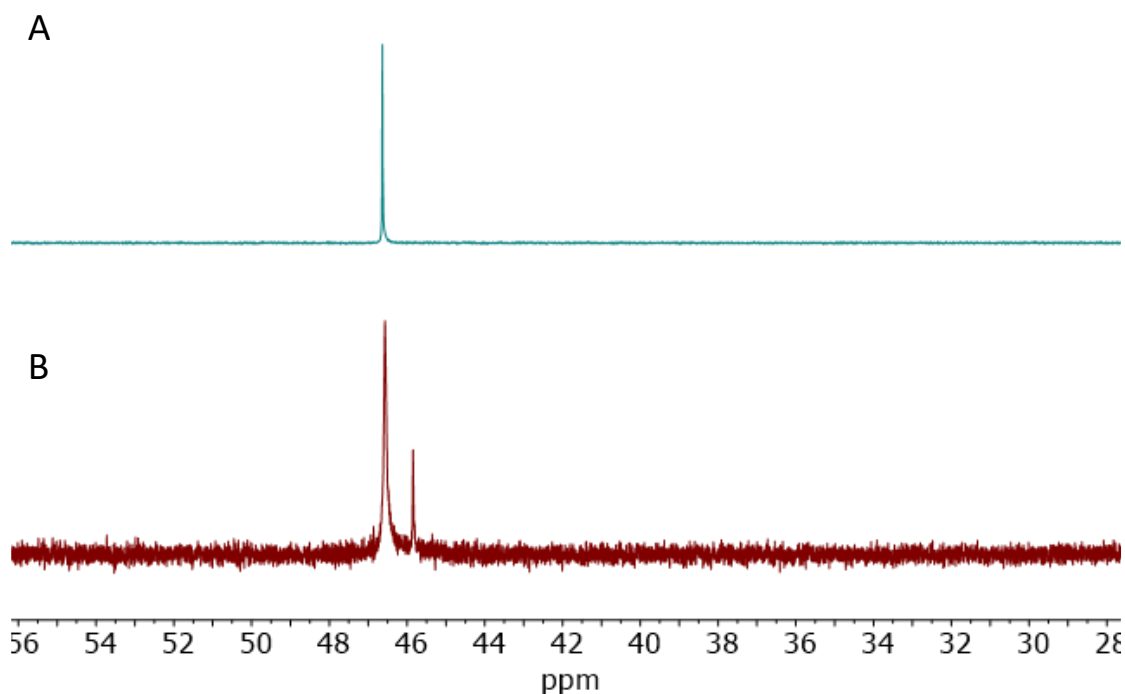
Figure 3.7. $^{31}P\{^1H\}$ NMR spectra (600 MHz, Me-THF) of a) **Ru-5**; and b) **Ru-5** combined with 10 equivalents of KOTf after 1 h after heating at 70 ºC.

It was then proposed that AgOTf would be a better candidate for the halide abstraction at elevated temperatures as there is a greater driving force due to the favourable formation of the AgCl byproduct rather than KCl potassium salts. **Ru-5** and AgOTf were combined in a mixture of MeCN and Me-THF and heated to 70 ºC for one h. No product formation was observed by $^{31}P\{^1H\}$ NMR spectroscopy, but many new sets of doublets appeared around 38 and 31 ppm (Figure 3.8). Due to the reaction complexity, this silver salt would not be a proper candidate for the *in-situ* halide abstractions. It was therefore decided that the halide abstraction would need to occur in the reaction vial with all components for catalysis present.
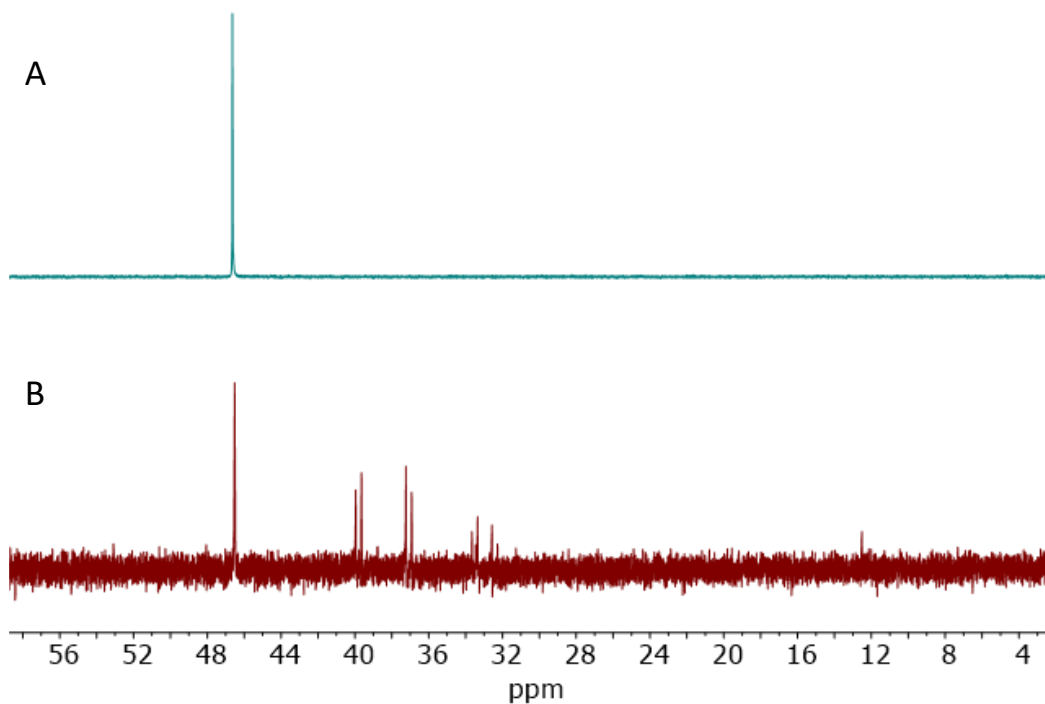
Figure 3.8. ^{31}P{^{1}H} NMR spectra (600 MHz, Me-THF) of A) **Ru-5**; and B) **Ru-5** combined with 10 equivalents of AgOTf after 1 h after heating at 70 ºC.

3.3.3 One Pot Halide Abstraction of **Ru-5** and Hydrofunctionalization of 2-EBA

Eight catalytic vials were prepared in a glovebox for the *in-situ* halide abstraction of **Ru-5** with the various WCAs for the hydrofunctionalization of 2-EBA (Scheme 3.11). The vials differed in their contents of potassium salt additive, MeCN and **Ru-4**. The reactions were heated at 70 ºC for 24 h, and then analyzed by GC-FID.
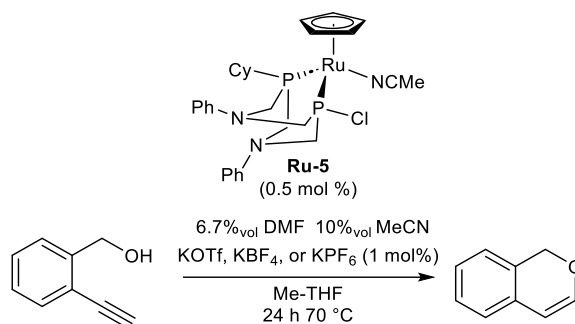
Scheme 3.11. *In-Situ* halide abstraction of **Ru-5** (0.5 mol%) with potassium salts KOTf, KBF$_4$, or KPF$_6$ (1 mol%), 6.7%$_{vol}$ DMF with or without 10%$_{vol}$ MeCN in Me-THF for 24 h at 70 ºC to generate the active catalyst species for the hydroalkoxylation of 2-EBA to isochromene.

The reaction of 2-EBA with 5 mol% **Ru-5** in the absence of any additives gave only 10% consumption of the starting material. The chloride ligand has very low lability which would have caused low conversions. Performing the same reaction with KOTf, KBF$_4$, or KPF$_6$ as additives gave 2-EBA conversions of 55, 30, and 66%, respectively. The increase in 2-EBA consumption when having these additives gives evidence that the halide abstraction occurred, and the active catalytic species was stabilized by MeCN. It is proposed that the PF$_6^-$ anion would be the least coordinating, followed by BF$_4^-$ followed by OTf$^-$ based on the atoms size and ability each anion had to delocalize the -1 charge about the entire ion.[54,74] The catalyst with counterion BF$_4^-$ gave the lowest conversion of 2-EBA, which was not expected. It was possible that BF$_4^-$ anion could have coordinated to the vacant coordination site of the active catalyst species through one of the fluorine substituents resulting in catalyst inhibition. It has been previously observed in this work and that of the Blacquiere group that halogenated solvents are not compatible with these complexes at elevated temperatures.[3,8,9,17,18,58] The catalyst with counterion KOTf$^-$ gave the second-best consumption of 2-EBA, which was not expected as it had less delocalization abilities compared to BF$_4^-$. PF$_6^-$ as the anion gave the highest consumption of 2-EBA at 67%, which was consistent with previously observed conversions when using **Ru-4** for the hydrofunctionalization of 2-EBA. When combining 2-EBA with the potassium salts in the absence of **Ru-5**, less than 10% consumption of 2-EBA was observed. A control reaction was performed by subjecting 2-EBA to catalytic conditions with the absence of any metal

complex or alkali salts. The error bars for the control reaction overlapped with the error bars of the reactions of 2-EBA with the potassium salt additives under catalytic conditions without any **Ru-5**. This proved that these potassium salts had no effect alone on the consumption of 2-EBA and **Ru-5** was required to perform the hydrofunctionalization reactions with high consumption of 2-EBA. A control reaction of 2-EBA, **Ru-5** with KPF_6 in only a mixture of DMF and toluene was performed to see the effect of having no acetonitrile present in the mixture. It was found that an average of 4% of 2-EBA was consumed over the allotted time. This result has two possible interpretations: 1) MeCN is required to generate the catalytic species, or 2) the vacant coordination site on the metal centre results in rapid decomposition of the catalytic species, and thus no catalytic conversion. Prior work has covered the thermal stabilities of complex **Ru-5** when heating the complex at 70 ºC. As previously stated in section 1.1, $[Ru(Cp)(P^{Ph}_2N^{Ph}_2)]^+$ complexes of this kind have the ability to stabilize their vacant coordination site in a ^{3}-(P, P, Ar) fashion.[3] However, this κ^3 coordination is rapidly displaces by addition of a Lewis base. Therefore, this coordination would be displaced by the addition of 2-EBA. MeCN may be required in the reaction to aid in the solvation of the potassium salts, although, solubility was not observed to be an issue. It is most likely that the halide abstraction did not occur at all under these conditions, thus, little catalytic activity was observed due to the low lability of the chloride ligand.
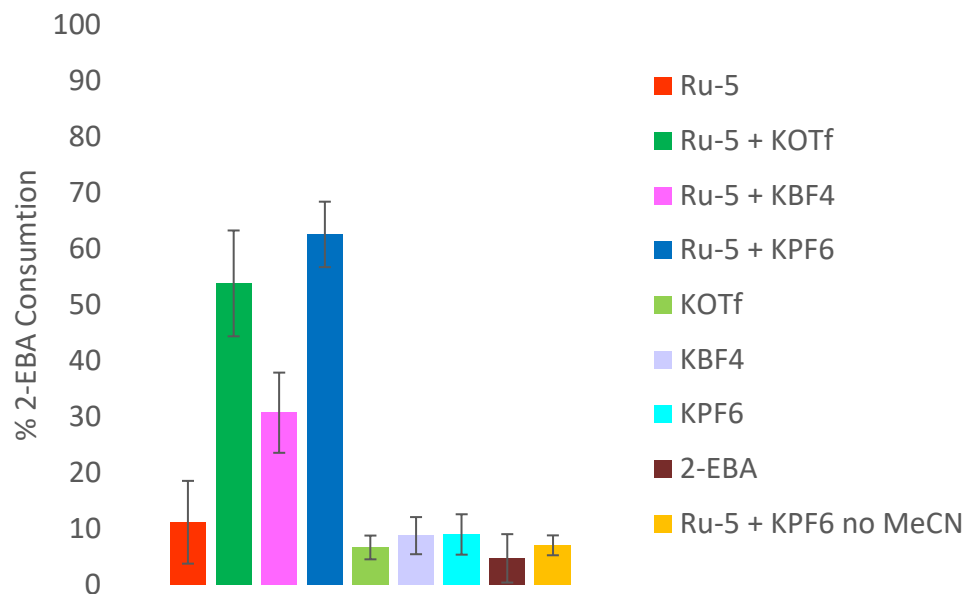
Figure 3.9. Results of the hydroalkoxylation of 2-EBA to isochromene using **Ru-5** and potassium salts.

3.4   Summary and Conclusion

In Chapter 3, it was demonstrated that electronic effects on the terminal alkyne under the selected conditions had negligible effect on metal-vinylidene rate formation. In contrast, a more sterically encumbered and electron rich metal centre has a higher rate of metal-vinylidene formation, suggesting that the RDS of vinylidene formation under these conditions is the dissociation of the labile MeCN ligand. Addition of alkali salts for the hydroalkoxylation of 2-EBA to isochromene results in a greater observed consumption of 2-EBA by GC-FID, emphasizing the importance of purity of the MLC complexes to ensure reproducible and reliable data. The PF_6^- WCA to the selected ruthenium cationic complex was found to give the greatest consumption of 2-EBA. This finding confirms that the best anion has been selected and used for these MLC complexes from previously established chemistry from the Blacquiere lab.

Chapter 4

4   Conclusions and Future Work

4.1   Conclusions

This research described in this thesis exploited the reactivity of various iron and ruthenium MLC complexes in order to gain greater understanding of their capabilities and search ways to improve reactivity.

In Chapter 2, complexes **Fe-1**, **Fe-2**, **Ru-1**, **Ru-2**, **Ru-3** were synthesized and reacted with phenyl acetylene to make vinylidenes *in-situ* to test their susceptibility towards nucleophilic attack by **1a**. **Ru-3**, the most electron poor and least sterically hindered MLC complex [Ru(Cp)($P^{Ph}_2N^{Ph}_2$)(NCMe)]PF_6 (**Ru-3**), was found to be the only complex whose vinylidene species was susceptible to nucleophilic attack of **1a**. Products from the stoichiometric reaction were unable to be isolated. The products of catalysis using **Ru-3** with dioxazolone **1a** and terminal alkyne **2a** were not found to form the desired *N*-acyl ketenimine, but rather, **Ru-3** and **1a** catalytically react to generate a large mixture of products that were not successfully separated. Trapping agents were employed in attempts to trap out the major product of catalysis between **Ru-3** and **1a**, where 1,2,4-triazole as the trapping agent gave the cleanest mixture of products. In order to understand the reaction pathway, a forced Curtius rearrangement was performed between 1,2,4-triazole and **1a**, where the major product of reaction was consistent with that of catalysis. Thus, indicating that complex **Ru-3** performs decarboxylative decomposition on **1a**. It is evident that the target chemistry cannot be performed with these MLC complexes. This means that these complexes are not able to perform nitrene-transfer chemistry with dioxazolones.

In Chapter 3, the rate of vinylidene formation with **Ru-3** and **Ru-4** as well as the capabilities for the hydroalkoxylation of 2-EBA with **Ru-4** and **Ru-5** were tested. A Hammett analysis was performed to gain further understanding on how the electronic parameters on terminal alkynes affect metal-vinylidene formation with **Ru-3** and alkynes **2a**, **2b**, **2c**, and **2d**. No distinct trends were found during this analysis. This was proposed to be the case as at the specified temperature MeCN ligand dissociation was the rate-

determining step. The steric and electronic effects of the rate of metal-vinylidene formation were then tested using **2a** and **2e** with **Ru-3**. The rate of vinylidene formation when using **2a** and **Ru-3** had a higher rate compared to vinylidene formation of **2e** and **Ru-3**. It was proposed that because **2e** is quite electron rich, the η^2-alkyne complex was the favoured configuration for vinylidene formation, resulting in a slow rate. The more electron rich and sterically encumbered **Ru-4** complex was found to have a higher rate of vinylidene formation than that of **Ru-3**. These vinylidene rate studies are essential to allow for selecting optimal conditions of reactions to obtain the highest yielding reactions. The hydroalkoxylation of 2-EBA by **Ru-4** with the addition of alkali salts was studied. It was found that when **Ru-4** and $NaPF_6$ are in solution together, the highest consumption of 2-EBA is observed. $LiPF_6$ and KPF_6 also increased 2-EBA consumption. It is proposed that the addition of alkali metals either aids in altering the isomerization of one of the six-membered amine rings of the $M-P_2N_2$ metallocycle or the salts themselves promote a different path of reactivity. This isomerization should allow for less steric hinderance about the vacant coordination site on the metal, and thus, more catalytic turnover. The addition of these salts also indicated that having impurities present in solution could generate false data. Therefore, it is important that catalyst purity is of utmost importance to obtain reliable, reproducible, and accurate results. In the absence of catalyst, the salts were observed to consume very small amounts of 2-EBA indicating that the salts themselves do not react with the substrate. The addition of alkali salts increase reactivity under these conditions. The *in-situ* halide abstraction of **Ru-5** using KOTf, KBF_4, and KPF_6 was performed. Products of these reactions were used towards the hydroalkoxylation of 2-EBA. It was found that the PF^- WCA gave the highest consumption of 2-EBA, which was expected. Interestingly, BF_4^- gave the lowest consumption of 2-EBA. This was rationalized by potential competitive coordination of the fluorine ions of the WCA to the metals vacant coordination site, resulting in catalyst inhibition. This revealed that the most optimal WCA has been used on the complexes made by the Blacquiere group.

4.2   Future work

Due to limited stocks of **1a**, complete characterization of the product formed by the Curtius rearrangement of **1a** with 1,2,4-triazole at elevated temperatures was not completed, but is

required. The proposed structure of the product has not yet been discovered. The synthesis of a single substrate containing both a dioxazolone and terminal alkyne functionalities must be completed. **1a** was found to be incompatible under the deprotecting reaction conditions and was later discovered that dioxazolones are incompatible with MeOH. Therefore, the TMS-protected terminal alkyne must be deprotected prior to dioxazolone formation. It is unknown whether terminal alkynes are stable under the conditions required to form dioxazolones. Therefore, the formation of dioxazolones on substrates containing terminal alkynes must be tested.
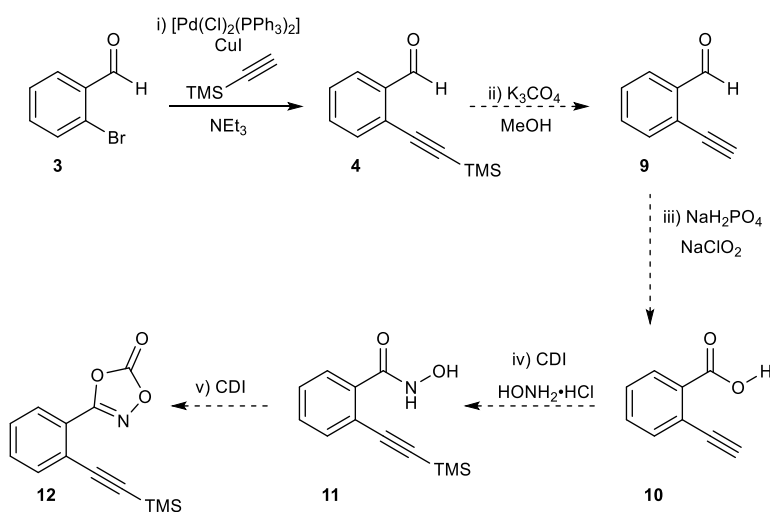
Scheme 4.1. Proposed formation of dioxazolone and terminal alkyne substrate by; i) sonogashira reaction of **3** to **4**; ii) removal of TMS-protecting group on **4** to generate **9**; iii) Pinnick Oxidation of **9** to generate carboxylic acid **10**; iv) installation of hydroxamic acid on **10** to generate **11**; V) cyclization of hydroxamic acid **11** to generate final dioxazolone **12**.

Validation of the rate determining step as the dissociation of MeCN for all vinylidene complexes at 70 ℃ should be confirmed. This can be evaluated by performing a VTNA study using **Ru-3** and phenylacetylene. By holding the concentration of **Ru-3** constant, the concentration of phenylacetylene can be altered. This data can be plotted on a graph with the X-axis labeled [phenylacetylene] and the Y-axis labelled d[Phenylacetylene]/d[time]. The same analysis can be performed for **Ru-3**. If there is a positive linear slope on the **Ru-3** graph, that would indicate that it is participating in the rate determining step. If this is the

case, the same data would need to be acquired at increasing temperatures to find the temperature where the rate determining step for vinylidene formation is dependent on both phenylacetylene and **Ru-3**. If the rate determining step is MeCN dissociation, the slope of the line for the graph for phenylacetylene should equal zero and the slope of the line for **Ru-3** should be positive and linearly increase. Once this is completed, it can be determined if and how sterics and/or electronics play a role in vinylidene formation. The greatly increased consumption of 2-EBA with the NaPF$_6$ salt additive with **Ru-4** should be further evaluated to determine if the proposed boat-to-chair isomerization was occurring. This can be done by performing a ^{31}P{^{1}H} NMR spectroscopic analysis of a mixture of **Ru-4** and NaPF$_6$. Na$^+$ will withdraw electron density from the pendant amines and therefore, from the phosphorus atoms of the P$_2$N$_2$ ligand. This is expected to result in an upfield shift from the starting MeCN complex to the chair complex. Attempts to crystalize the product should also be attempted to further characterize the product by crystallography. If the salts are found to have this isomerization effect of the P$_2$N$_2$ ligand, their catalytic capabilities for hydrofunctionalization reactions can be improved and should be revisited. It was suggested that the product of these reactions was the Markovnikov product, which could possibly have the same retention time as isochromene. This Markovnikov product should be injected into the GC-FID instrument in order to validate this hypothesis, If the two products do overlap in the chromatograph using the selected method, the products of the reaction should be analyzed using ^{1}H NMR spectroscopy. Finally, additional WCAs should be used with **Ru-5** for the hydroalkoxylation of 2-EBA. The trends found in this study were not as expected, where BF$_4$$^-$ gave lower overall consumption of 2-EBA in comparison to OTf$^-$. Using more WCAs containing halogens such as BAr^{F-}, TFA$^-$, or SbF$_6$$^-$ will give more information on the role they play, if any, during catalysis. These insights promise to enhance comprehension of the capabilities and applications inherent in these MLC complexes. Their potential for application in the synthesis of novel target products may be investigated for innovative methodologies or organic transformations employing inorganic compounds.

Chapter 5

5 Experimental

5.1 General Experimental Procedure

Unless otherwise stated, all reactions were conducted under an inert argon or nitrogen atmosphere following standard Schlenk line or glovebox techniques, respectively. All NMR tubes and glassware were dried in an oven at 150 °C for at least 3 h and cooled under an inert atmosphere or vacuum before use. Unless otherwise stated, all solvents were dried and degassed using an Innovative Technology 400-5 Solvent Purification system, degassed by bubbling with argon. Solvents were stored over activated 4 Å molecular sieves for at least 24 h except acetonitrile, ethanol, and methanol, which were stored over activated 3 Å molecular sieves before use. Molecular sieves were purchased from Fluka and activated under vacuum at 150 °C for at least 12 h prior to use. $CDCl_3$ and C_6D_5Br were degassed and stored over activated 4 Å sieves. CD_2Cl_2, $(CD_6)_2O$, C_6D_6, and $C_6D_5CD_3$ were purchased from Sigma Aldrich as ampules and used directly without anu purification under an inert atmosphere. All other reagents were purchased from Alfa Aesar, Sigma Aldrich, or Fisher Scientific and used without any further purification unless otherwise stated. $RuCl_3 \cdot (H_2O)_x$ was left overnight under vacuum at room temperature to remove excess water and re-weighed prior to use.

All NMR spectra were recorded on a Bruker 400, Bruker 600 MHz, or INOVA 600 MHz instrument at 25 °C unless stated otherwise. ^1H NMR spectra were acquired in $CDCl_3$, $(CD_6)_2O$, C_6D_6, $C_6D_5CD_3$, and C_6D_5Br and were referenced internally against the residual solvent signal ($CHCl_3$ at 7.26 ppm, $(CD_6)_2O$ at 2.09 ppm, C_6D_6 at 7.15 ppm, $C_6D_5CD_3$ at 7.09 ppm, and C_6D_5Br at 7.19 ppm) to tetramethylsilane (0 ppm). $^{31}P\{^1H\}$NMR spectra collected in proteo solvents were referenced externally to TMS (0 ppm) or an internal standard triphenylphosphine oxide (29.23 ppm). Assigned multiplicities are abbreviated as: singlet (s), doublet (d), triplet (t), and multiplet (m). Infrared spectra were collected on solid samples using a Bruker ALPHA II FTIR spectrometer. Catalytic performance was measured using an Agilent 7890a gas chromatograph instrument with flame ionization detector (GC-FID), fitted with an HP-5 column.

5.2 Synthesis of Substrates

5.2.1 Synthesis of 3-Phenethyl-1,2,4-dioxazol-5-one (**1a**)

The preparation for the two-step synthesis follows a known literature procedure.[40] The only difference was the purification of the final crude material *via* crystallization from hexanes (15 mL) by dissolving the material in and storing it in the freezer for 1-24 h to afford **1a** (white crystalline solid, 804 mg, 4.21 mmol, 76% yield). ^{1}H NMR (600 MHz, CDCl$_3$) δ: 7.33 (t, *J* = 7.2 Hz, 2H), 7.29-7.23 (m, 1H), 7.19 (d, *J* = 7.2 Hz, 2H), 3.03 (t, *J* = 7.6 Hz, 2H), 2.94 (t, *J* = 7.6 Hz, 2H).

5.2.2 Synthesis of 3-Phenyl-1,2,4-dioxazol-5-one (**1b**)

The preparation for the two-step synthesis follows a known literature procedure.[40] The only difference was the purification of the final crude material *via* crystallization in hexanes by dissolving the material in 15 mL and storing it in the freezer for 1-24 h to afford **2a** (white crystalline solid, (345 mg, 2.12 mmol, 71% yield). ^{1}H NMR (600 MHz, CDCl$_3$) δ: 7.89 – 7.85 (m, 2H), 7.69 – 7.63 (m, 1H), 7.58 – 7.53 (m, 2H).

5.2.3 Attempted Synthesis of Intramolecular Species **8**

2-(Trimethylsilyl)ethynyl]benzaldehyde (**4**) was synthesized following literature protocols of a sonogashira reaction and obtained in good yield, (777 mg, 3.84 mmol, 71% yield).[70] The crude material **4** was subjected to the Swern oxidation to afford 2-(Trimethylsilyl)ethynyl]benzoic acid (**5**) following literature protocols and obtained in excellent yield, (800 mg, 3.66 mmol, 95% yield).[71] **5** was used to afford 2-(Trimethylsilyl)ethynyl]hydroxamic acid (**6**) following a modified literature protocol.[40] Further purification was required, therefore, a gradient column was performed using an eluent system of 100% hexanes to 75:25 ratio of hexanes to ethyl acetate to afford product **6** in poor yield, (yellow oil, 65 mg, 0.28 mmol, 10% yield), ^{1}H NMR (600 MHz, CDCl$_3$) δ: 7.88 (d, *J* = 7.2 Hz,1H), 7.6 (d, *J* = 7.6 1H), 7.48 (d, *J* = 7.6 1H), 7.39 (t, *J* = 7.2 1H), 3.61 (m, 1H), 2.05 (m, 1H) 0.24 (s, 9H).

5.3 Synthesis of MLC Complexes

5.3.1 Synthesis of [Fe(Cp*)(P$^{Ph}_2$N$^{Ph}_2$)(NCMe)]PF$_6$ (**Fe-2**)

Fe-2 was synthesized following a modified literature procedure.[58] The workup and purification differed where the crude mixture was filtered through Celite, and the Celite was washed with DCM (50 mL) until the washings were clear. The solvent of the filtrate was removed, and the crude material was washed with Et$_2$O (3 x 5 mL) and the solid was dried under vacuum, (red solid, 103 mg, 0.12 mmol, 54%). ^{1}H NMR spectroscopic data matched that of literature.

5.3.2 Synthesis of [Ru(Cp*)(P$^{t-Bu}_2$N$^{Ph}_2$)(NCMe)]PF$_6$ (**Ru-1**)

Ru-1 was synthesized following a literature procedure.[17] **Ru-1** was obtained (red solid, 0.589 g, 0.72 mmol, 60% yield) where ^{1}H NMR matched that of literature.

5.3.3 Synthesis of [Ru(Cp)(P$^R_2$N$^{Ph}_2$)(NCMe)]PF$_6$ (**Ru-2**, **Ru-3** & **Ru-4**)

Ru-2, **Ru-3**, and **Ru-4** were synthesized following a modified literature procedure.[3,9,17]

[Ru(Cp)(P$^{t-Bu}_2$N$^{Ph}_2$)(NCMe)]PF$_6$ (**Ru-2**) spectroscopic data matched that of literature (reddish-orange solid, 180 mg, 0.24 mmol, 76% yield).

[Ru(Cp)(P$^{Ph}_2$N$^{Ph}_2$)(NCMe)]PF$_6$ (**Ru-3**) spectroscopic data matched that of literature (reddish-orange solid, 206 mg, 0.26 mmol, 47% yield).

[Ru(Cp)(P$^{Cy}_2$N$^{Ph}_2$)(NCMe)]PF$_6$ (**Ru-4**) spectroscopic data matcher that of literature (red solid, 174 mg, 0.21 mmol, 17% yield).

5.3.4 Synthesis of Ru(Cp)(P$^{Cy}_2$N$^{Ph}_2$)Cl (**Ru-5**)

Ru-5 was synthesized following a modified literature procedure.[9] Spectroscopic data matched that of literature (yellow powder, 213 mg, 0.31 mmol, 23% yield).

5.4 Reaction Procedures

5.4.1 General Procedure for Stoichiometric Reactions of Metal-Vinylidenes and Dioxazolone **1a**

In a glovebox, stock solutions for dioxazolone **1a** (150 mM), phenylacetylene (**2a**) (200 mM), and the transition metal complexes **Fe-1**, **Fe-2**, **Ru-1**, **Ru-2**, and **Ru-3** (250 mM) were made in anisole. Metal complex (250 µL) and **2a** (150 µL) were taken from the stock solutions, combined in an NMR tube, and placed in a pre-heated 110 °C oil bath for 2-5 h to form the metal-vinylidene. The reaction was monitored by $^{31}P\{^1H\}$ NMR spectroscopy. Once complete conversion was observed, **1a** (200 µL) was added to the tube, which was then heated in a pre-heated oil bath set to 70 °C for 1-24 h until a new complex, regeneration of the transition-metal complex, or no reactivity was observed by $^{31}P\{^1H\}$ NMR spectroscopy.

5.4.2 General Catalytic Procedures for NMR Scale Reactions with **Ru-3**, **1a**, and **2a**

In a glovebox, stock solutions of substrates dioxazolone **1a** and phenylacetylene **2a** (600 mM) were prepared in anisole. A catalyst stock solution of $[Ru(Cp)(P^{Ph}_2N^{Ph}_2)(NCMe)]PF_6$ (**Ru-3**) (35 mM) was prepared in anisole. A screw cap vial (4 mL) containing a stir bar was charged with 150 µL of each stock solution and topped off with anisole to a total volume of 600 µL for use as a time = 0 sample. A separate screw cap vial (4 mL) containing a stir bar was charged with 150 µL of each substrate stock solution, 129 µL of the metal complex stock solution and topped off with anisole to obtain a total volume of 600 µL. The vial was capped, sealed with electric tape, removed from the glovebox and heated to 70 °C for 24 h on a metal heating block. Once time had elapsed, the vial was removed from the heat, opened to ambient air, and placed under vacuum to remove the solvent. The dried crude material was washed with ether (3 x 10 mL) to separate the organic products from the metal complex, and ^1H NMR spectroscopic data was acquired from the obtained products.

5.4.3 Control Reactions with **1a** and Trapping Agents

In a glovebox, stock solutions of dioxazolone **1a** (600 mM) , phenylacetylene **2a** (600 mM) and each trapping reagents 1-butyric acid, 4-acetamidobenzene sulfonylazide, 2,3-

dimethyl-1,3-butadiene, 3-methyl-1-butanol, 1,2,4-triazole, 4-phenyl-1,2-triazoline-3,5-dione, and TMS-azide (1200 mM) were prepared in Me-THF, respectively. In a 4 mL screw cap vial equipped with a stir bar, 150 µL stock solutions of **1a** and **2a** were added to nine different vials. 150 µL of each trapping agent was added to one of the nine vials and topped off with 150 µL of Me-THF. The vials were capped and secured with electrical tape, removed from the glove box and left to stir for 24 h on a pre-heated heating block at 70 °C. After the time had elapsed, the solvent was removed under vacuum and the products were analyzed by ^{1}H NMR spectroscopy.

5.4.4   Catalytic Reaction with **1a**, 1,2,4-Triazole, and **Ru-3**

In a glovebox, stock solutions of **1a** (600 mM) and 1,2,4-triazole (1200 mM) were prepared in Me-THF. A stock solution of **Ru-3** (35 mM) was prepared in anisole. In a 4 mL screw cap vial equipped with a stir bar, 150 µL of each stock solution of **1a**, 1,2,4-triazole, **Ru-3** was added, along with 50 µL of Me-THF. The vial was capped and secured with electrical tape, removed from the glove box, and left to stir for 24 h on a pre-heated heating block at 70 °C. After the time had elapsed, the solvent was removed under vacuum and the organics were separated by washing the solids with ether (3 x 15 mL). The organic products were dried *in-vacuo* and observed using ^{1}H NMR spectroscopy.

5.4.5   Curtius Rearrangement with **1a** and 1,2,4-Triazole

In a 100 mL round-bottom-flask equipped with a stir bar, **1a** (100 mg, 0.529 mmol, 1 equiv.) and 1,2,4-triazole (364 mg, 5.29 mmol, 10 equiv.) were dissolved in anisole (10 mL). The flask was heated to 110 ºC and left to stir for 24 h. The mixture was cooled to room temperature and filtered through Celite. The solvent was removed *in-vacuo* to afford a crude mixture. The crude mixture was dissolved in hexanes (30 mL) and filtered through silica and the solvent was removed *in-vacuo* to afford a yellow solid which was analyzed by ^{1}H NMR spectroscopy.

5.4.6   General Procedure for Rate Analysis of Vinylidene Formation

In a glovebox, stock solutions of **Ru-3** or **Ru-4** (120 mM), O=PPh$_3$ (160 mM), and terminal alkyne   phenylacetylene,   4-ethynyl   toluene,   4-ethynyl   anisole,   4-

(trifluoromethyl)phenylacetylene, or 1-octyne (1200 mM) were prepared in anisole, in separate 4 mL vials. Portions of **Ru-3** or **Ru-4** (250 µL) and of O=PPh$_3$ (250 µL) stock solutions were combined in an NMR tube sealed with electrical tape. The tube was capped, secured with electrical tape, and removed from the glove box to obtain the first time point. The NMR tube was brought back into the glovebox and the terminal alkyne stock solution (100 µL) was added to the tube to reach a total volume of 600 µL. The tube was capped, sealed with electrical tape and brought out of the box, loaded in an I600 NMR instrument and heated to 70 °C. The instrument was heated from 25 ℃ to 70 ℃ over a 10-minute time span. After five additional minutes the spectrometer equilibrated to the desired temperature. Time points were taken every 10 minutes for 1.5 h. Conversion of the acetonitrile complex to the vinylidene was calculated *via* integration of the P$_2$N$_2$ ligand peaks for each complex relative to the internal standard. The integration value of the internal standard was set to 1, and the SM$_{tot}$ value was acquired by dividing the integration of the MeCN complex at t=0 to that of the internal standard. Integrations of both **Ru-3** and each vinylidene complex were acquired at each time point. To determine concentration of each species at each time point, the integration of the species was divided by the SM$_{tot}$ value and multiplied by 100 to give the percent concentration of each species at each time point. This was repeated three times to ensure reproducibility and accuracy, and the average values of all three runs were plotted to acquire the slope from time 20 to 80 minutes, or rate, of vinylidene formation. The slope of each run was then compared directly to that of the slope when using phenylacetylene for vinylidene formation. The log of their ratio was then plotted to observe the electronic trends with respect to their σ values in a Hammett analysis (Figure 3.1).

Equation 5.1. Equations for calculating percent starting material and percent vinylidene by ^{31}P{^{1}H} NMR spectroscopy with IS as O=PPh$_3$ where the integral of IS was set to one, SM as **Ru-3** or **Ru-4**, and V as the vinylidene of **Ru-3** or **Ru-4** with phenylacetylene, 4-ethynyl toluene, 4-ethynyl anisole, 4-(trifluoromethyl)phenylacetylene, or 1-octyne.

$$SM_{tot} = SM_0/IS_0$$

$$\%SM = (SM_t/SM_{tot})*100\%$$

$$\%V = (V_t/SM_{tot})*100\%$$

Table 5.1 Ru-3 consumption and vinylidene formation using phenylacetylene (**2a**).

Time (min)	Run 1		Run 2		Run 3	
	%SM$_t$ $\delta = 44.4$ ppm	%V$_t$ $\delta = 42.4$ ppm	%SM$_t$	%V$_t$	%SM$_t$	%V$_t$
0	100	0	100	0	100	0
10	97.26	5.48	95	3.33	92.65	8.83
20	86.30	10.96	86.67	8.33	86.76	11.76
30	87.67	13.69	86.67	10	85.29	13.23
40	79.45	16.43	78.33	15	79.41	20.58
50	68.49	23.28	71.67	21.67	75	26.47
60	67.12	28.76	69.67	23.33	73.52	30.88
70	64.38	32.89	65	28.33	69.11	32.45
80	60.27	38.35	61.67	30	66.17	35.29

Table 5.2. **Ru-3** consumption and vinylidene formation using 4-ethynyl anisole (**2b**).

Time (min)	Run 1		Run 2		Run 3	
	$\%SM_t$ $\delta = 44.4$ ppm	$\%V_t$ $\delta = 43.0$ ppm	$\%SM_t$	$\%V_t$	$\%SM_t$	$\%V_t$
0	100	0	100	0	100	0
10	93.87	7.14	98.61	4.16	97.14	4.29
20	90.81	9.18	95.83	11.11	95.71	5.71
30	85.71	13.26	88.88	13.88	90	12.85
40	80.61	17.34	83.33	19.44	85.71	17.14
50	75	21	80.55	20.83	84.28	21
60	73	22	73.61	27.77	78.57	24.28
70	69	28	72.22	30.55	75.71	27.14
80	65	29	68.05	30.55	71.43	30

Table 5.3. **Ru-3** consumption and vinylidene formation using 4-ethynyl toluene (**2c**).

Time (min)	Run 1		Run 2		Run 3	
	%SM$_t$ $\delta = 44.4$ ppm	%V$_t$ $\delta = 42.5$ ppm	%SM$_t$	%V$_t$	%SM$_t$	%V$_t$
0	100	0	100	0	100	0
10	98.27	5.17	96.92	3.08	95.45	2.27
20	93.10	6.89	89.23	9.23	92.90	9.09
30	87.93	10.34	84.61	10.53	91.78	11.36
40	86.20	13.79	78.84	12.30	90.90	13.63
50	75.86	17.24	73.46	21.54	82.40	15.91
60	72.41	22.41	70.84	23.01	77.27	17.48
70	70.69	24.13	69.23	27.23	75	27.59
80	68.96	27.58	68.75	29.69	74.98	21.27

Table 5.4. **Ru-3** consumption and vinylidene formation using 4-(trifluoromethyl)phenylacetylene (**2d**).

Time (min)	Run 1		Run 2		Run 3	
	%SM$_t$ $\delta = 44.4$ ppm	%V$_t$ $\delta = 41.7$ ppm	%SM$_t$	%V$_t$	%SM$_t$	%V$_t$
0	100	0	100	0	100	0
10	97.05	1.47	95.41	1.83	100	5
20	94.12	2.34	94.49	5.50	92.45	5.32
30	95.58	4.46	92.74	0.91	93.45	8.33
40	88.23	6.94	93.24	6.42	92.45	11.67
50	95.58	10.29	87.16	8.25	84.56	18.33
60	89.70	11.78	84.40	11.92	85.24	14.24
70	83.17	13.25	86.23	11.01	83.28	17.67
80	77.94	13.94	75.23	12.84	79.26	15.23

Table 5.5. **Ru-3** consumption and vinylidene formation using 1-octyne (**2e**).

Time (min)	Run 1		Run 2		Run 3	
	%SM$_t$ $\delta = 44.4$ ppm	%V$_t$ $\delta = 45.8$ ppm	%SM$_t$	%V$_t$	%SM$_t$	%V$_t$
0	100	0	100	0	100	0
10	98.30	1.69	99.85	1.51	98.53	1.47
20	96.61	2.45	95.45	4.45	97.06	4.41
30	94.35	5.98	92.42	6.06	92.64	5.88
40	92.18	6.77	89.59	10.60	89.71	10.29
50	88.13	16.94	87;87	13.63	85.29	13.23
60	88.13	16.94	85.98	15.15	80.89	14.71
70	82.48	18.46	83.33	18.18	80.89	17.64
80	80.14	20.33	81.81	19.70	79.41	19.11

Table 5.6. **Ru-4** consumption and vinylidene formation with phenylacetylene (**2a**).

Time (min)	Run 1		Run 2		Run 3	
	%SM$_t$ $\delta = 45.9$ ppm	%V$_t$ $\delta = 44.8$ ppm	%SM$_t$	%V$_t$	%SM$_t$	%V$_t$
0	100	0	100	0	100	0
10	99.63	9.23	99.79	3.99	95.46	8.69
20	90.77	14.14	95.79	16.18	91.32	12.84
30	85.86	21.71	83.82	24.16	87.16	21.14
40	78.39	27.85	75.84	34.14	78.86	29.44
50	73.14	33.98	65.86	38.43	70.56	31.52
60	66.02	36.75	61.57	40.13	68.48	36.50
70	63.25	42.87	59.87	44.12	58.94	41.01
80	57.12	47.11	55.88	50.12	53.96	46.04

5.4.7 Rate Data for Vinylidene Formation

The rates of each vinylidene substrate were extrapolated from each curve of time (min) v.s. % vinylidene formation from 20 to 80 minutes. The Hammett analysis was conducted taking the slope of each line for vinylidene formation with phenylacetylene, 4-ethynylanisole, 2-ethynyltoluene, and 4-(trifluoromethyl)phenylacetylene with **Ru-3** and inoutting the data into Equation 2. K is the slope of each rate line, respectively. This data was plotted on a graph where the σ values correspond to each substituent on the terminal alkyne backbone.

Equation 5.2. Hammett analysis calculation.

$$Log(K_{Phenylacetylene}/K_{substrate})$$

5.5   Hydrofunctionalization Data

5.5.1   2-EBA Calibration Curve

A calibration curve was constructed by preparing vials of 2-EBA differing in concentrations ranging from 0 mM to 15 mM in GC vials using a dilution scheme. A stock solution of 2-EBA (100 mM) in MeCN was prepared. 0, 5, 10, 20, 50 100, and 150 µL of this solution was dispensed into separate GC vials. Each vial was topped off with the appropriate amount of MeCN to obtain an overall volume of 1000 µL. The vials were then loaded into the GC-FID instrument for analysis. Each vial was run twice to ensure accuracy. Each vial corresponded to a peak area on the spectrometer. This process was repeated three times to get reliable data and ensure consistency in sample preparation. There is a clear linear positive correlation between the increasing concentration of 2-EBA and peak area, validating the method.

Table 5.7 Dilution scheme for construction of 2-EBA calibration curve.

Vial	2-EBA (100 mM) Stock Solution added (µL)	MeCN added (µL)
1	0	1000
2	5	995
3	10	990
4	20	980
5	50	950
6	100	900
7	150	850
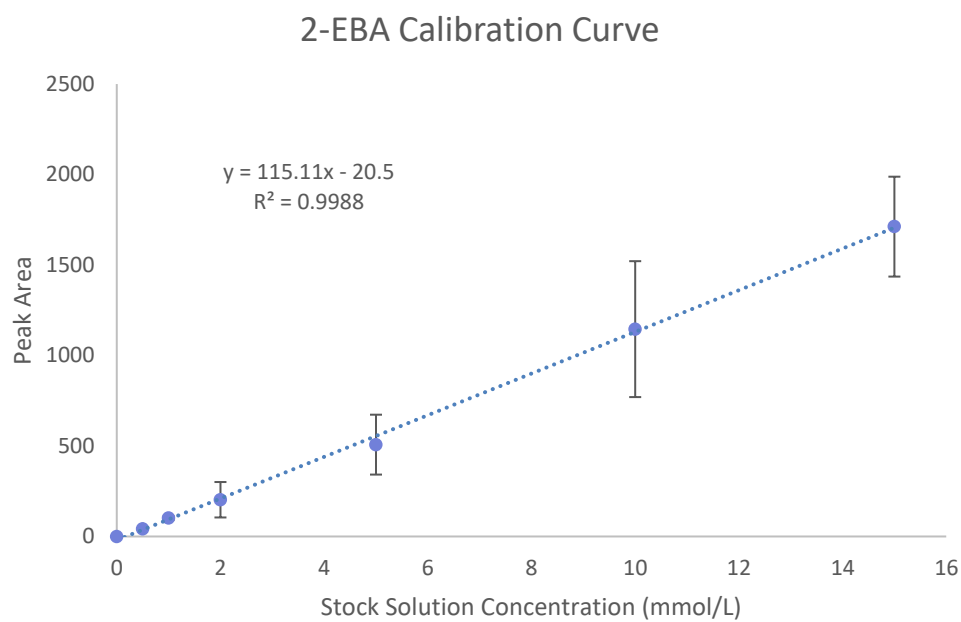
Figure 5.1. Calibration curve for 2-EBA.

5.5.2 General Procedure for Hydroalkoxylation of 2-EBA with Alkali Salt Additives

In a glovebox, stock solutions of **Ru-4** (15 mM) in acetone, alkali salts (80 mM) in DMF, 2-EBA (300 mM) and tetralin (390 mM) in Me-THF were prepared. 20 µL of the **Ru-4** stock solution was dispensed into four clean 4 mL vials and the solvent was removed *in-vacuo*. 38 µL was then added to the "cat" vial. 38 µL of each alkali salt stock solution mixture was dispensed into two 4 mL vials, one containing **Ru-4** and one absent from any catalyst. 200 µL of the 2-EBA and tetralin stock solution mixture was dispensed into all eight 4 mL vials. The vials were then each topped up with Me-THF to obtain a final volume of 600 µL. The vials were closed and secured with electrical tape, brought out of the glovebox and left on a pre-heated heating block at 70 ºC for 24 h. Once the time had elapsed, the vials were opened to air. 100 µL of each sample was dispensed into separate GC vials. Each vial was topped off with 900 µL of MeCN and loaded onto the GC-FID instrument. Each sample was run twice to ensure reproducibility. The experiment was repeated in triplicate to ensure accuracy and reproducibility.

Table 5.8. Alkali salt additive test: hydroalkoxylation of 2-EBA catalytic vial contents.

Contents of Stock Solutions	Catalytic Vials								
	T_0	Cat	Cat + NaPF$_6$	Cat + LiPF$_6$	Cat + KPF$_6$	NaPF$_6$	LiPF$_6$	KPF$_6$	2-EBA
Ru-4	X	✓	✓	✓	✓	X	X	X	X
2-EBA and Tetralin	✓	✓	✓	✓	✓	✓	✓	✓	✓
NaPF$_6$	X	X	✓	X	X	✓	X	X	X
LiPF$_6$	X	X	X	✓	X	X	✓	X	X
KPF$_6$	X	X	X	X	✓	X	X	✓	X

5.5.3 General Procedure for *In-Situ* Halide Abstraction of **Ru-5** for the Hydroalkoxylation of **2-EBA**

In a glovebox, stock solutions of **Ru-5** (7.5 mM) in a mixture of Me-THF, MeCN, and DMF, alkali salts (50 mM) in DMF, 2-EBA (600 mM) and tetralin (770 mM) in Me-THF were prepared. 40 µL of the **Ru-5** stock solution was dispensed into four clean 4 mL vials. 10 µL of each alkali salt stock solution mixture was dispensed into two 4 mL vials, one containing **Ru-5** and one absent from any catalyst. 100 µL of the 2-EBA and tetralin stock solution mixture was dispensed into all nine 4 mL vials. The vials were then each topped up with Me-THF to obtain a final volume of 600 µL. The vials were closed and secured with electrical tape, brought out of the glovebox and left on a pre-heated heating block at 70 ºC for 24 h. Once the time had elapsed, the vials were opened to air. 100 µL of each sample was dispensed into separate GC vials. Each vial was topped off with 900 µL of MeCN and loaded onto the GC-FID instrument. Each sample was run twice to ensure

reproducibility. The experiment was repeated in triplicate to ensure accuracy and reproducibility.

Table 5.9. Coordinating different WCAs to **Ru-5**: hydroalkoxylation of 2-EBA catalytic vial contents.

Contents of Stock Solution	Catalytic Vials								
	T_0	Cat	Cat + KOTf	Cat + KBF$_4$	Cat + KPF$_6$	KOTf	KBF$_4$	KPF$_6$	2-EBA
Ru-4	X	✓	✓	✓	✓	X	X	X	X
2-EBA and Tetralin	✓	✓	✓	✓	✓	✓	✓	✓	✓
KOTf	X	X	✓	X	X	✓	X	X	X
KBF$_4$	X	X	X	✓	X	X	✓	X	X
KPF$_6$	X	X	X	X	✓	X	X	✓	X

6 References

(1) Woodrick, M. D.; Hu, X., *Nat. Rev. Chem.,* **2017**, *2* (0099), 1-7.

(2) Wiedner, E. S.; Appel, A. M.; Raugei, S.; Shaw, W. J.; Bullock, M., *Chem. Rev.* **2022**, *122* (14), 12427-12474

(3) Chapple, D. E.; Boyle, P. D.; Blacquiere, J. M., *Chem. Cat. Chem.*, **2021**, *31* (17), 3789-3800.

(4) Lynam, J. M., *Chem. Eur. J.*, **2010**, *16* (28), 8238-8247.

(5) Antonova, A. B.; Kovalenko, S. V; Korniyets, E. D.; Johansson, A. A.; Struchkov, Y. T.; Ahmedov, A. I.; Yanovsky, A. I., *J. Org. Chem.*, **1983**, *244* (1), 35-45.

(6) Roh, S. W.; Choi, K.; Lee, Chulbom, L., *Chem Rev.*, **2019**, *119* (6), 4293-4356.

(7) Bruneau, C.; Dixneuf, P. H., *J. Am. Chem. Soc.,* **1999**, *32* (4), 311-323.

(8) Bridge, B. J.; Boyle, P. D.; Blacquiere, J. M., *Organometallics*, **2020**, *39* (14), 2570-2574.

(9) Chapple, D. E.; Hoffer, M. A.; Boyle, P. D.; Blacquiere, J. M., *Organometallics*, **2022**, *41* (12), 1532-1542

(10) Jiménez-Tenorio, M.; Carmen Puerta, M.; Valerga, P.; Moreno-Dorado, J.; Guerra, F. M.; Massanet, G. M., *J. Am. Chem. Soc.*, **2021**, *1* (22), 2324-2325.

(11) Nair, R. N.; Lee, P. J.; Rheingold, A. L.; Grotjahn, D. B., *Eur. J. Chem.*, **2010**, *16* (27), 7992-7995.

(12) Watanabe, T.; Mutoh, Y.; Saito, S., *J. Am. Chem. Soc.,* **2017**, *139* (23), 7749-7752.

(13) Varela-Fernández, A.; Varela, J. A.; Saá, C., *Adv. Synth. Catal.*, **2011**, *353* (11), 1933-1937.

(14) Pickup, O. J. S.; Khazal, I.; Smith, E. J.; Whitwood, A. C.; Lynam, J. M.; Bolaky, K.; King, T. C.; Rawe, B. W.; Fey, N., *Organometallics*, **2014**, *33* (7), 1751-1761

(15) Arita, A. J.; Cantada, J.; Grotjahn, D. B.; Cooksy, A. L., *Organometallics,* **2013**, *32* (23), 6867–6870.

(16) Cadierno, V., *J. Org. Chem.*, **2020**, *11-12*, 886-898.

(17) Stubbs, J. M.; Chapple, D. E.; Boyle, P. D.; Blacquiere, J. M., *Chem. Cat. Chem.*, **2018**, *10* (17), 3694–3702.

(18) Stubbs, J. M.; Bridge, B. J.; Blacquiere, J. M., *Dalton Trans.* **2019**, *48* (22), 7928–7937.

(19) Gong, L.; McAllister, M. A.; Tidwell, T. T., *J. Am. Chem. Soc.*, **1991**, *113* (16), 6021-6028.

(20) Lu, P.; Wang, Y., *Chem. Soc. Rev.,* **2012**, *41* (17), 5687–5705.

(21) Krow, G. R., *Angew. Chem. Int. Ed.*, **1971**, *10* (7), 435-528.

(22) Sung, K., *J. Chem. Soc. Perkin. Trans.,* **2000**, *2*, 847-853.

(23) Shaabani, A.; Sarvary, A.; Ghasemi, S.; Rezayan, A. H.; Ghadari, R.; Ng, S. W., *Curr. Green Chem.,* **2011**, *13* (3), 582–585.

(24) Bae, I.; Han, H.; Chang, S., *J. Am. Chem. Soc.,* **2005**, *127* (7), 2038–2039.

(25) Sauers, R. R.; Van Arnum, S. D., *Phosphorus, Sulfur, Silicon Relat. Elem.,* **2003**, *178* (10), 2169–2181.

(26) Van Vliet, K. M.; Polak, L. H.; Siegler, M. A.; Van Der Vlugt, J. I.; Guerra, C. F.; De Bruin, B., *J. Am. Chem. Soc.,* **2019**, *141* (38), 15240–15249.

(27) Jung, B.; Kim, H.; Park, B. S., *Tetrahedron Lett.*, **1996**, *37* (23), 4019-4022.

(28) Bestermann, H.; Harder, R.; Winter, H.; Wentrup, C., *Angew. Chem. Int. Ed.*, **1980**, *19* (7), 564-566.

(29) Montalbetti, C. A. G. N.; Falque, V., *Tetrahedron*, **2005**, *61* (740), 10827-10852.

(30) Kumar, V.; Bhatt, V.; Kumar, N., *J. Nat. Prod.,* **2018**, *56*, 287-333.

(31) Zhang, R.; Zhang, Z.; Zhou, Q.; Yu, L.; Wang, J., *Angew. Chem. Int. Ed.,* **2019**, *131* (17), 5800–5804.

(32) Kumar, Y. K.; Kumar, G. R.; Reddy, M. S., *J. Org. Chem.,* **2014**, *79* (2), 823–828.

(33) Bi, X.; Liu, Z.; Cao, S.; Wu, J.; Zanoni, G.; Sivaguru, P., *ACS Catal.,* **2020**, *10* (21), 12881–12887.

(34) Dodd, R.; Cariou, K.; Ketenimines, K. C.; Dodd, R. H. *Chem. Eur. J.,* **2018**, *24* (10), 2297-2304.

(35) Yang, W.; Huang, D.; Zeng, X.; Zhang, J.; Wang, X.; Hu, Y., *Tetrahedron,* **2019**, *75* (3), 381–386.

(36) Shi, M.; Ye, N.; Chen, W.; Wang, H.; Cheung, C.; Parmentier, M.; Gallou, F.; Wu, B., *Org. Process Res. Dev.,* **2020**, *24* (8), 1543–1548.

(37) Matsuda, F.; Itoh, S.; Hattori, N.; Yanagiya, M.; Matsumoto, T., *Tetrahedron*, **1985**, *41* (18), 3625-3631.

(38) Bousfield, T. W.; Pearce, K. P. R.; Nyamini, S. B.; Angelis-Dimakis, A.; Camp, J. E., *Green Chem.,* **2019**, *21* (13), 3675–3681.

(39) Gupta, P. K.; Hussain, M. K.; Asad, M.; Kant, R.; Mahar, R.; Shukla, S. K.; Hajela, K., *New J. Chem.,* **2014**, *38* (7), 3062–3070.

(40) Tian, X.; Li, X.; Duan, S.; Du, Y.; Liu, T.; Fang, Y.; Chen, W.; Zhang, H.; Li, M.; Yang, X.; Li, M.; Yang, X., *ACS Catal.,* **2020**, *363* (4), 1050-1058.

(41) Powell, W. H., *Pure & Appl. Chem.*, **1993**, *65* (6), 1357-1455.

(42) Van Vliet, K. M.; De Bruin, B., *J. Am. Chem. Soc.,* **2020**, *10* (8), 4751-4769.

(43) Sheng, Y.; Zhou, J.; Gao, Y.; Duan, B.; Wang, Y.; Samorodov, A.; Liang, G.; Zhao, Q.; Song, Z., *J. Org. Chem.,* **2021**, *86* (3), 2827–2839.

(44) Park, Y.; Park, K. T.; Kim, J. G.; Chang, S., *J. Am. Chem. Soc.,* **2015**, *137* (13), 4534–4542.

(45) Li, D.; Wu, T.; Liang, K.; Xia, C., *Org. Lett.,* **2016**, *18* (9), 2228–2231.

(46) Entelis, S. G.; Nesterov, O. V., *Russ. Chem. Rev.,* **1966**, *35* (12), 917-930.

(47) Knopf, R. J.; Brotherton, T. K., *JCED.*, **1967,** *12* (3), 421-425.

(48) Papadopoulos, E. P., *J. Org. Chem.,* **1977**, *42* (24), 3925-3930.

(49) Lapprand, A.; Boisson, F.; Delolme, F.; Méchin, F.; Pascault, J. P., *Polym. Degrad. Stab.*, **2005**, *90*, 363-373.

(50) Chen, M.; Sun, N.; Chen, H.; Liu, Y., *ChemComm.,* **2016**, *52* (37), 6324–6327.

(51) Zhao, Y.; Hu, Y.; Wang, C.; Li, X.; Wan, B. *J. Org. Chem.,* **2017**, *82* (7), 3935–3942.

(52) Mayer, K. K.; Sauer, J., *Tetrahedron Lett., 3*, 319-324.

(53) Evano, G.; Lecomte, M.; Thilmany, P.; Theunissen, C., *Synthesis*, **2017**, *49*, 3183-3214.

(54) Krossing, I.; Raabe, I., *Angew. Chem. Int. Ed.,* **2004**, *43*, 2066-2090.

(55) Beck, W.; Sunkel, K., *Chem. Rev.* **1988**, *88*, 1405-1421.

(56) Fisher, S. P.; McArthur, S. G.; Tej, V.; Lee, S. E.; Chan, A. L.; Banda, I.; Gregory, A.; Berkley, K.; Tsay, C.; Rheingold, A. L.; Guisado-Barrios, G.; Lavallo, V., *J. Am. Chem. Soc.,* **2020**, *142* (1), 251–256.

(57) Jenne, C.; Wegener, B., *Z., Greem Chem.,* **2018**, *644* (18), 1123–1132.

(58) Stubbs, J. M.; Firth, K. F.; Bridge, B. J.; Berger, K. J.; Hazlehurst, R. J.; Boyle, P. D.; Blacquiere, J. M., *Dalton Trans.* **2017**, *46* (3), 647–650.

(59) Biasiolo, L.; Trinchillo, M.; Belanzoni, P.; Belpassi, L.; Busico, V.; Ciancaleoni, G.; D'Amora, A.; Macchioni, A.; Tarantelli, F.; Zuccaccia, D.*, Eur. J, Chem.,* **2014**, *20* (45), 14594–14598.

(60) Macchioni, A., *Chem. Rev.,* **2005**, *105*, 2039-2073

(61) Macchioni, A.; Bellachioma, G.; Cardaci, G.; Travaglia, M.; Zuccaccia, C.; Milani, B.; Corso, G.; Zangrando, E.; Mestroni, G.; Carfagna, C.; Formica, M. *Organometallics,* **1999**, *18* (16), 3061–3069.

(62) Kennedy, A. R.; Kerr, W. J.; Moir, R.; Reid, M., *Org. Biomol. Chem.,* **2014**, *12* (40), 7927–7931.

(63) Youn Hong, S.; Park, Y.; Hwang, Y.; Bum Kim, Y.; Baik, M.-H.; Chang, S.,

(64) Sung, K.; Wu, S. H.; Wu, R. R.; Sun, S. Y. *Journal of Organic Chemistry* **2002**, *67* (12), 4298–4303.

(65) Rao, V. V. R.; Wentrup, C., *J. Chem. Soc., Perkin Trans.,* **1998**, *1*, 2583-2586.

(66) Salvatore, R. N.; Chu, F.; Nagle, A. S.; Kapxhiu, E. A.; Cross, R. M.; Woon Jung, K.

(67) Yoshitake, M.; Hayashi, H.; Uchida, T. *Org. Lett.,* **2020**, *22* (10), 4021–4025.

(68) Li, D.; Wu, T.; Liang, K.; Xia, C. *Org. Lett.,* **2016**, *18* (9), 2228–2231.

(69) Sonawane, R. B.; Rasal, N. K.; Bhange, D. S.; Jagtap, S. V., *Chem. Cat. Chem.,* **2018**, *10* (17), 3907–3913.

(70) Stephen, A.; Hashmi, K.; Hofmann, J.; Shi, S.; Schütz, A.; Rudolph, M.; Lothschütz, C.; Wieteck, M.; Bührle, M.; Wçlfle, M.; Rominger, F., *Chem,. Eur. J.,* **2012**, *19* (1), 382-389.

(71) Mancuso, R.; Ziccarelli, I.; Fini, F.; Della Ca', N.; Marino, N.; Carfagna, C.; Gabriele, B., *Adv. Synth. Catal.,* **2019**, *361* (4), 690–695.

(72) Libretexts, *Elecrophilic Additions Reactions of Alkynes*, 916.

(73) Fackler, J. P.; Douglas, B. E.; Busch, D. H.; Worrell, J. H.; Kaesz, H. D.; Ginsberg, A. P.; Bennet, M. A.; Calderazzo, F.; Fischer, E. O.; Lewis, J.; Malatesta, L.; Poilblanc, R.; Roesky, H. W.; Stone, F. G. A.; Yamamoto, A.; Angelici, R. J., *Reagents for Transition Metal Complex and Organometallic Synthsis,* **1990**, *28*, 270-273.

(74) Strauss, S. H., *Chem. Rev.*, **1993**, *93*, 927-942.

(75) Mercier, A.; Yeo, C.; Chou, J.; Chaudhuri, D.; Bernardinelli, G.; Kündig, E. P., *ChemCom.*, **2009**, *35*, 5227-5229.

7   Appendix
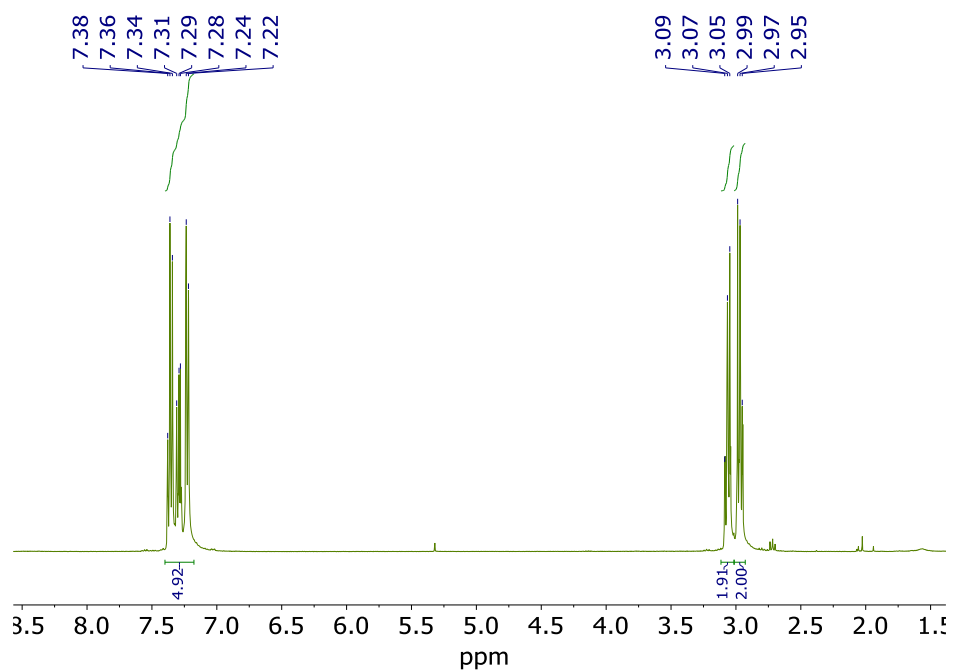
Appendix 7.1. ¹H NMR spectrum (600 MHz, CD$_2$Cl$_2$) of **1a**.
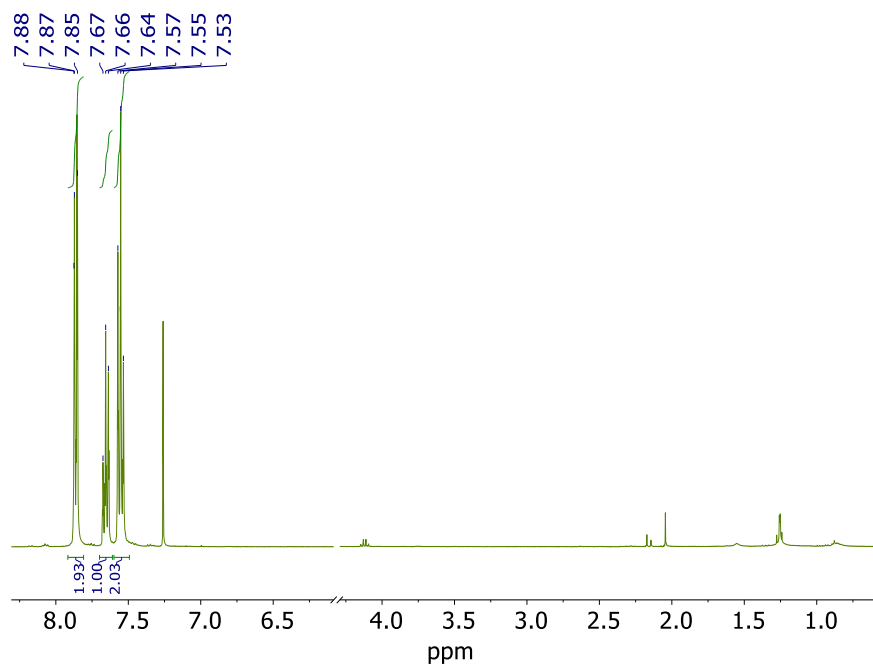
Appendix 7.2. ¹H NMR spectrum (600 MHz, CD$_2$Cl$_2$) of **1b**.

7.35
7.28
7.00
6.88

3.89
3.65
3.56

1.99

4.03
6.00

2.28
4.03
2.13

5.18

7.6 7.2 6.8 6.4 6.0 5.6 5.2 4.8 4.4 4.0 3.6 3.2 2.8 2.4 2.0 1.
ppm
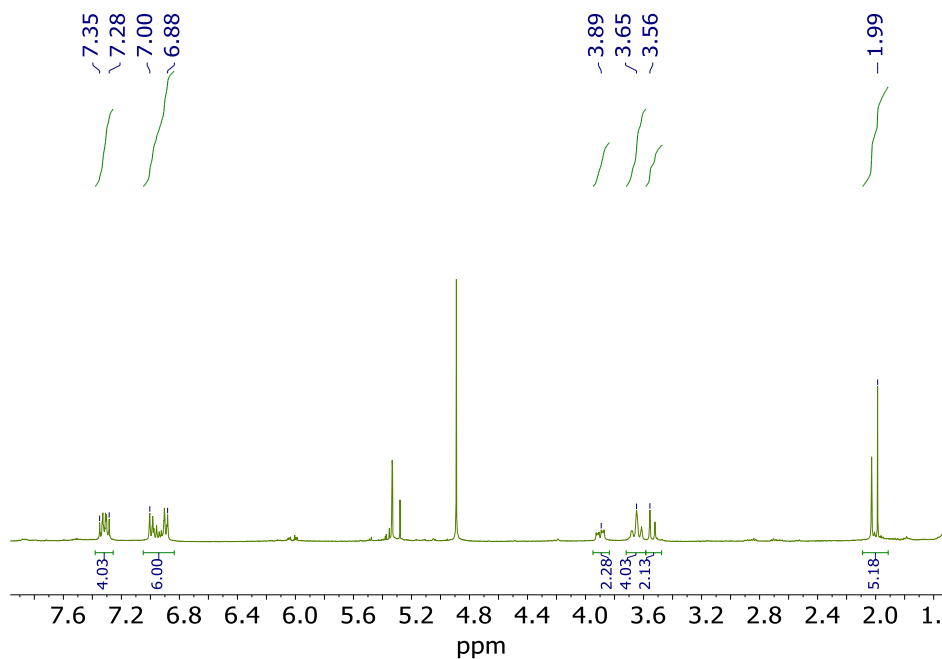
Appendix 7.3. ^{1}H NMR spectrum (600 MHz, Acetone-d_6) of **Ru-1**.

−40.77

−−144.24

80   50   20   −10   −40   −70   −100   −130   −160   −190   −220   −2
ppm
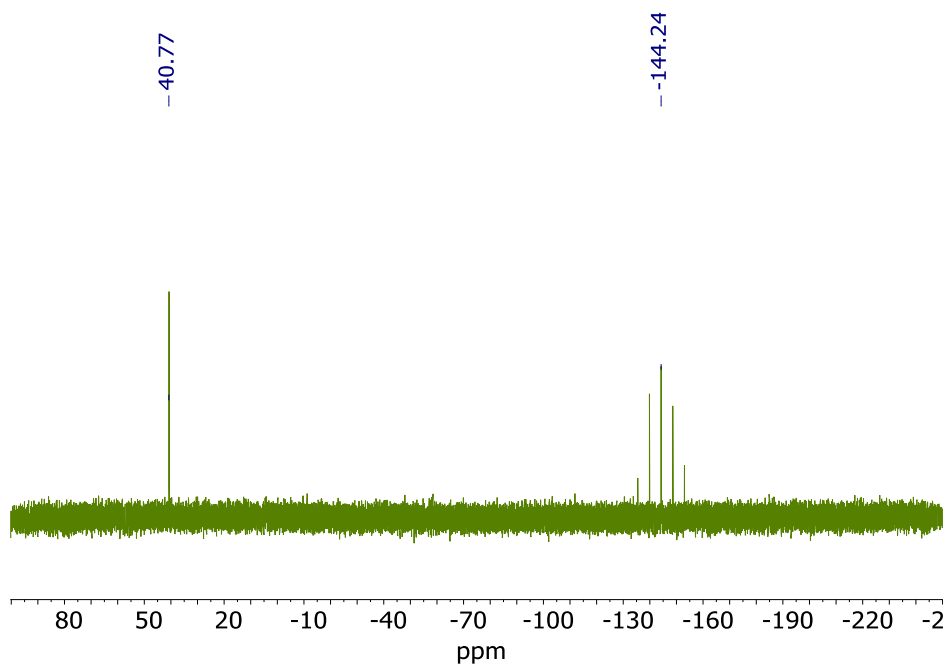
Appendix 7.4. ^{31}P{^{1}H} NMR spectrum (600 MHz, Acetone-d_6) of **Ru-1**.
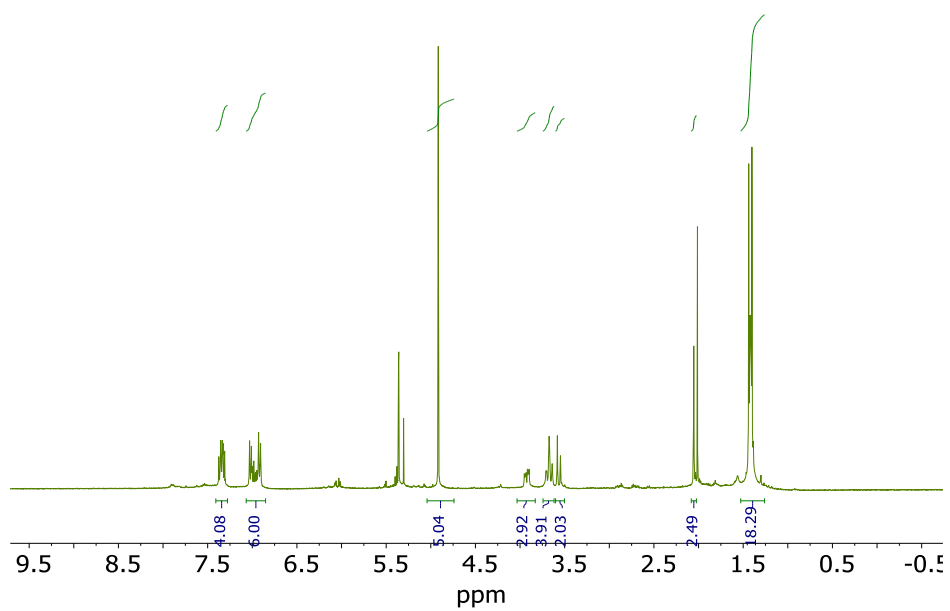
Appendix 7.5. ^{1}H NMR spectrum (600 MHz, CD$_2$Cl$_2$) of **Ru-2**.
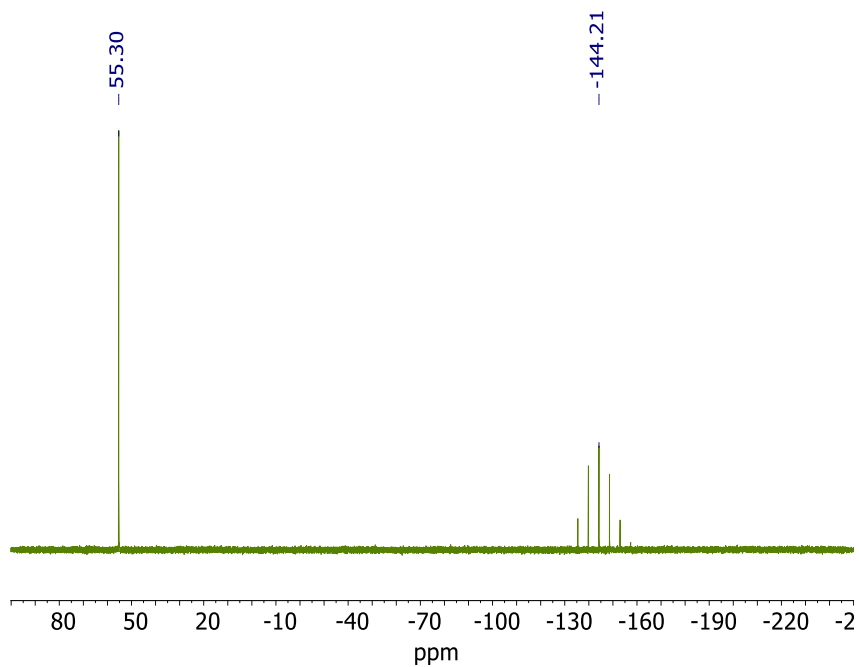
Appendix 7.6. ^{31}P{^{1}H} NMR spectrum (600 MHz, CD$_2$Cl$_2$) of **Ru-2**.
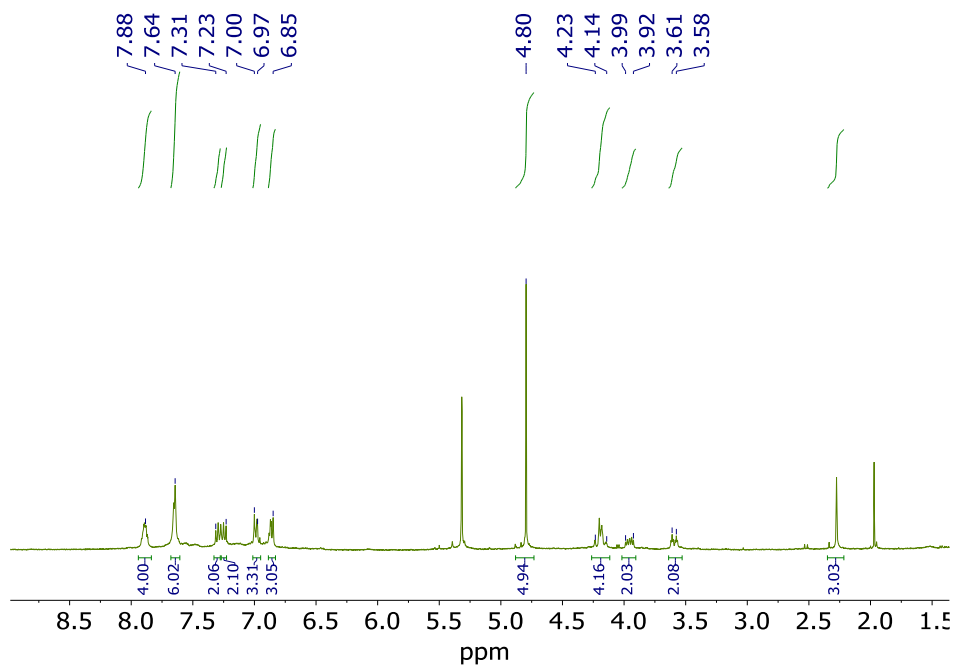
Appendix 7.7. ^{1}H NMR spectrum (600 MHz, CD$_2$Cl$_2$) of **Ru-3**.
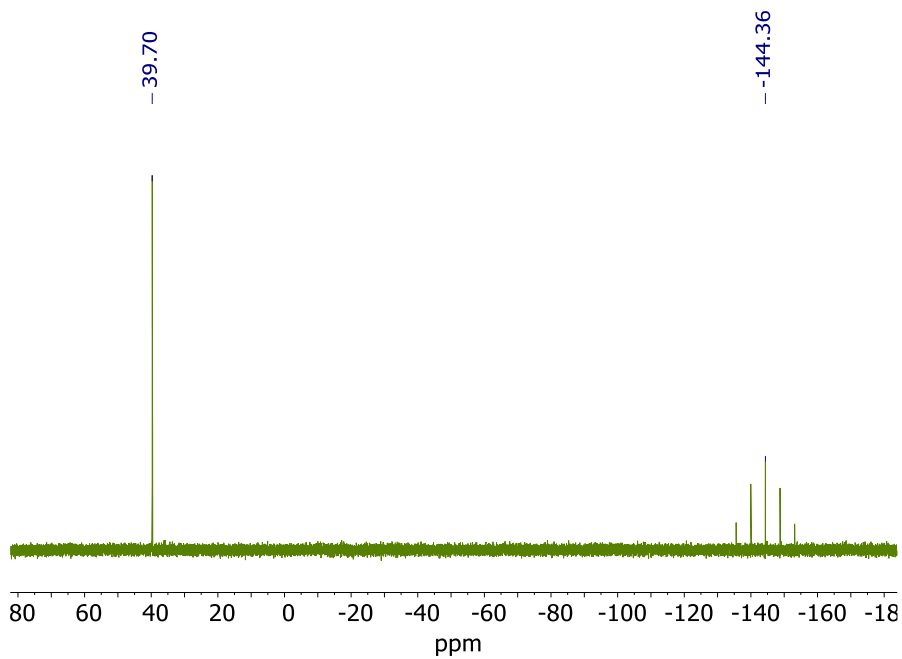
Appendix 7.8. ^{31}P{^{1}H} NMR spectrum (600 MHz, CD$_2$Cl$_2$) of **Ru-3**.
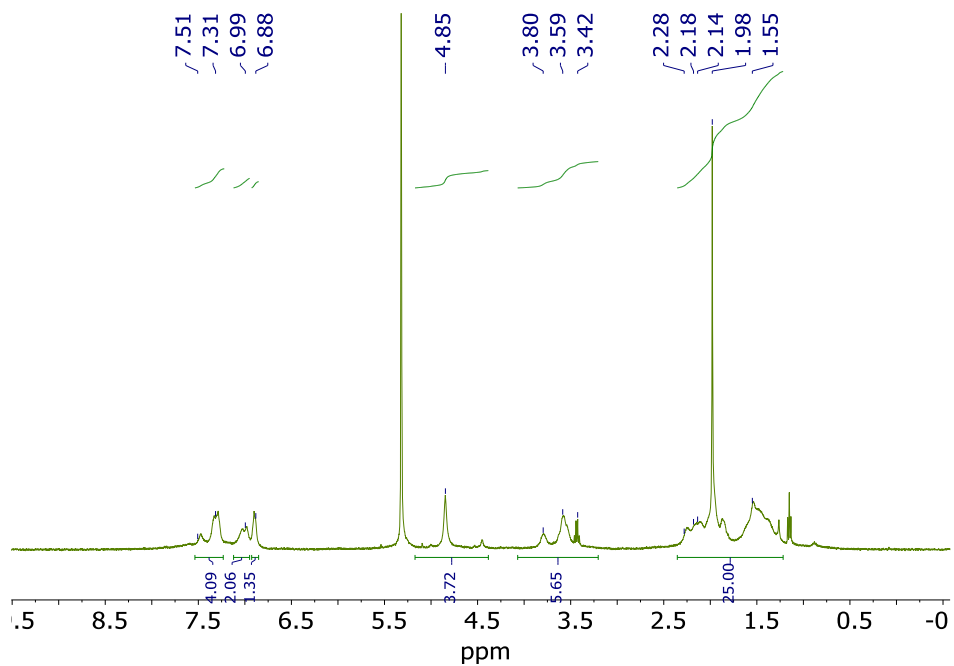
Appendix **7.9**. ¹H NMR spectrum (600 MHz, CD₂Cl₂) **Ru-4**.
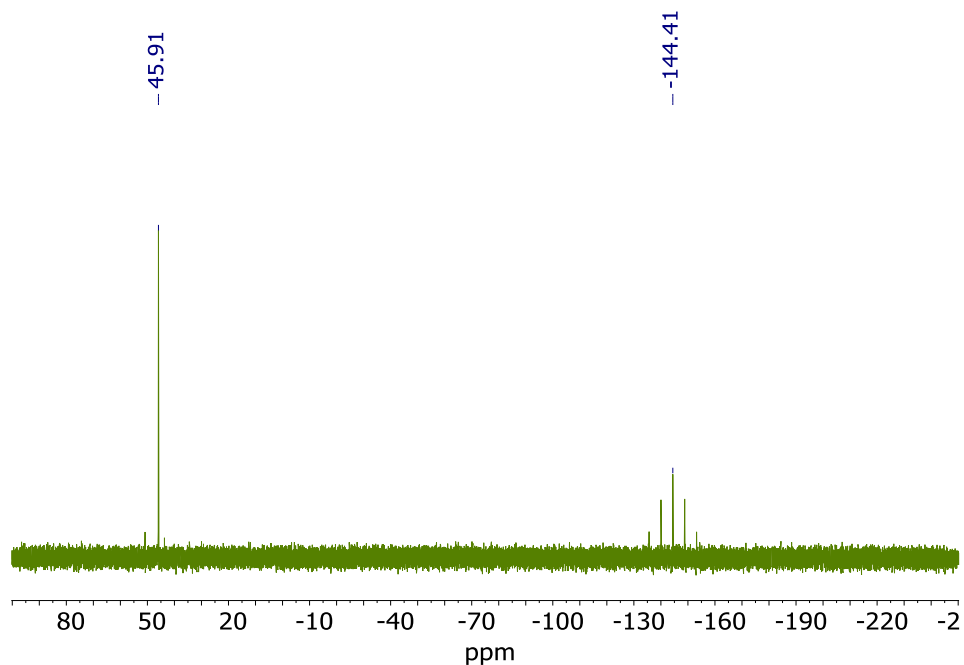
Appendix 7.10. ³¹P{¹H} NMR spectrum (600 MHz, CD₂Cl₂) of **Ru-4**.
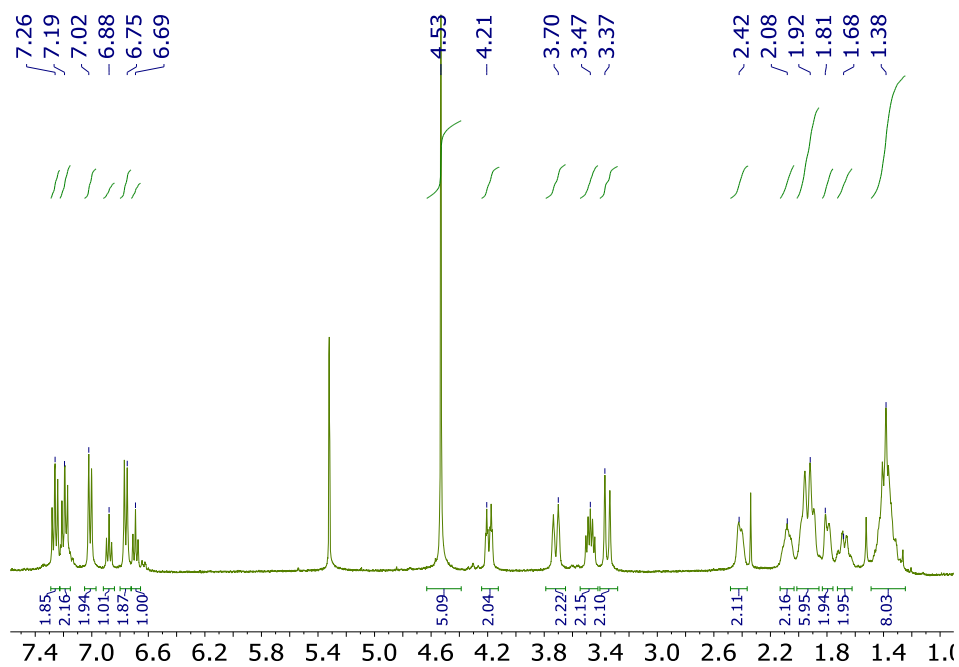
Appendix 7.11. ^{1}H NMR spectrum (600 MHz, CD$_2$Cl$_2$) of **Ru-5**.
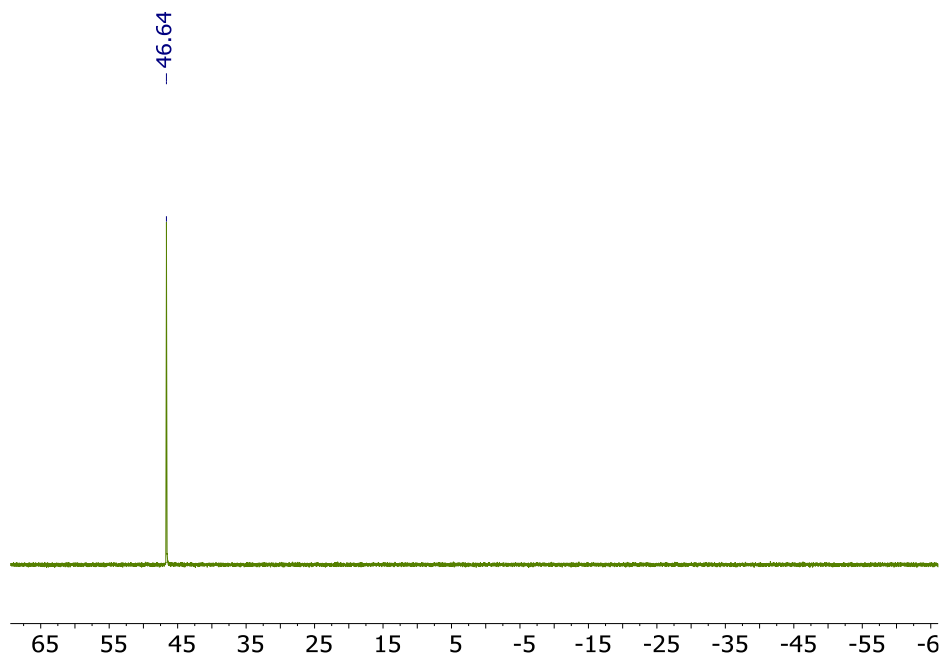
Appendix 7.12. ^{31}P{^{1}H} NMR spectrum (600 MHz, CD$_2$Cl$_2$) of **Ru-5**.
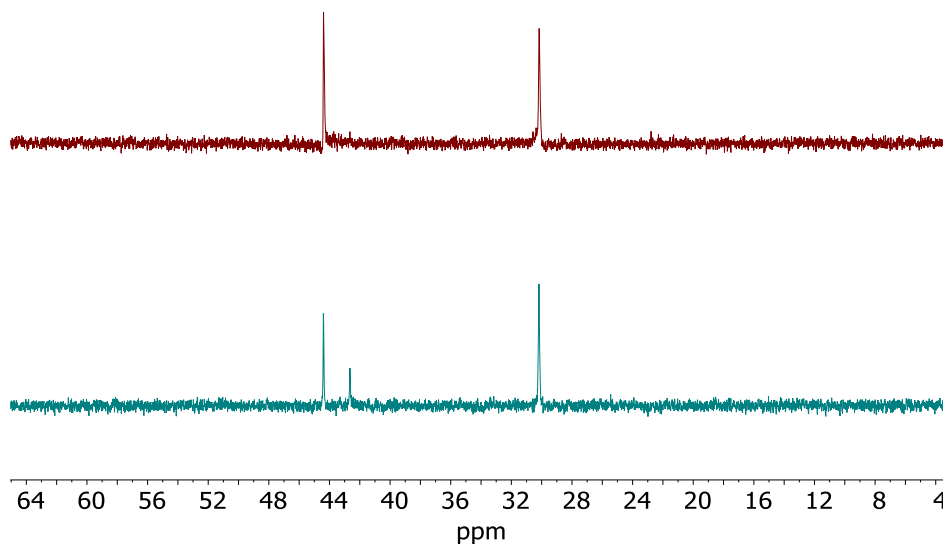
Appendix 7.13. $^{31}P\{^1H\}$ NMR spectrum (600 MHz, Anisole) of top) **Ru-3**; and bottom) **Ru-3** with **2a** after 80 min at 70 ºC.
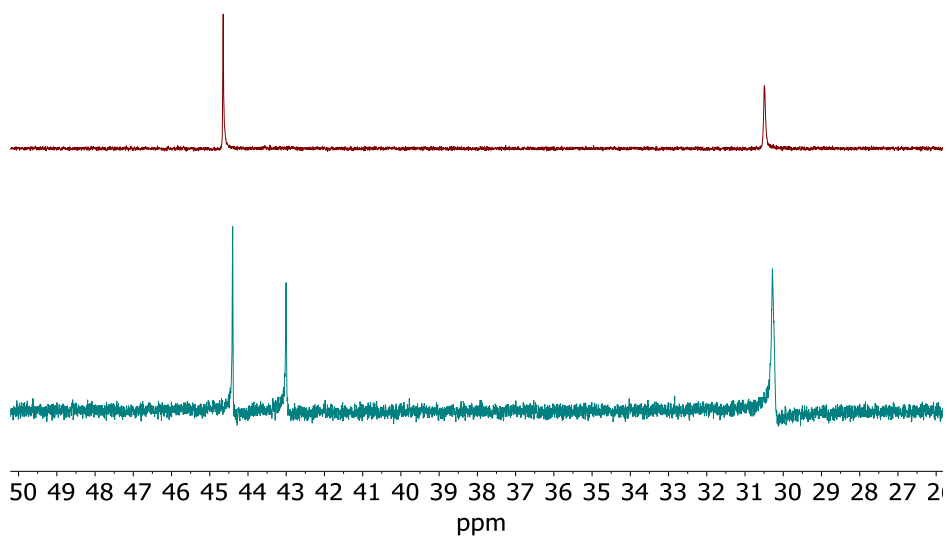
Appendix 7.14. $^{31}P\{^1H\}$ NMR spectrum (600 MHz, Anisole) of top) **Ru-3**; and bottom) **Ru-3** with **2b** after 80 minutes at 70 ºC.
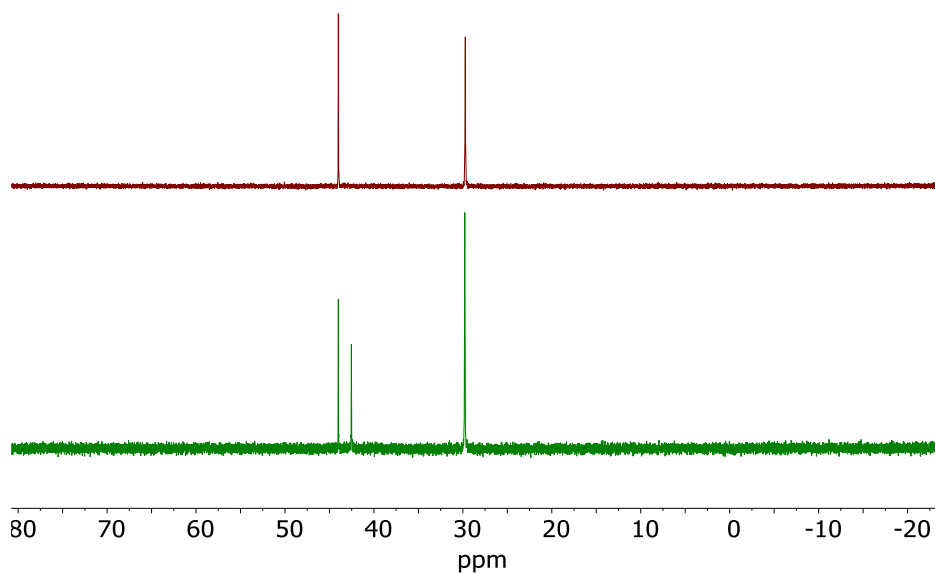
Appendix 7.15. $^{31}P\{^1H\}$ NMR spectrum (600 MHz, Anisole) of top) **Ru-3**; and bottom) **Ru-3** with **2c** after 80 minutes at 70 ℃.
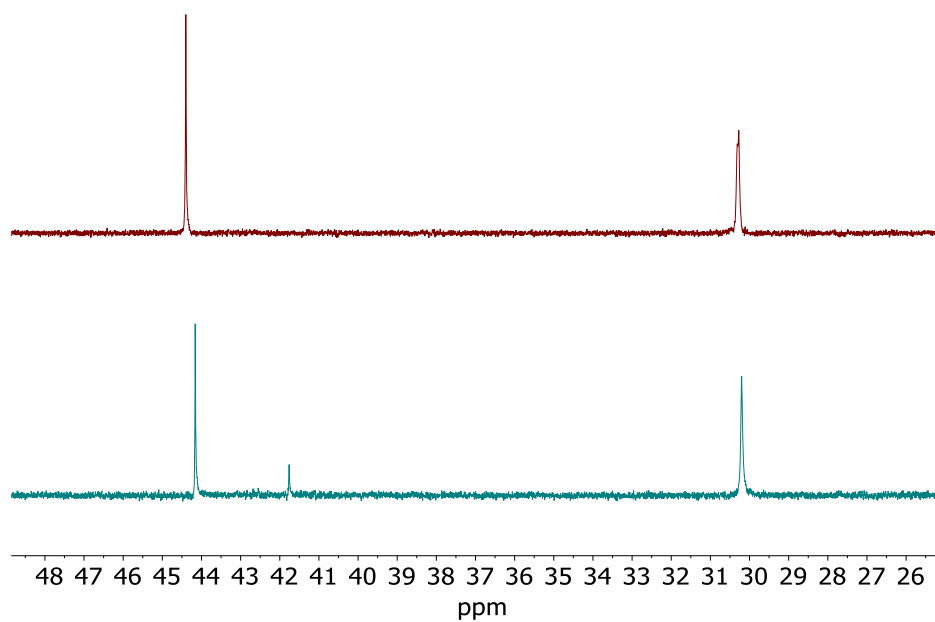
Appendix 7.16. $^{31}P\{^1H\}$ NMR spectrum (600 MHz, Anisole) of top) **Ru-3**; and bottom) **Ru-3** with **2d** after 80 minutes at 70 ℃.
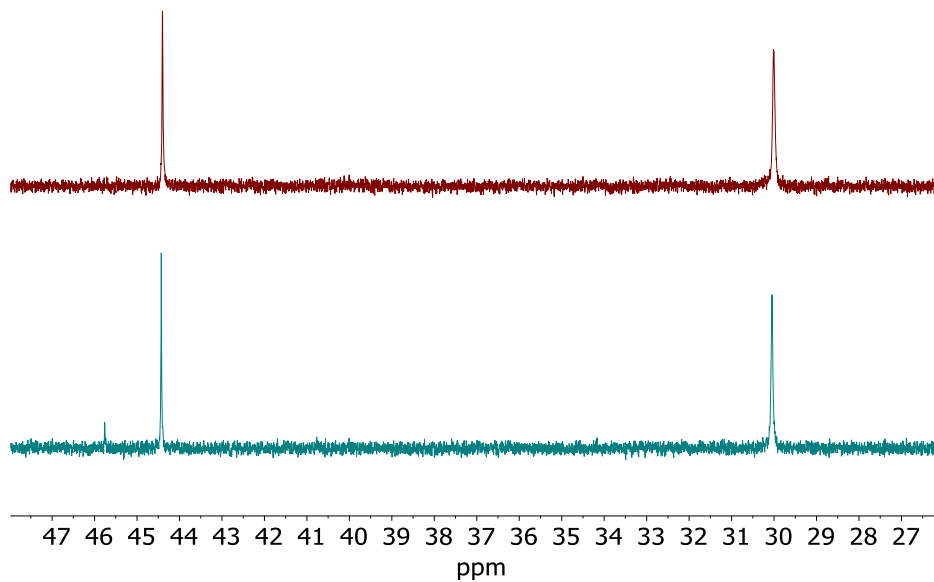
Appendix 7.17. ^{31}P{^{1}H} NMR spectrum (600 MHz, Anisole) of top) **Ru-3**; and bottom) **Ru-3** with **2e** after 80 minutes at 70 ºC.
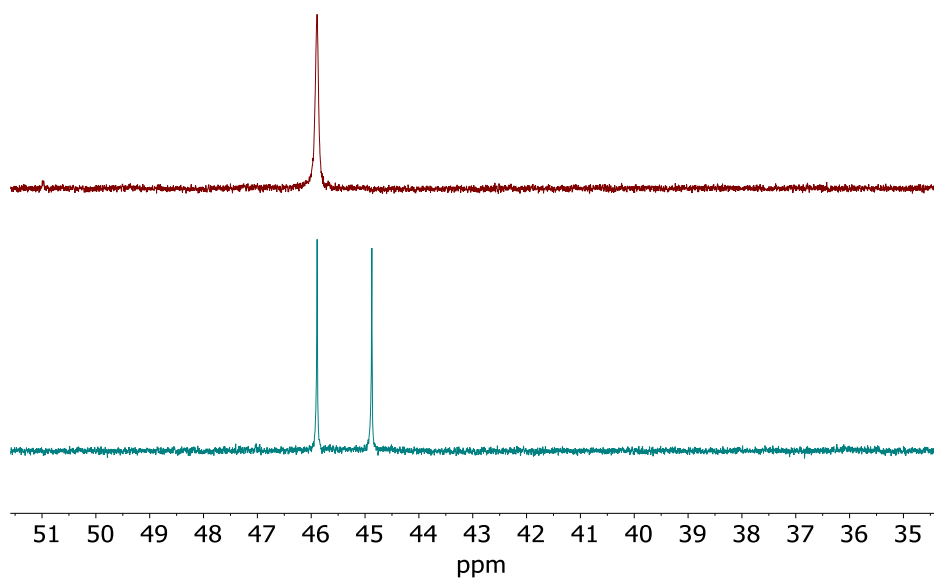
Appendix 7.18. ^{31}P{^{1}H} NMR spectrum (600 MHz, Anisole) of top) **Ru-4**; and bottom) **Ru-4** with **2a** after 80 minutes at 70 ºC

Appendix 7.19. Response factor calculated for hydroalkoxylation of 2-EBA to isochromene using **Ru-5** with various WCAs.

Vial Contents	Average 2-EBA Remaining	Average Isochromene Produced	Response Factor Required
2-EBA	98.6%	2.5%	1.01
2-EBA + **Ru-5**	88.8%	17.6%	0.94
2-EBA + **Ru-5** + KOTf	48.2%	58.9%	0.93
2-EBA + **Ru-5** + KBF$_4$	69.4%	47.8%	0.86
2-EBA + **Ru-5** + KPF$_6$	37.3%	71.8%	0.92
2-EBA + KOTf	91.2%	11.9%	0.97
2-EBA + KBF$_4$	91.0%	13.2%	0.96
2-EBA + KPF$_6$	95.3%	8.4%	0.97
2-EBA + **Ru-5** + KPF$_6$ + No MeCN	92.3%	9.1%	0.99

Appendix 7.20. Response factor calculated for hydroalkoxylation of 2-EBA to isochromene using **Ru-4** with alkali salt additives.

Vial Contents	2-EBA Remaining	Isochromene Produced	Required Response Factor
2-EBA	98.6%	2.5%	1.01
2-EBA + **Ru-4**	31.7%	66.2%	1.02
2-EBA + **Ru-4** + NaPF$_6$	2.5%	93.4%	1.04
2-EBA + **Ru-4** + LiPF$_6$	17.7%	74.7%	1.08
2-EBA + **Ru-4** + KPF$_6$	31.7%	64.2%	1.04
2-EBA + NaPF$_6$	85.7%	18.4%	0.96
2-EBA + LiPF$_6$	91.7%	4.5%	1.04
2-EBA + KPF$_6$	91.0%	2.8%	1.07

Curriculum Vitae

Name: Megan A. Hoffer

Post-secondary Education and Degrees:
Western University
London, Ontario, Canada
2017-2021 BSc

Honours and Awards:
Dean's Honour List
Western University
2020-2021

Undergraduate Student Research Internship
Western University
Summer   2021

Related Work Experience
Teaching Assistant | Inorganic Chemistry of the Main Group Elements
Western University
Jan. 2023-Apr. 2023

Mentor | Sisters in Science Mentorship Program
Western University
Oct. 2022-Present

President | Chemistry Graduate Student Association (CGSA)
Western University
Sept. 2022-Aug. 2022

Teaching Assistant | Structure and Bonding in Inorganic Chemistry
Western University
Sept. 2022-Dec. 2022

Teaching Assistant | Organic Chemistry for Life Science
Western University
May 2022

Teaching Assistant | Inorganic Chemistry of the Main Group Elements
Western University
Jan. 2022-Apr. 2022

Teaching Assistant | Discovering Chemical Energetics
Western University
Jan. 2022-Apr. 2022

Vice President Social | CGSA
Western University
Sept. 2021-Sept. 2022

Publications:	D.E. Chapple, <u>M.A. Hoffer</u>, P.D. Boyle, J.M. Blacquiere* Alkyne Hydrofunctionalization Mechanism Including an Off-Cycle Alkoxycarbene Deactivation Complex, *Organometallics*, **2022**, *41*, 12, 1532-1542. DOI: 10.1021/acs.organomet.2c00170
Conferences:	IDW Poster Session November 2022 Brock University "Exploration of Nucleophilic Reactivity of Dioxazolones" Canadian Chemistry Conference and Exhibition Poster Session Sumer 2021 Virtual Conference "Highly Selective Iron Catalyst Affording *Endo*-Oxygen-Heterocycles"